Leveraging Next Generation Sequencing to Elucidate the Spectrum of Genetic Alterations Underlying Head and Neck Cancer and Identify Potential Therapeutic Targets

by

Matthew Louis Hedberg

Bachelor of Arts in Chemistry, University of Utah, 2009

Submitted to the Graduate Faculty of

The University of Pittsburgh School of Medicine

in partial fulfillment of the requirements for the degree of

Doctor of Philosophy

University of Pittsburgh

2015

UNIVERSITY OF PITTSBURGH

SCHOOL OF MEDICINE

This dissertation was presented

by

Matthew L. Hedberg

It was defended on

July 27, 2015

and approved by

Donald B. DeFranco, PhD, Department of Pharmacology and Chemical Biology

Adrian Lee, PhD, Department of Pharmacology and Chemical Biology

Ben Van Houten, PhD, Department of Pharmacology and Chemical Biology

Yuri Nikiforov, MD, PhD, Department of Pathology

Dissertation Advisor:

Jennifer R. Grandis, MD, Department of Pharmacology and Chemical Biology

Leveraging Next Generation Sequencing to Elucidate the Spectrum of Genetic Alterations Underlying Head and Neck Cancer and Identify Potential Therapeutic Targets

Matthew L. Hedberg, PhD

Head and neck squamous cell carcinoma (HNSCC), is a cancer of the upper aerodigestive tract epithelium. Risk factors for HNSCC are smoking, alcohol use, and infection with oncogenic human papillomavirus (HPV). HPV(+)HNSCC has a better prognosis than HPV(-)HNSCC in the absence of smoking. Multimodal therapy, combining surgery, radiation therapy, and chemotherapy, is the standard of care for HPV(+) and HPV(-) HNSCC. Despite improvements in care, all stage survival rates for HNSCC (~60% and ~50%, at 5 and 10 years respectively), have only modestly improved in the last 3 decades.

Cetuximab, an antibody against the epidermal growth factor receptor (EGFR), and only FDA-approved targeted therapy in HNSCC, is efficacious in only a subset of patients, and no known biomarkers can identify which patients will respond. Traditionally, a lack of knowledge regarding the genetic alterations underlying HNSCC has stymied the development of additional targeted agents. We conducted whole exome sequencing (WES) studies that reveal a compendium of genetic alterations observed in primary, metastatic, and recurrent HNSCC. Which, together with functional analyses in preclinical models, have identified new potential therapeutic targets in HNSCC.

WES of 151 HNSCC tumors identified the phosphoinositol-3-kinase (PI3K) pathway and phosphatidylinositol-4,5-bisphosphate 3-kinase, catalytic subunit alpha (*PIK3CA*) as the most commonly mutated oncogenic pathway and oncogene in HNSCC. *PIK3CA* alterations were

found to promote growth, survival, and invasion in engineered HNSCC cell lines. PI3K inhibitors were effective in preclinical models of HNSCC, especially in those harboring endogenous *PIK3CA* mutations.

WES of patient-matched tumor pairs from 23 patients with metastatic or recurrent disease reveals a spectrum of inter-tumor genetic heterogeneity. Genetically, paired primary tumors are more similar to synchronous lymph node metastases than metachronous recurrent tumors. Newly acquired mutations in the discoidin domain receptor 2 (*DDR2*) gene were found in a subset of recurrent tumors. Mutations in this gene have been found to confer sensitivity to Src family kinase (SFK) inhibitors in other malignancies, and we found HNSCC cell lines with endogenous or engineered *DDR2* mutations to be sensitive to dasatinib. These studies shed light on the underlying pathophysiology of HNSCC, and identify potential therapeutic targets for further investigation.

TABLE OF CONTENTS

LIST OF TABLES

LIST OF FIGURES

PREFACE

I would like to acknowledge all of my scientific collaborators and mentors to date for the contributions they have made to my training. I would like to make special mention of my primary undergraduate mentors at the University of Utah: Drs. James Metherall, Malay Haldar, and Mario Capecchi. As well as my primary graduate mentors Drs. Clayton Wiley, Richard Steinman, Bruce Freeman, Patrick Pagano, Simion Chiosea, Yuri Nikiforov, Ben Van Houten, Adrian Lee, Donald DeFranco, and Jennifer Grandis. These individuals, along with the countless fellow students, technicians and senior staff scientists who now number amongst my friends and colleagues, have been absolutely integral to my development as a scientist, and none of this work would be possible without their tremendous contributions.

Most of all, I wish to thank my family. They have made continual sacrifices for my benefit since the day I was born. Every opportunity I've had is made possible only through them, and the credit for any success I may have had is owed to them.

Some of the material contained in this dissertation has already been published. Any material(s), including text, tables, or figures, that have been reproduced in part or in whole in this manuscript have been used with the express written consent of the publishing entities to whom the copyright belongs. Documentation of these permissions, which give me the right to reproduce these works in part or in whole for this purpose, is contained in the appendix.

1.0 GENERAL INTRODUCTION AND REVIEW OF LITERATURE

The Human Genome Project, initiated in 1990, represents the culmination of more than a century of research, dating back to Gregor Mendel's 1865 experiments in plant hybridization. Largely using bacterial artificial chromosome (BAC) cloning and Sanger sequencing techniques originally developed in the 1970s, this international consortium of geneticists produced the first full sequence of the human genome over the course of 13 years, at a cost of approximately $2.7 billion.(*1*) As the draft sequence was completed, a new sequencing technology, called massively parallel sequencing (MPS), was developed by Lynx Therapeutics.(*2*) This technology combined and miniaturized *in vitro* cloning/amplification and sequencing techniques, resulting in the simultaneous generation of millions of parallel reaction reads, and provided the framework for additional high-throughput next generation sequencing (NGS) technologies, developed shortly thereafter.(*3*) The profound reductions in cost and time to sequence that NGS technologies offer, from years and millions of dollars to days and thousands of dollars, have resulted in the application of genome, exome, and targeted NGS to virtually every known disease. As cancer is a genetic disorder, these technologies present a tremendous opportunity to expand our understanding of this disease and develop new therapeutics.

Cancer is a collection of disease states characterized by uncontrolled growth of atypical cells with the potential to invade, overtake and damage otherwise normal tissues throughout the body. Specific types of cancer are diagnosed and defined by the cells and organs they originate

from, and increasingly, by their molecular characteristics. These underlying molecular characteristics, namely the genetic and epigenetic abnormalities that accumulate throughout the evolution of these atypical cells, are the root cause of cancer.

Since 1998, in the United States, there has been a sustained decline in overall cancer mortality, and the most recent data demonstrate a 0.5% decrease in the incidence rate of cancer in the general population from 2002 to 2011.(*4*) Cancer remains however, a leading cause of morbidity and mortality in this country; with an estimated 1,658,370 new cases of cancer and 589,430 deaths from cancer in the United States this year, costing in excess of $125 billion to treat.(*5*)

1.1 HEAD AND NECK SQUAMOUS CELL CARCINOMA

1.1.1 Epidemiology and Clinical Considerations

Head and neck squamous cell carcinoma (HNSCC) is a cancer of the upper aerodigestive tract epithelium that accounts for >90% of the cancers of the head and neck.(*6*) It arises in the oral cavity (~51%), pharynx (~26%), and larynx (~23%).(*7*) Worldwide, HNSCC is the 7th most common cancer by incidence, with over 600,000 new cases each year; more than 50,000 of which are estimated to occur in the United States.(*8*) Men are at least two times more likely to be diagnosed with HNSCC than women, due largely to differences in behavioral risk factors, and the incidence rate of HNSCC has increased by ~55% in men and ~20% in women over the last 10 years, according to US incidence data.(*4*) Classically, tobacco use and alcohol consumption are the two most important behavioral risk factors for the development of HNSCC in developed

countries, and their contributions to risk are synergistic. Underlying the increased incidence of oropharyngeal cancer, infection with oncogenic strains of the human papillomavirus (HPV), primarily HPV-16, is now a well-established independent risk factor; with approximately 20% of all HNSCC, and more than 60% of HNSCC arising in the oropharynx, being HPV(+).(*4, 9-11*) The prevalence of HPV in the general population appears to increasing as well, a recent meta-analysis found the prevalence in the general male population to be 8.8% in studies before the year 2000, and 28.5% in studies conducted afterwards.(*12*) This virally-associated subtype of HNSCC has been found to have a favorable prognosis, compared to HPV(-) subtypes, in the absence of smoking.(*13*) The Epstein-Barr virus, though primarily a risk factor for nasopharyngeal carcinoma, has also been associated with HNSCC.(*14, 15*) Greatly increased susceptibility to HNSCC is seen in some heritable conditions of impaired genome maintenance, such as Fanconi Anemia.(*16*)

HNSCC is staged via the tumor, node, metastasis (TNM) staging system which, along with HPV status and tobacco use, is strongly predictive of prognosis.(*13, 17*) Early-stage tumors generally have a favorable prognosis, and are treated with surgery or radiation therapy (RT). Most patients however, present with advanced stage tumors and cervical lymph node metastases.(*18*) More than 90% of these patients are treated with curative intent multimodal combination therapy featuring surgery, RT, and chemotherapy (CT).(*19*) To date, the anatomic site of the primary tumor has in large part dictated the treatment approach; tumors in the oral cavity are surgically resected, and tumors of the pharynx and larynx are treated with chemo-radiation therapy (CRT).(*17, 19*) All stage survival rates in HNSCC, 61% and 50% at 5 and 10 years respectively, have been largely stagnant over the last 3 decades.(*6*) Significant toxicities and morbidities including pain, mucositis, immunosuppression, dysphagia and dysphonia; which

can result in long term dependency on gastric feeding tubes, tracheostomies and voice prostheses, are associated with these treatment modalities.(*20*) HNSCC recurs in more than 25% of patients.(*21*) Recurrence in HNSCC is often resistant to standard therapy, and is generally considered incurable, illustrating the need for improved therapy.(*21, 22*)

A major area of focus in the effort to improve HNSCC therapy is the development of targeted therapeutics. The most mature target to date is the epidermal growth factor receptor (EGFR). Overexpression and hyper activation of *EGFR* is known to contribute to oncogenesis, and is seen in >80% of HNSCC tumors; where high protein levels have been shown to correlate with reduced survival.(*23*) Cetuximab, a chimeric IgG1 monoclonal antibody (mAb) against EGFR, was approved in 2006 and remains the only FDA-approved targeted therapy in HNSCC to date. In a phase III randomized trial of 424 previously untreated HNSCC patients, median overall survival for patients treated with cetuximab and RT was 49.0 months versus 29.3 months in the RT-alone group.(*24*) A randomized trial of 442 patients with recurrent HNSCC found that the addition of cetuximab to platinum-based CT improved median overall survival from 7.4 to 10.1 months.(*25*) When added to CRT in a phase III randomized trial of 891 patients, cetuximab failed to improve outcomes.(*26*) When used alone, response to cetuximab is only observed 10-13% of patients, and resistance is known to develop.(*27*) Given these limitations, additional targeted therapies are clearly needed in HNSCC. In order to develop such agents, an improved understanding of the pathogenesis and molecular characteristics of HNSCC is required.

1.1.2 Oncogenic Progression

The field cancerization theory, proposed in 1953 by Slaughter *et al*., posits that HNSCC evolves clonally through the progressive acquisition of mutations from one or more precancerous field(s)

of atypical mucosal epithelium to an invasive carcinoma (Figure 1). This theory offers a partial explanation as to the risk of local recurrence (as high as 61% in cancers with high risk features) and rate of metachronous second primary tumor formation (6-9% annually for life) in HNSCC.(*28*, *29*)

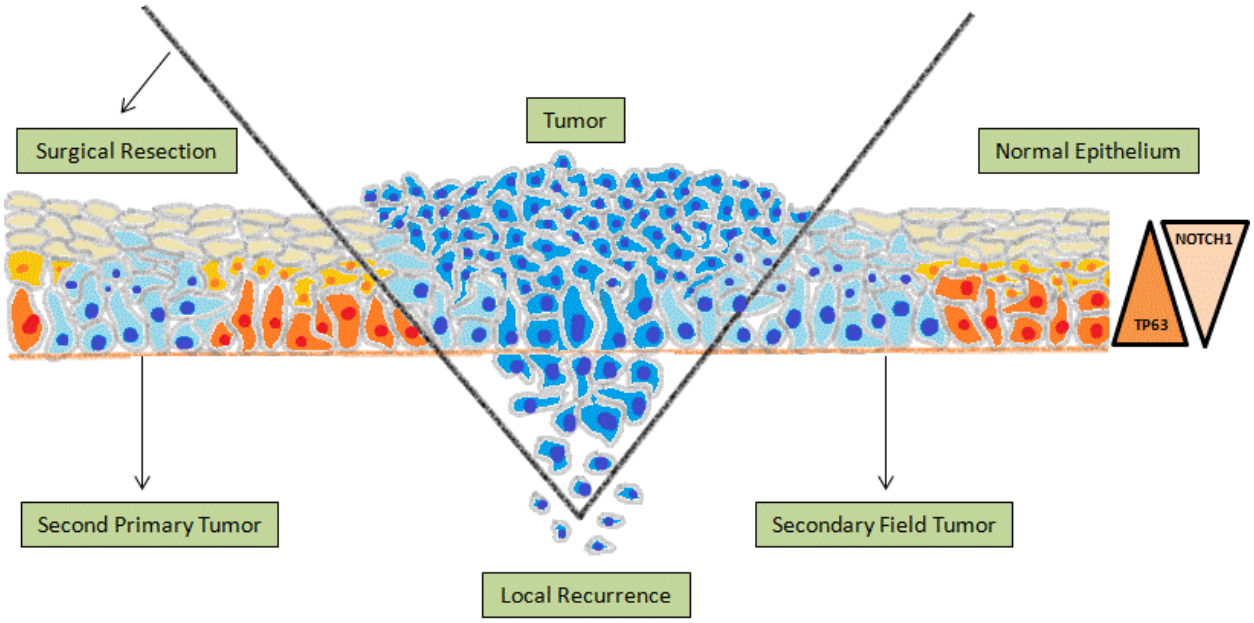

Figure 1. The Field Cancerization Theory.

Exposure of the aerodigestive mucosal tract to carcinogens, i.e. tobacco smoke, results in the presence of one or more mucosal areas consisting of epithelial cells with cancer-associated genetic or epigenetic alterations. A precursor field (*light blue*) is monoclonal but does not show invasive growth or metastatic behavior, which are the hallmarks of an invasive carcinoma (*dark blue*). A field is preneoplastic by definition; it may or may not have histological alterations characteristic of dysplasia. The clinical manifestation of a field is known as a leukoplakia, though most fields are clinically invisible. Additional genetic changes are needed to transform a field into a carcinoma. The field and primary tumor share genetic alterations and have a common clonal origin. Clinically, a field may be the source of local recurrences, second field tumors, and second primary tumors after surgical resection of the initial carcinoma. These legions are clinically distinguished on the basis of their distance from the index tumor, and/or the time interval after which they develop. A local recurrence (*lower center*) arises from residual tumor cells and is less than 2 cm away from, and/or occurs within 3 years of, the primary tumor. A second primary

tumor (*lower left*) is more than 2 cm away from, and/or occurs more than 3 years after, the primary tumor. Tumors that arise from a contiguous portion of the same field that gave rise to the original primary tumor have been described as second field tumors (*lower right*). The normal process of squamous differentiation in mucosa is controlled in part by a *TP63* and *NOTCH1* expression gradient (*far right*). *TP63* is expressed in keratinocytes of the basal layer, where it maintains their proliferative potential and regulates expression of basal keratins. Expression of *NOTCH1* results in terminal differentiation of cells in the spinous and granular layers, and the expression of alternative keratins. Perturbation of this gradient is believed to be a component of precancerous fields and invasive HNSCC legions.(*30-35*) This figure is artwork by Matthew Hedberg as published in The Molecular Pathogenesis of Head and Neck Cancer in Mendelsohn J, Howley PM, Israel MA, Gray JW, and Thompson CB (Eds), The Molecular Basis of Cancer. Philadelphia, PA: Elsevier Inc.

1.1.3 Molecular Pathogenesis

The well documented histological progression of HNSCC from leukoplakia through progressive phases of hyperplasia, dysplasia, carcinoma *in situ* and ultimately invasive carcinoma, is believed to correspond with the accumulation of genetic alterations.(*36*) In HNSCC, one of the earliest initiating events is likely the clonal proliferation of precancerous cells with inactive Tumor Protein 53 (*TP53)*.(*37*) The genetic alterations that accumulate within clonal subpopulations following this initiation event remain the subject of active investigation. Our understanding of the genetic alterations that underlie the development and progression of the primary subtypes of HNSCC (Figure 2) is evolving rapidly with the advent of whole exome sequencing (WES) studies in HNSCC.

Please note: the remaining introductory subsections provide a summary of the current understanding of the molecular pathogenesis of HNSCC, and are intended as a general review. Several components will not be addressed beyond this introduction as they do not directly pertain

to the materials of Chapters 2 and 3, which present the contributions made through our WES studies in primary, metastatic, and recurrent HNSCC.

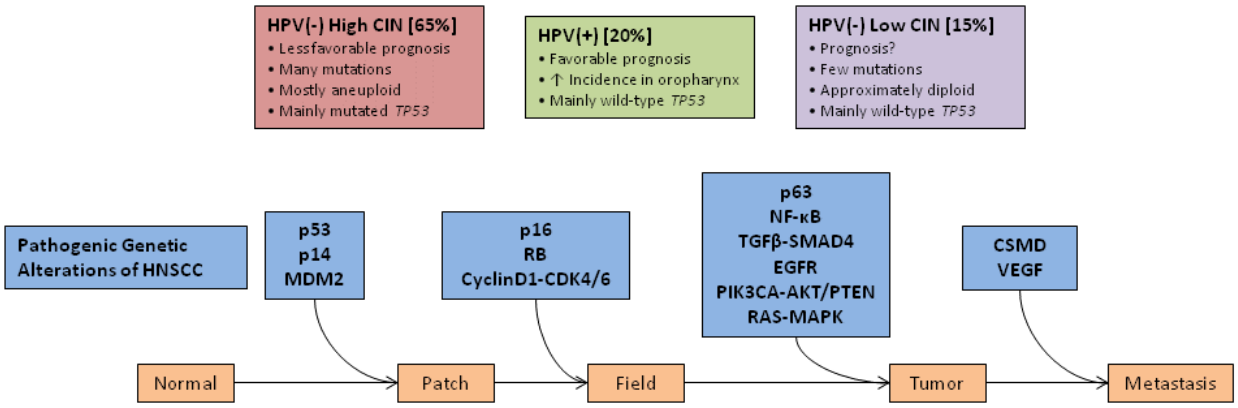

Figure 2. Hypothetical Model of HNSCC Development.

An outline of the genetic alterations implicated in HNSCC oncogenesis. The model is a generalization and thus is varyingly accurate among subtypes of HNSCC. Three steps are critical in this model: A progenitor or adult stem cell acquires one (or more) genetic alterations, usually including an alteration of p53, and forms a patch containing clonal, genetically altered daughter cells. Then, by escaping normal growth control and/or gaining growth advantage, this clonal patch develops into an expanding field. Eventually, through a further accumulation of genetic alterations, a subclone in the field evolves into an invasive cancer and progresses to metastasis. Both aneuploidy and the accumulation of cancer-associated genetic changes in fields are linked to the risk of malignant progression. The three main clinicopathologic subtypes of HNSCC are depicted: HPV(+)HNSCC, HPV(-)HNSCC with many genetic changes (high CIN), and HPV(-)HNSCC with few genetic changes (low CIN). Although drawn as distinct steps for the purpose of illustration, the actual order of acquisition of distinct alterations is not known at this time. CDK: Cyclin-dependent kinase, CSMD: CUB and SUSHI multiple domain protein, NF-κB: nuclear factor-κB, *PIK3CA:* phosphoinositide-3 kinase subunit-α, TGFβ: transforming growth factor-β, *VEGF*: vascular endothelial growth factor. This figure is artwork by Matthew Hedberg as published in The Molecular Pathogenesis of Head and Neck Cancer in Mendelsohn J, Howley PM, Israel MA, Gray JW, and Thompson CB (Eds), The Molecular Basis of Cancer. Philadelphia, PA: Elsevier Inc.

Genetic, and epigenetic, alterations drive the manifestation of cancerous cellular phenotypes in HNSCC. Conceptually, six major hallmarks define our current understanding of a cancerous cellular phenotype: sustaining proliferative signaling, evading growth suppressors, resisting cell death, enabling replicative immortality, inducing angiogenesis, and activating invasion and metastasis.(*38*) Research to date indicates that the altered oncogenes and tumor suppressors of HNSCC act primarily in functional pathways known to largely determine cellular proliferation, cell survival, squamous epithelial differentiation, and invasion and metastasis. Individual genes may function in more than one pathway, and the pathways themselves interface with, and influence, each other (Figure 3).

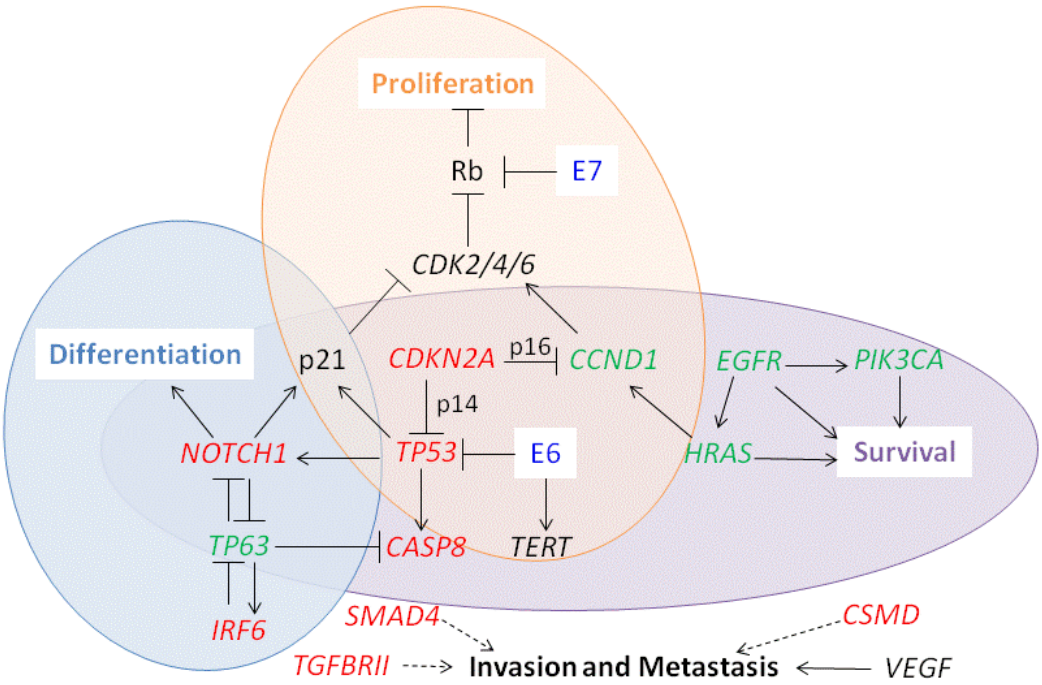

Figure 3. Interfacing Genetic Alterations of HNSCC

Putative oncogenes (*green*), tumor suppressors (*red*), and signaling pathways that mediate the hallmarks of HNSCC. Loss of *TP53* and *CDKN2A*, either through mutation or expression of the HPV E6 and E7 proteins (*blue*), along with

amplification of *CCND1* favors survival and permits proliferation through the increased activity of cyclin-dependent kinases and loss of p53-dependent apoptosis. Although intact differentiation programs and alternative apoptotic programs may restrict abnormal cell cycling for a time, loss of *NOTCH1* and/or abnormal expression of *TP63*, along with the acquisition of alterations in other survival genes, such as *CASP8*, *PIK3CA*, and *EGFR*, remove additional barriers to tumor cell proliferation and survival. Upregulation of pro-angiogenic genes permits the growth of tumors, and the loss of cell adhesion genes allows for the release of cells from the mucosal lining. Invasion through the basement membrane is promoted by TGFβ-SMAD signaling, the loss of which initially contributes to tumorigenesis, and whose later reactivation drives metastasis. Several genes and signaling pathways, including *TP53*, *TP63*, and *NOTCH1*, contribute to more than one hallmark by influencing each other's expression and/or activity. This figure is artwork by Matthew Hedberg as published in The Molecular Pathogenesis of Head and Neck Cancer in Mendelsohn J, Howley PM, Israel MA, Gray JW, and Thompson CB (Eds), The Molecular Basis of Cancer. Philadelphia, PA: Elsevier Inc.

1.1.3.1 Cell Cycle and Proliferation

The genetic pathology observed in HNSCC is characterized by a large degree of inter-tumor mutational heterogeneity and mutation rates that generally exceed 50 somatic mutations per tumor, on average, with loss of tumor suppressor gene functions and, somewhat less commonly, gain of proto-oncogene functions.(*10*, *39-41*) Foremost among these tumor suppressors is the *TP53* gene product: p53. A nuclear phosphoprotein that, among other mechanisms, promotes the expression of its key downstream partner: cyclin-dependent kinase inhibitor 1 (p21), p53 can influence both the G1 and G2 checkpoints of the cell cycle, though it is traditionally thought of as the primary G2 regulator. Canonically, in response to DNA damage, p53 activation inhibits cell cycle progression and prevents apoptosis, allowing the cell time to repair the damaged DNA. If the DNA damage cannot be repaired, apoptosis ensues. Loss of p53 function allows cells with damaged DNA to proliferate freely, resulting in the accumulation of potentially oncogenic mutations in the genome of affected cells.

In HPV(-)HNSCC, mutation of *TP53* is the earliest and most frequent mutation event that is observed. Occurring in greater than 50% of cases, *TP53* mutation is significantly associated with decreased survival.(*42*) The majority of *TP53* mutations are found in exons 5-9, the DNA binding region, with mutations at several specific codons known to be associated with tobacco exposure.(*43*) In most HNSCC tumors without somatic *TP53* mutations, the activity of p53 is compromised by other mechanisms including: viral E6 gene expression in HPV(+) cancers, which inactivates p53, and overexpression and/or amplification of the MDM2 proto-oncogene E3 ubiquitin ligase (*MDM2*), which promotes the degradation of p53. Overall, p53 function is believed to be downregulated through one or more mechanisms, in at least 80% of HNSCC.(*10*)

Chromosomal loss of 9p21, which contains the locus encoding the cyclin-dependent kinase inhibitor 2A (*CDKN2A*), has been reported in 70-80% of dysplastic oral mucosa legions progressing to HNSCC.(*10*) Two *CDKN2A* protein products, $p16^{INK4A}$ and $p14^{ARF/INK4B}$, are involved in cell cycle regulation. Specifically, $p14^{ARF/INK4B}$ is known to downregulate *MDM2*, thereby regulating p53 levels.(*44*) Whereas $p16^{INK4A}$ regulates the Retinoblastoma pathway, the primary G1 checkpoint regulator, by inhibiting the Cyclin D1/Cyclin-Dependent Kinase (*CCND1*/CDK) complex that normally functions to inactivate Retinoblastoma 1 (*RB*) encoded pocket proteins via phosphorylation. Phosphorylation of *RB* proteins permits the dissociation and activation of Elongation Factor-2 and subsequent entry into S phase. Inactive, phosphorylated *RB* pocket proteins are unable to block the G1 to S phase transition in the setting of $p16^{INK4A}$ loss.(*44*) In addition to chromosomal loss of 9p21, recent studies have demonstrated *CDKN2A* mutations in approximately 7% of HNSCC tumors and copy number losses in another 20-30%.(*39, 41*) The mechanism of $p16^{INK4A}$ loss has been shown to be of prognostic value in oral SCC; with epigenetic silencing found to be associated with higher recurrence rates, and deletion

with increased rates of nodal metastases.(*45*) Analogous to the inhibition of p53 by HPV E6 expression, viral E7 gene expression in HPV(+)HNSCC inactivates the retinoblastoma pathway by binding *RB* proteins. Inhibition of *RB* by E7 reduces the selective pressure for $p16^{INK4A}$ loss in HPV(+)HNSCC allowing immunohistochemical staining for $p16^{INK4A}$ to be utilized clinically as a surrogate marker for HPV infection in HNSCC, along with PCR based methods, and *in situ* hybridization.(*46*) Further evidence of the important role of the retinoblastoma pathway in HNSCC is that the commonly found amplification of 11q13, in combination with other potential mechanisms, results in the overexpression of *CCND1* in up to 80% of HPV(-) tumors.(*10*)

Intriguingly, *CDKN2A* loss and *CCND1* gain, though seemingly redundant mechanisms to evade the G1 checkpoint, are not mutually exclusive events in HNSCC. Both occur frequently, and remain under investigation as independent and synergistic markers of poor prognosis. (*47*) Cyclin D1 has been found to sequester certain *CDK* inhibitors, bind transcription factors such as PPARγ, and various DNA repair proteins such as Rad51.(*48*) Whether or not any of these interactions contributes to a consequential non-canonical *CCND1* function in HNSCC, remains to be established.

Telomerase reverse transcriptase (*TERT*) also promotes limitless replicative potential in HNSCC. The activity of telomerase is detectable by immunostaining in approximately 80% of HNSCC cases analyzed, and 5p amplifications, overlapping *TERT*, are common in HNSCC.(*40*) In most *in vitro* HNSCC models, Telomerase activity is generally necessary for immortalization of cell lines. However, keratinocytes transfected with E7 have been shown to elongate their telomeres in the absence of detectable telomerase expression, and the exact role of *TERT* in HNSCC is under investigation.(*10*)

1.1.3.2 Differentiation and Mesenchymal Transition

Many of the expression profile studies in HNSCC contain a large number of genes that are thought to reflect the process of epithelial-to-mesenchymal transition (EMT), especially profiles of metastatic HNSCC.(*49*) EMT is a biological process, wherein cells change from an epithelial phenotype to a mesenchymal-like phenotype. As epithelial cells do not possess the cellular plasticity for metastatic dissemination, this process is a common occurrence in cancer cells.(*10*) *TP63* codes for p63, a p53-related transcription factor that, via its target genes such as p57Kip2, regulates differentiation in stratified epithelium, lineage specification, and subsequently proliferative potential. Mice lacking *TP63* undergo total failure of epidermal maturation.(*32, 34*) In normally differentiated mature epithelium, *TP63* expression is present as a gradient; with the highest levels in the basal epithelial cells, where it serves to antagonize *NOTCH1* expression. Rising superficially through the strata, *TP63* levels decrease and *NOTCH1* levels increase driving terminal differentiation of the epithelial cell type (Figure 1). In dysplastic mucosa, this patterning is lost, and *TP63* expression is evident throughout all layers of the epithelium. Additionally, *TP63* overexpression and/or amplification is seen in the majority of HNSCC.(*35*) An isoform of *TP63*, ΔNp63, is known to contribute to cell survival by inhibiting senescence, and modulating growth factor signaling, and has be found to be upregulated in HNSCC.(*33, 41*)

NOTCH mutations are found by exome sequencing in up to 25% of HNSCC tumors, with *NOTCH1* being the most commonly mutated family member, 12-19%.(*39-41*) NOTCH signaling has been shown to influence cell survival, self-renewal capacity, and cell cycle exit; in addition to driving epithelial differentiation in concert with p63 and other signaling pathways. Ligands on adjacent cells bind to the NOTCH receptor, resulting in the cleavage of intracellular portions of

the receptor, that subsequently translocate to the nucleus, and drive the transcription of NOTCH target genes such as Cyclin D1 and p21.(*30*) Over activation of this pathway is believed to be tumorigenic in diffuse large B-cell lymphoma, T-cell acute lymphoblastic leukemia, and chronic lymphocytic leukemia. In those hematologic malignancies, translocations and activating mutations within NOTCH receptor genes have been observed.(*50-52*) In contrast, the *NOTCH* mutations observed in HNSCC appear to be predominantly inactivating mutations (truncation mutations, widespread distribution of SNVs across gene length, as opposed to hotspot enrichment); suggesting that it acts as a tumor suppressor in HNSCC, likely due to its role in driving epithelial differentiation.(*31, 39, 40*) The exact role of NOTCH signaling in HNSCC remains to be elucidated, and is likely tissue and/or context dependent; as has been observed in mouse models of epidermal and hematopoetic malignancies.(*53, 54*)

1.1.3.3 Invasion and Metastasis

HNSCC tumors metastasize primarily to the regional lymph nodes. The number of lymph node metastases in the neck, distant metastases, and the presence of extranodal spread are important prognostic factors predictive of disseminated disease and survival. While expression profile signatures of primary tumors that are predictive of metastasis have been identified, attempts to elucidate the mechanisms driving HNSCC metastasis are preliminary, and in some cases conflicting.(*10*) Metastasis is a multi-faceted process that ultimately results in a primary tumor “seeding” a distant anatomical site in the body. It involves several steps, one of which is invasion via the degradation of the extracellular matrix surrounding the primary tumor, in order to gain access to other areas of the body via the bloodstream or lymph system. Many studies have investigated the involvement of the matrix metalloproteinases (MMPs), which facilitate the degradation of the extracellular matrix. To date, strong associations have not been found, and

treatments targeting MMPs have not achieved appreciable success, in HNSCC, and first generation inhibitors generally have been plagued by a lack of specificity in most clinical trials.(*55, 56*)

In the context of invasion, the transforming growth factor β pathway (TGFβ), which normally functions to inhibit growth, has been implicated in HNSCC. TGFβ ligands bind to the receptors TGFBR1 and TGFBR2, resulting in phosphorylation of TGFBR1, which then activates the proteins SMAD2 and SMAD3. A SMAD complex is formed with the addition of SMAD4. This complex enters the nucleus and binds transcription factors, co-activators and co-repressors, which modulate the expression of TGFβ target genes, several of which are known to suppress cell proliferation, such as the cell cycle inhibitors *CDKN2A*. In addition, the TGFβ pathway has been implicated in the EMT process.(*57*)

18q deletion, containing *SMAD2*, *SMAD3*, *SMAD4*, and *TGFBR2* is common in HNSCC.(*10*) A recent mouse model found that conditional deletion of *SMAD4* in the head and neck epithelium was sufficient to generate invasive HNSCC. The loss of *SMAD4* expression in these animals correlated with increased expression of *TGFBR1* and increased activation of SMAD3, while the Fanconi Anemia DNA repair pathway was found to be downregulated.(*58*) Significant rates (~4%) of missense mutations in *TGFBR2* and rare mutations in *SMAD2* and *SMAD4* have been reported in HNSCC tumors and cell lines.(*39-41, 59, 60*) Recently, it has been demonstrated that reduced activity of the TGFβ pathway correlates with increased NF-κβ signaling in HNSCC. The TGFβ pathway has also been implicated in tumor suppression and although alterations in TGFβ and NF-κβ signaling have long been implicated in cancer, the exact mechanism(s) of their interaction, as well as their independent and/or cooperative contributions to invasion and metastasis in HNSCC are still being defined.(*61, 62*)

Tumors require blood vessels in order to grow to sizes larger than a few millimeters in diameter. These vessels facilitate nutrient and oxygen delivery, as well as metabolic byproduct disposal. The exploitation of neo-angiogenesis, usually by producing angiogenic factors, is common to all solid tumors. Of the many inducers of angiogenesis, the strongest is vascular endothelial growth factor (VEGF). Many studies have linked VEGF expression to HNSCC prognosis, including a meta-analysis which found a significantly increased risk of mortality, as well as an association between VEGF expression and metastasis to lymph nodes.(*10*) Although this data suggests a link between VEGF expression and outcome, as was also seen with respect to EGFR expression, HPV status remains the superior prognostic indicator.(*63*)

CSMD3, a putative adhesion factor, and *CSMD1*, a putative tumor suppressor, are altered in HNSCC by mutation, and by 8p deletion, which is common.(*39-41*) Loss of *CSMD1* is associated with high tumor grade and poor prognosis in other cancers, and the role of these two genes remains an area of active investigation in HNSCC.(*64*) Functional studies are required to determine if alterations in these genes may underlie a mechanism permitting the dissociation of cells from an otherwise cohesive sheet of cancerous epithelium, allowing for migration and metastasis of HNSCC tumors.

1.1.3.4 Apoptosis and Survival

Cell cycle alterations, reduced immunogenicity, promotion of angiogenesis, and inhibition of apoptosis are some of the many mechanisms underlying enhanced cancer cell survival in HNSCC. These cancerous traits are generated by genetic and epigenetic alterations in several pathways. Of particular importance in HNSCC, are the receptor tyrosine kinase (RTK) based signaling pathways. The class 1a phosphatidyl-inositol-3 kinases (PI3K) are heterodimeric kinases that are activated, directly or through adaptor molecules, downstream of RTKs, such as

EGFR. The PI3K signaling pathway mediates cellular metabolism, cell cycle progression, and apoptosis (Figure 4). Activated PI3K generates the lipid second-messenger phosphatidylinositol (3,4,5)-trisphosphate (PIP3). Which, together with phosphoinositide-dependent kinase-1 (PDPK1) and the MTORC2 complex, serves to activate protein kinase B (AKT). AKT is a serine/threonine kinase that, when activated, phosphorylates many downstream transcription factors, apoptotic proteins, cell cycle inhibitors, and other proteins; regulating their activity in a manner that ultimately promotes cell survival and proliferation. This pathway is held in check by the action of the tumor suppressor, phosphate and tensin homolog (PTEN), which dephosphorylates PIP3, thereby deactivating AKT. If PTEN activity is compromised, PI3K signaling can be constitutively activated by RTK stimulation.(*65*)

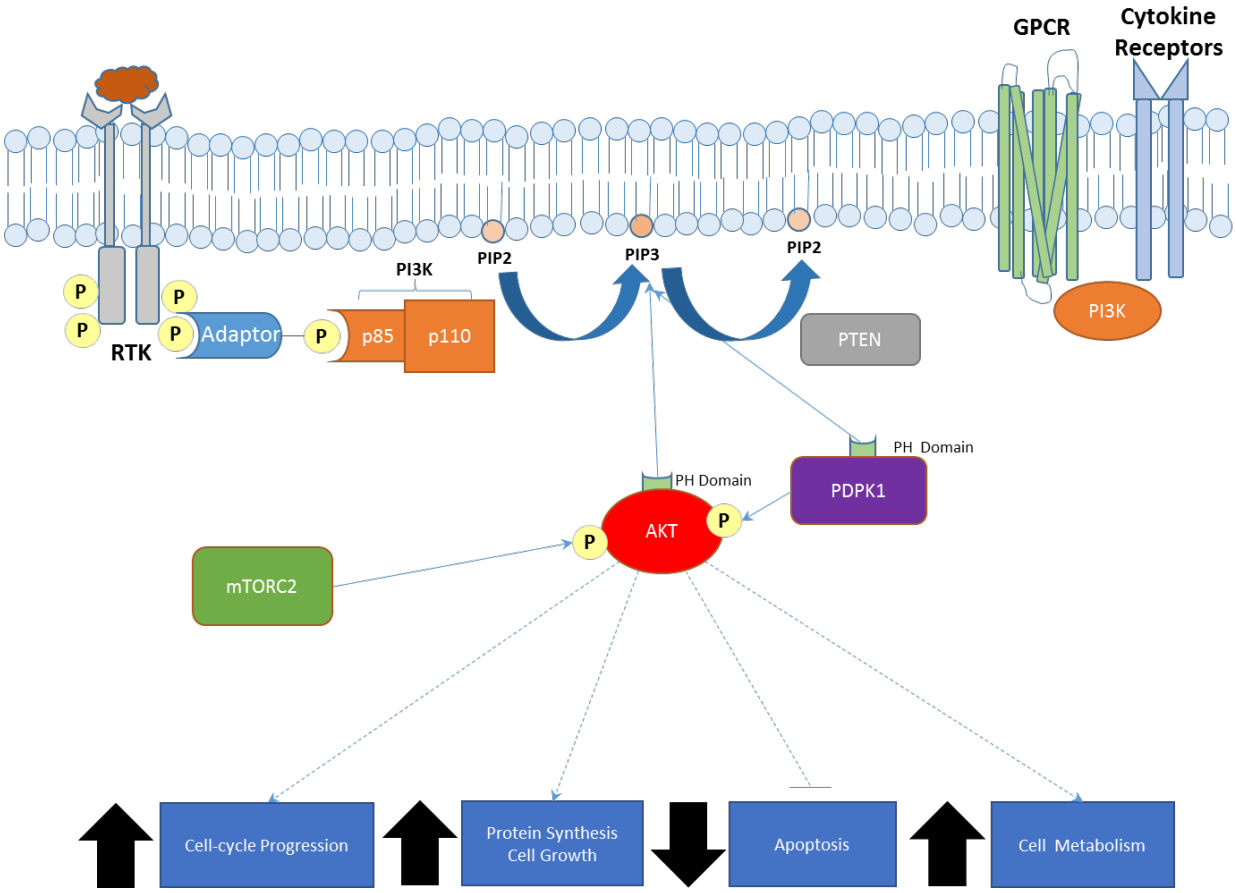

Figure 4. The PI3K Signaling Pathway

PI3K is activated by a variety of ligand-bound surface receptors, generally a receptor tyrosine kinase, and it phosphorylates phosphatidylinositol (4,5)-bisphosphate (PIP2) to PIP3. The reverse reaction is catalyzed by *PTEN*. PIP3 recruits several proteins to the plasma membrane by interacting with the pleckstrin homology (PH) domains of the recruited proteins. Two of the proteins recruited by this mechanism include the serine/threonine kinase PDPK1, and the primary signaling molecule downstream of PIP3, AKT. AKT is partially activated through phosphorylation by PDPK1, and fully activated through further phosphorylation by the mTORC2 complex. Fully activated AKT phosphorylates a wide range of substrates, with over 100 putative targets reported in the literature. When signaling through AKT is hyperactivated, via oncogenic mutations in *PIK3CA* or deletion of *PTEN*, the target proteins phosphorylated by AKT are either activated or inhibited in a manner that ultimately contributes to a series of cancer-associated phenotypes such as enhanced growth, enhanced protein synthesis, enhanced proliferation and survival through numerous mechanisms. HNSCC tumors with mutations in PIK3CA have elevated levels of phosphorylated AKT, suggesting that mutations in *PIK3CA* can indeed hyperactivate the signaling pathway in HNSCC patients.(*40*)

Inactivating *PTEN* mutations have been reported in about 3-10% of HNSCC, PTEN expression is undetectable in nearly 30% of tongue cancers, and loss of heterozygosity of the *PTEN* locus has been observed in up to 40% of HNSCC.(*66*) Furthermore, recent evidence suggests that loss of even a single *PTEN* allele can contribute to tumorigenesis.(*67*) Three different "hot-spot" activating mutations have been reported in *PI3KCA*, which codes for the catalytic subunit of the major PI3K isoform.(*68*) Notably, the frequency of *PI3KCA* mutations and amplification is higher in HPV(+)HNSCC, suggesting a possible interaction between the PI3K pathway and the E6/E7 proteins of HPV; which has been suggested to be contributory to the development of invasive SCC in cervical cancer.(*39, 41, 69*) The PI3K pathway is of consequence therapeutically, with numerous targeted inhibitors now in clinical trials.(*70, 71*)

RAS family GTPases (HRAS, KRAS, and NRAS) are molecular switches that cycle between 2 conformational states: an active GTP bound form, and an inactive GDP bound form.

The first RAS effector pathway to be identified was the RAS-RAF-MEK-MAPK pathway. The pathway is a common and essential element of mitogenic signaling driven by RTKs, resulting in a diverse array of cellular responses. RAF proteins are serine/threonine kinases that bind to the effector region of RAS-GTP. This interaction induces translocation of the protein to the plasma membrane. There, RAF proteins are activated and phosphorylated by different protein kinases. Active RAF phosphorylates MEK that, in turn, phosphorylates and activates MAPK. Activated MAPK serves as the terminal effector of the pathway, influencing cellular growth, differentiation, inflammation, apoptosis, and senescence. Mutated, constitutively active RAS genes are known to be oncogenic, and are found in approximately 25% of human tumors.(*72*)

Of the three prototypical RAS genes whose expression varies amongst tissue types, *HRAS* mutations are found in ~4% of HNSCC, and are more prevalent than *KRAS* or *NRAS* mutations.(*39-41*) These *HRAS* mutations are known to be associated with HNSCC in smokers, and in mouse models exposed to chemical carcinogens.(*73*) The exact contribution of *HRAS* mutations to oncogenesis remains under investigation in HNSCC, and there is evidence of both direct and indirect interaction between the RAS-MAPK and PI3K signaling pathways.(*72*) Additionally, *HRAS* mutations have been detected in HPV(+) tumors, allowing for the possibility of interaction with oncogenic viral proteins.(*39, 41*) Recent *in vitro* evidence suggests that even a single *HRAS* mutation, in the background of HPV and *MYC* alteration, can contribute to tumorigenesis.(*74*) Though the success of therapies targeting RAS proteins has been limited to date, several attempts to target their downstream effectors have shown promising results in preclinical models.(*75*)

RTKs lie upstream of both the RAS-MAPK and PI3K pathways. One of the most important and well-studied RTKs in HNSCC is *EGFR* (7p12), which codes for the prototypical

ErbB family Type I RTK. Signaling through EGFR influences a variety of cellular processes, including survival and differentiation. EGFR has an extracellular ligand-binding domain, a transmembrane portion, and an intracellular kinase domain with five autophosphorylation sites. Ligand binding by EGFR monomers drives homodimerization or heterodimerization with another RTK, resulting in the initiation of downstream survival and proliferation signaling pathways, such as the RAS-MAPK and PI3K pathways. These two independent cascades converge via the ultimate upregulation of Cyclin D1. Furthermore, when bound to EGF, EGFR itself can translocate to the nucleus where it acts as a transcription factor for several genes including *CCND1*, and as a co-activator for other transcription factor proteins, such as the Signal Transducer and Activator of Transcription (STAT) proteins.(*10*)

EGFR is expressed in most epithelial tissues, and its dysregulation has been repeatedly shown to contribute to epithelial oncogenesis. In HNSCC, EGFR expression levels are nearly ubiquitously elevated in tumor and tumor-adjacent tissue compared to corresponding normal mucosa. Higher EGFR expression levels and copy number gain correlate with decreased survival, and have not been predictive of improved response to EGFR directed therapy. In HNSCC, there are three agents in common clinical use known to inhibit EGFR; gefitinib and erlotinib, both TKIs, and cetuximab, a monoclonal antibody against EGFR, which is the only targeted agent that is FDA-approved for use in HNSCC. These agents have shown modest efficacy as monotherapies to date, showing activity in about 20% of patients in large multicenter trials, generally in combination with radiation and/or chemotherapy.(*76*) Expression of EGFRvIII, an *EGFR* allele harboring a large in-frame deletion of exons 2-7, can confer resistance to anti-EGFR therapy. The prevalence of the EGFRvIII variant remains controversial in HNSCC, with various studies reporting its expression to be present in anywhere from 0-42%

of the tumors assayed.(*77-80*) Investigations into EGFRvIII mechanism(s) of oncogenesis continue, as therapies specifically directed against EGFRvIII have shown promise in glioblastoma, and may be applicable in refractory HNSCC.(*80*) Another genetic alteration, reported in some cases of HNSCC, that is believed to contribute to anti-EGFR therapy resistance, is mutation or amplification of the *MET* gene, which codes for another RTK.(*81, 82*) *MET* has been implicated as a cancer gene in HNSCC, that influences cell growth, motility, and angiogenesis.(*10*) This too, may be of particular clinical consequence, as there are both monoclonal antibodies and small molecule inhibitors that are FDA-approved in other cancers, with the ability to inhibit MET kinase activity.(*83, 84*)

In addition to the growth factor signaling pathways that indirectly influence apoptosis, recent studies in HNSCC have found alterations directly within apoptotic proteins. *CASP8*, a proteolyase responsible for initiating the caspase cascade that drives apoptosis, was found to be mutated in 5-8% of HNSCC by exome sequencing; and *BCL2*, which prevents apoptosis, has been observed to be overexpressed in some HNSCC cell lines, usually coincident with the reduced expression of p63.(*33, 40, 41*)

1.2 SUMMARY AND RATIONALE

HNSCC is a malignancy of the upper aerodigestive tract mucosa. Most patients present with advanced disease and are treated with multimodal therapy, in a manner dependent upon a variety of parameters specific to the clinical presentation such as stage, anatomic location, and the presence or absence of significant co-morbidities. HNSCC treatments are morbid, therapeutic options are limited for patients who relapse, and cures are only achieved in approximately 50%

of patients.(*18*) An improved understanding of the genetic alterations underlying the pathophysiology of HNSCC tumors is needed in order to establish predictive biomarkers to guide therapy, and facilitate the development of new treatments.

As such, we and others, notably Agrawal *et al.*, Stransky *et al.*, and The Cancer Genome Atlas (TCGA) project performed a series of large-scale genomic profiling studies that have begun to shed light on the molecular diversity of HNSCCs, and provide data to the field for the generation of new hypotheses.(*39-41, 85*)

As they were originally proposed, my thesis goals only included the study of primary HNSCC. Our analysis of the mutational profiles of 151 HNSCC tumors via whole exome sequencing (WES) identified the Phosphoinositol-3-Kinase (PI3K) pathway as the most commonly mutated mitogenic pathway in HNSCC. We proposed the following specific aims:

Specific Aim 1: Determine the genetic alterations of *PIK3CA*, found in HNSCC, that mediate cancerous phenotypes and PI3K pathway inhibitor sensitivity in HNSCC preclinical models in vitro.

To identify *PIK3CA* alterations that contribute to cancerous phenotypes in HNSCC, we engineered HNSCC cell lines, with unaltered *PIK3CA*, to express mutant *PIK3CA* or over express WT *PIK3CA* (to mimic amplification) and used proliferation assays and matrigel invasion assays to identify "driver" *PIK3CA* events. Cell lines with and without *PIK3CA* alterations (endogenous and engineered) were treated with PI3K inhibitors to assess sensitivity. The results of these experiments are reported in Chapter 2. We intended to use reverse phase protein arrays (RPPA), to define signaling pathway phenotypes generated by each driver mutation, and to identify signaling pathways affected by PI3K inhibitors in HNSCC cells. This may have elucidated how *PIK3CA* driver mutations effect cancerous phenotypes and aberrant

cell signaling in HNSCC, and evaluate the efficacy and mechanism of PI3K inhibitors in these cells. The RPPA analysis has not yet been performed in cell lines. While cellular phenotypes such as survival and invasion were reproducible, limitations of the retroviral infection system hindered our ability to appreciate reproducible signaling pathway alterations. We therefore propose to perform RPPA analyses in future studies using CRISPR/Cas9 techniques to generate *PIK3CA* altered HNSCC models which will hopefully yield more reproducible phenotypes at the level of cellular signaling as the engineered alterations will be under the control of endogenous expression mechanisms at the natural loci, as opposed to viral promoters integrated randomly across the genome.

Specific Aim 2: Elucidate the *in vivo* sensitivity of patient-derived HNSCC tumors to small molecule inhibitors targeting the PI3K pathway.

We hypothesized that PI3K alterations will enhance sensitivity to treatment with PI3K inhibitors. We treated mice with heterotopic tumorgrafts, implanted directly from surgically-resected patient tumors, with and without *PIK3CA* mutations with the PI3K inhibitor BYL-719 and compared the treatment sensitivities of these models and performed RPPA analysis to provide *in vivo* mechanistic insight into the predictive value of PI3K pathway status in HNSCC. Results to date from these experiments are reported in Chapter 2.

Specific Aim 3: Define the spectrum of *PIK3CA* mutations in a prospective HPV(+)HNSCC cohort.

HPV(+)HNSCC is of great interest on account of its increasing incidence and seemingly unique biology as outlined earlier in the introduction. HPV(+) tumors had been underrepresented in WES studies at the time of my original proposal. Prior to the completion of this aim however, a sequencing study focusing on HPV(+)HNSCC was completed by Seiwert *et al*, which limited

the contribution our efforts would have made to the field.(*86*) Accordingly, we modified this aim, and chose to invest our resources in an alternative sequencing project that aimed to determine if there was a therapeutic benefit of NSAID treatment in *PIK3CA* mutated and/or amplified HNSCC. Such a benefit has recently been reported in the setting of colorectal cancer, and would present an immediately actionable therapeutic option for patients if the same benefits were observed in HNSCC.(*87*) While data collection for this aim has been completed, the analysis is ongoing and is not presented in this dissertation.

Chapter 3 of this dissertation presents an additional project in which we used WES to study the genetics of HNSCC metastasis and recurrence using patient-matched tumor pairs. This project was not formally a part of my original thesis proposal, but represents a large share of the work that I ultimately performed during my time as a graduate student, and is a significant contribution to the field which has been accepted for publication at the *Journal of Clinical Investigation.*

2.0 GENETIC ALTERATIONS IN PRIMARY HNSCC: THE PI3K PATHWAY

2.1 INTRODUCTION

HNSCC is a frequently lethal cancer with few effective therapeutic options. In an effort to elucidate the genetic underpinnings of this disease and identify new therapeutic targets, Agrawal *et al.,* and Stransky *et al.,* performed WES on 32 and 74 HNSCC tumor-normal pairs, respectively.(*39, 41*) These studies were published simultaneously in *Science* in 2011, and revealed a spectrum of genetic aberrations that varied widely within and between tumors. This pronounced mutational heterogeneity, coupled with the relatively small cohort sizes, limited the contributions these reports were able to make with respect to guiding and improving therapy for HNSCC patients.

TP53 mutation is the only single-gene mutational event identified in an outright majority of HNSCC, and the loss of function of this tumor suppressor gene has remained challenging to exploit therapeutically. Mitogenic pathways are crucial for cancer development and progression. Gain of function mutations in mitogenic pathway genes have been shown to result in pathway activation, enhanced tumor growth, and increased sensitivity to agents targeting the mutated pathway. However, the potential of genomics-based therapy selection has not been widely investigated in HNSCC.

In an effort to identify mutationally-altered, targetable mitogenic pathways in HNSCC, we analyzed the WES results of an additional 45 HNSCC tumor-normal pairs from patients treated at the University of Pittsburgh, sequenced on the Illumina platform, under the auspices of the TCGA project. Combined with the previously published results, this cohort of 151 HNSCC mutation profiles allowed us to evaluate the mutations found in the genes composing three major mitogenic pathways that have been previously implicated in HNSCC pathophysiology; the mitogen-activated protein kinase (MAPK), Janus kinase/signal transducer and activator of transcription (JAK/STAT), and phosphoinositide-3-kinase (PI3K) pathways.(*39-41, 85, 88, 89*) These key mitogenic pathways are targetable in human cancers with a variety of agents currently in various stages of clinical and preclinical development.

2.2 MATERIALS AND METHODS

2.2.1 Cells and Reagents

HNSCC cell lines were genotypically verified and grown in a humidified cell incubator at 37°C and 5% CO_2. UMSCC47, CAL-33, FaDu, Detroit 562, UPCI 090, and UPCI-52 (SD-1) cells were maintained in DMEM containing 10% FBS and 1× penicillin/streptomycin solution (Invitrogen) whereas PE/CA-PJ34 cells were maintained in IDMEM containing 10% FBS, 2 mM L-glutamine, and 1× penicillin/streptomycin solution. HSC2 and JHU 022 cells were maintained in 1640 RPMI containing 10% FBS, 2 mM L-glutamine, and 1× penicillin/streptomycin solution. PLAT-A cells were maintained in DMEM, 10% fetal calf serum (FCS), 1 μg/mL puromycin, 10 μg/mL blasticidin, penicillin and streptomycin. FaDu, Detroit 562 cell lines were obtained from

ATCC whereas PE/CA-PJ34 cells were obtained from Sigma-Aldrich. CAL-33 cells were obtained from Gerard Milano (Centre Antoine Lacassagne, Nice, France). HSC2 and JHU 022 cells were obtained from Jian Yu (University of Pittsburgh Cancer Institute) UMSCC47 cells were obtained from Dan Johnson (University of Pittsburgh Cancer Institute) UPCI 090 cells were obtained from Robert Ferris (University of Pittsburgh Cancer Institute) PLAT-A cells were purchased from Cell Biolabs. The UPCI-52 (SD-1) cell line was obtained by clonal selection of the parental UPCI-52 cell line (University of Pittsburgh Cancer Institute) by rounds of graded serum selection. In brief, PCI-52 parental cell lines were plated as single cells, which grew as single clones. These single clones were subjected to serum deprivation (0% FBS) for 1–2 wk, followed by assessment of cell growth by 3-[4,5-dimethylthiazol-2-yl]-2,5 diphenyl tetrazolium bromide (MTT) assay. The PCI-52-SD1 subline was the most serum-sensitive subline, which died (>99.8%) upon complete serum deprivation.

2.2.2 Mutation Databases, Comparison, and Co-mutation Analysis

HNSCC mutation analyses were based on the published WES data from 32 and 74 tumors and the TCGA WES data on 45 tumors accessed through the cBio Portal.(*39, 41, 90*) Data was aggregated into Microsoft Excel where a match macros allowing for side-by-side comparison between multiple groups (2 or more) to identify and quantify common mutational events amongst the groups was used to compare the reported HNSCC mutations to reference lists generated for each mitogenic pathway of interest. A cancer gene list was generated in each subgroup of tumors by comparing the Cancer Gene Census list (COSMIC Database) with non-synonymous mutation gene lists of each tumor subgroup (the PI3K-mutated tumors, tumors without PI3K-mutation, etc.) using this comparison program.

2.2.3 Clinical Data

De-identified data was available to HIPPA-trained, IRB-approved researchers for the tumors from the University of Pittsburgh through the Head and Neck SPORE and Organ Specific Database.

2.2.4 Mutation Modeling

The PyMol Molecular Graphics System and Evolutionary Action Scoring Algorithm were used in collaboration with Drs. Van Houten, Kastonis, and Lichtarge to model select mutations as described in results.(*91*, *92*)

2.2.5 Cloning and Mutagenesis

WT Human *PIK3CA* was cloned into the retroviral vector, pMXs-puro (Cell Biolabs, Inc., San Diego, CA). The pMXs-puro-*PIK3CA* vector was used as a template for site directed mutagenesis using the QuikChange XL Site-Directed Mutagenesis Kit (Stratagene, La Jolla, CA). Mutagenesis of the *PIK3CA* WT gene was performed according to the manufacturer's instructions. Each mutant was generated and confirmed by sanger sequencing with the primers outlined below.

Table 1. *PIK3CA* Mutation Primers

	AA Change	Codon Change	Forward Mutation Primer	Reverse Mutation Primer
PIK3CA	WT	N/A	N/A	N/A
	p.R38H	c.(112-114)CGT>CAT	5'-gtgactttagaatgcctccatgaggctacattaataacc-3'	5'-ggttattaatgtagcctcatggaggcattctaaagtcac-3'
	p.R88Q	c.(262-264)CGA>CAA	5'-agaatttttgatgaaacaagacaactttgtgaccttcggctttttc-3'	5'-gaaaaagccgaaggtcacaaagttgtcttgtttcatcaaaaaattct-3'
	p.E110del	c.(325-327)GAAdel	5'-aaccagtaggcaaccgtgaaaagatcctcaatcga-3'	5'-tcgattgaggatctttcacggttgcctactggtt-3'
	p.R115L	c.(343-345)CGA>CTA	5'-cgtgaagaaaagatcctcaatctagaaattggttttgctatcg-3'	5'-cgatagcaaaaccaatttctagattgaggatctttcttcacg-3'
	p.G118D	c.(352-354)GGT>GAT	5'-tcctcaatcgagaaattgattttgctatcggcatgcc-3'	5'-ggcatgccgatagcaaaatcaatttctcgattgagga-3'
	p.G363A	c.(1087-1089)GGA>GCA	5'-aacaggtatctaccatgcaggagaacccttatgtg-3'	5'-cacataagggttctcctgcatggtagatacctgtt-3'
	p.E542K	c.(1624-1626)GAA>AAA	5'-cacgagatcctctctctaaaatcactgagcaggag-3'	5'-ctcctgctcagtgattttagagagaggatctcgtg-3'
	p.E545K	c.(1633-1635)GAG>AAG	5'-gagatcctctctctgaaatcactaagcaggagaaaga-3'	5'-tctttctcctgcttagtgatttcagagagaggatctc-3'
	p.C971R	c.(2911-2913)TGC>CGC	5'-gattagtaaaggagcccaagaacgcacaaagacaagagaattt-3'	5'-aaattctcttgtctttgtgcgttcttgggctcctttactaatc-3'
	p.R975S	c.(2923-2925)AGA>AGT	5'-caagaatgcacaaagacaagtgaatttgagaggtttcagga-3'	5'-tcctgaaacctctcaaattcacttgtctttgtgcattcttg-3'
	p.H1047R	c.(3139-3141)CAT>CGT	5'-aacaaatgaatgatgcacgtcatggtggctggacaac-3'	5'-gttgtccagccaccatgacgtgcatcattcatttgtt-3'

Table 2. *PIK3CA* Sequencing Primers

Primers for Plasmid Fragment Sequencing	(Forward Primers Only)
Primer Name	Primer Sequence (5'-3')
pMXs-Puro-PIK3CA-WT seq 1	tggtacctcacccttaccga
pMXs-Puro-PIK3CA-WT seq 2	cccccaagaatcctagtaga
pMXs-Puro-PIK3CA-WT seq 3	ggcatgccagtgtgtgaat
pMXs-Puro-PIK3CA-WT seq 4	gtgtgtggatgtgatgaatacttcc
pMXs-Puro-PIK3CA-WT seq 5	ttcctgatcttcctcgtgct
pMXs-Puro-PIK3CA-WT seq 6	ccacgcaggactgagtaaca
pMXs-Puro-PIK3CA-WT seq 7	ggttcgaggttttgctgttc
pMXs-Puro-PIK3CA-WT seq 8	agttgagcaaatgaggcgac
pMXs-Puro-PIK3CA-WT seq 9	gtcaatcggtgactgtgtgg
pMXs-Puro-PIK3CA-WT seq 10	cgagaacgtgtgccat

2.2.6 Retroviral Infection

Retroviruses were generated using the Platinum-A Retroviral Packaging Cell Line System (Cell Biolabs, San Diego, CA) according to manufacturer's instructions. Briefly, $2x10^6$ PLAT-A cells were plated overnight in 10cm tissue culture dishes without antibiotics and transfected the next day with 3 µg of retroviral vector carrying the gene of interest (pMXs-puro-*EGFP* as control, pMXs-puro-*PIK3CA* WT, pMXs-puro-*PIK3CA* mutants) using the Fugene HD kit (Promega)

according to manufacturer's instructions. Two days after transfection, fresh retroviruses (in the supernatant of the PLAT-A cells) were collected by filtering through a 0.45 µm syringe filter. Fresh retroviruses were used for infection of HNSCC cells. HNSCC cells were plated to 20% confluence in a T25/T75 flask without antibiotics one day before infection. Infection of HNSCC cells was performed by adding 1.5/4.5ml of retrovirus to the cells mixed with 2.5/5.5ml of complete culture media without antibiotics. Then, 18-20 µl of polybrene (4 µg/µl, Sigma-Aldrich, St. Louis, MO) was added to the cells with gentle mixing. Cells were then incubated at 37°C and 5% CO_2 for additional 72 hrs, and the infection medium was replaced with fresh complete medium after infection. In the case of the UPCI-52(SD-1) cells engineered to express *PIK3CA* constructs, two weeks of selection with 01.ug/ml puromycin media was performed as these cells were expanded for functional experiments which were performed using pooled puromycin resistant colonies.

2.2.7 Western/Immuno Blotting

Lysates were collected as described and resolved on sodium dodecyl sulfate polyacrylamide gel electrophoresis (SDS-PAGE) gels and transferred to nitrocellulose membranes prior to antibody staining. Primary antibodies for p110α, p-AKT(T308), p-AKT(Ser473), and AKT were purchased from Cell Signaling Technology, Inc. (Boston, MA). Anti-tubulin antibody was from Abcam (Cambridge, MA). Secondary antibodies were from BioRad (Hercules, CA). Densitometry was performed using ImageJ.

2.2.8 RT-PCR and Sanger Sequencing

RNA was extracted from 1 to 2 million HNSCC cells engineered to express retroviral vectors using the RNeasy Mini Kit (Qiagen) according to the manufacturer's instructions. Isolated RNA was treated with DNase I, Amplification Grade (Invitrogen) according to the manufacturer's instructions and used as template for RT-PCR using the SuperScript® III One-Step RT-PCR System with Platinum® Taq DNA Polymerase (Life Technologies) according to the manufacturer's instructions. Thermocycler settings: 1 cycle--[55C for 30 min, 94C for 2min], 40 cycles—[94C for 30 sec, Anneal 55C for 30 sec, Extend 68C for 30 sec], 1 cycle—[68C for 5min, 4C hold]. The resulting cDNA was purified on a 1.0% agarose gel, extracted using the QIAquick Gel Extraction Kit (Qiagen) according to manufacturer's instructions and assessed by Sanger sequencing. Results viewed with Applied Biosystems Sequence Scanner v1.0. Primers used for RT-PCR and sequencing below.

Table 3. Primers for RT-PCR and Sequencing

RT-PCR Primer	Sequence
Non-hotspot sense	5'- ATGCCTCCAAGACCATCATC-3'
Non-hotspot anti-sense	5'- CCCTAAGATCCACAGCTTCTTT-3'
Helical hotspot sense	5'- AATTGGTCTGTATCCCGAGAAG -3'
Helical hotspot anti-sense	5'-CATAGCCTGTTCAGGTTTGATTG-3'
Kinase hotspot sense	5'-TCGACAGCATGCCAATCTC-3'
Kinase hotspot anti-sense	5'-TTGTGTGGAAGATCCAATCCAT-3'
Sequencing Primer	**Sequence**
Non-hotspot forward	5'-CCCCCAAGAATCCTAGTAGA-3'
Helical hotspot forward	5'-AGTAACAGACTAGCTAGAGA-3'
Kinase hotspot forward	5'-GACCCTAGCCTTAGATAAAAC3'

2.2.9 *In vitro* Drug Treatments

HNSCC cells were plated at the densities indicated in the figure legends in 48 well culture plates overnight and treated with various concentrations of BKM-120 or BYL-719 (Novartis, USA) dissolved in DMSO for the amount of time indicated in the figure legends, and assessed by proliferation assays or immunoblot assays as indicated in the figure legends.

2.2.10 Proliferation Assays

HNSCC cells were plated at the densities indicated in the figure legends in 48 well culture plates overnight and subjected to the treatments indicated in the figure legends, at which point, MTT or MTS (Sigma-Aldrich) was performed as indicated according to manufacturer's instructions. For MTT, following a 30 min incubation at 37°C and 5% CO_2 DMSO solubilized extracts were measured at 570nm, for MTS, following a 2 hour incubation at 37°C and 5% CO_2 aqueous solutions were measured at 590nm, in a uQuant spectrophotometer, to determine formazan production in subject versus control cells. Each subject or control reaction was run in replicates, and repeated as indicated in figure legends. Average proliferation values as bar graphs and growth curves were generated using GraphPad Prism 6 software as outlined in the legends.

2.2.11 Invasion Assays

Invasion of HNSCC cells in the presence or absence of *PIK3CA* mutant expression was tested using Biocoat migration and Matrigel® coated invasion Chambers (BD Biosciences), according to the manufacturer's instructions. Briefly, 3.0×10^4 UPCI-52 (SD-1) cells suspended in DMEM

stably expressing *EGFP*, WT or mutant *PIK3CA* constructs were plated inside migration (uncoated) chambers or invasion (matrigel coated) chambers submerged in 10% FBS media for 24 hrs. Cells were counted and averaged from 4 photomicrographs (20x objective) of each membrane, and the invasion/migration ratios were calculated. Bar graphs and statistical analysis generated in GraphPad Prism 6 as outlined in the figure legend.

2.2.12 Patient Derived HNSCC Xenograft Models and Drug Treatment

Following HNSCC tumor resection, tissues are collected under the auspices of an IRB-approved tissue bank protocol. Patient samples are quality controlled by UPMC surgical pathologists for a composition of at least 70% tumor, de-identified and delivered to the lab in antibiotic/antimycotic solution. Clinical correlates such as p16 status are noted and any excess material is stored for molecular analyses such as DNA sequencing. Approximately 25mg pieces of tumor are implanted into the flanks of NOD SCIDγ mice to establish PDXs. For treatment experiments the four indicated PDXs were selected, expanded, treated and assessed as indicated in the legend of Figure 17. BYL-719 (Novartis, USA.) was administered as a suspension in 1% (w/v) carboxymethylcellulose (CMC) + 0.5% (w/v) Tween 80. Solvent sans drug used as vehicle control.

2.2.13 Proteomic Profiling by Reverse Phase Protein Array (RPPA)

Quantitative proteomic analysis (reverse phase protein array) was performed in collaboration with Dr. Gordon B Mills in the RPPA Core Facility at the MD Anderson Cancer Center. The

platform techniques have been published.(*93*) An up-to-date listing of their evolving protocols and services is available (http://www.mdanderson.org/education-and-research/resources-for-professionals/scientific-resources/core-facilities-and-services/functional-proteomics-rppa-core/index.html) I collected and prepared BYL-719 and vehicle treated PDX samples for analysis by RPPA, lysing them according to the recommended protocol (see website). The results they deliver include normalized linear expression values for each antibody/sample analyzed. I plotted these values in GraphPad Prism 6 to interrogate the effects of BYL-719 treatment on PI3K signaling and AXL expression as described in the legends of Figure 18 and Figure 19.

2.3 RESULTS

2.3.1 The PI3K Pathway is the Most Commonly Mutated Mitogenic Pathway in HNSCC

We compiled the WES results of 106 HNSCC tumors published by Agrawal *et al.* and Stranksy *et al.*, along with the WES results of an additional 45 HNSCC tumors collected at the University of Pittsburgh and sequenced as a part of the TCGA HNSCC project (Table S1 in Lui, Hedberg, Li, *et al.* 2013).(*39, 41, 85*) With the aim of identifying mutationally-altered, targetable mitogenic pathways in HNSCC, we assessed the JAK/STAT, MAPK and PI3K pathways. Pathway component genes were defined as follows: JAK/STAT pathway (*JAK1*, *JAK2*, *JAK3*, *STAT1*, *STAT2*, *STAT3*, *STAT4*, *STAT5A*, *STAT5B*, *STAT6*, *SOCS3*, *SHP2*, *IL6ST*, *IL6R and IL6*), MAPK pathway (*ERK1*, *ERK2*, *MEK1*, *MEK2*, *RAF1*, *ARAF*, *BRAF*, *HRAS*, *KRAS*, *NRAS*, *SHC1*, *SHC2*, *SHC3*, and *GRB2*) and PI3K pathway (*PIK3CA*, *PIK3AP1*, *PIK3C2A*, *PIK3C2B*,

PIK3C2G, PIK3CB, PIK3CD, PIK3CG, PIK3IP1, PIK3R1/2/3/4/5/6, AKT1/2/3, MTOR, PTEN, PDK1, TSC1/2, RICTOR and RPTOR).

Strikingly, almost one third of all HNSCC tumors analyzed in our combined cohort (30.5%; 46/151 tumors) harbored PI3K-pathway mutations, while only 9.3% (14/151) and 8.0% (12/151) of tumors harbored mutations in the JAK/STAT or MAPK pathways, respectively (Figure 5A).(*85*) These results demonstrate that despite the mutational heterogeneity of HNSCC, the components of the PI3K pathway are mutated in >30% of tumors; identifying this pathway as a potential therapeutic target in a substantial subset of patients. Similar analyses of these pathways in WES data of other cancer types is reported in the supplemental data of our published paper.(*85*)

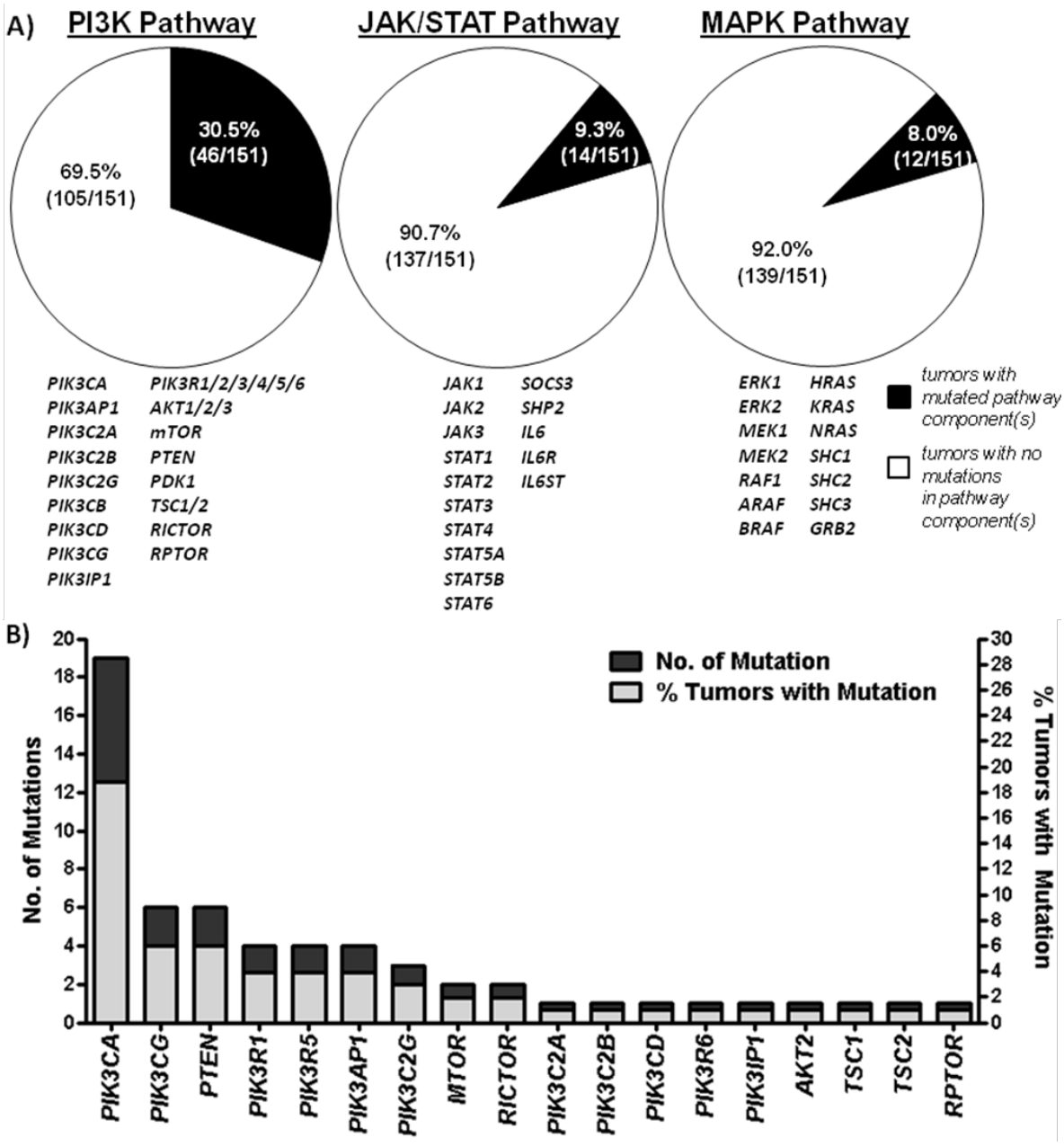

Figure 5. Mutations in Mitogenic Signaling Pathways in HNSCC.

(A) Mutation rates of the major mitogenic pathways (the PI3K pathway, the MAPK pathway and the JAK/STAT pathway) in 151 HNSCC patient tumors determined by whole exome sequencing. Components of each pathway examined are displayed underneath each pie chart. **(B)** Bar graph detailing the number of mutations (dark bars) of each particular component of the PI3K pathway as well as the number of HNSCC tumors harboring these mutations (grey bars). This figure is adapted from Lui, Hedberg, Li *et al* 2013. Sequencing data was obtained and analyzed as

outlined in the methods. I performed the data analysis and interpretation for this portion of the paper, and generated this figure.

A detailed analysis of the mutations identified in the PI3K pathway revealed that 19 of the 151 tumors (12.6%) harbor a *PIK3CA* mutation, making it the most commonly mutated oncogene in our cohort (Figure 5). This mutation rate is higher, but similar, to rates reported previously by Kozaki *et al.* (7.4%) and Cohen *et al.* (10.8%), in targeted *PIK3CA* sequencing studies of HNSCC tumors.(*94, 95*) *PIK3CG* and *PTEN* were mutated in 4.0% (6/151) of HNSCC tumors; while *PIK3R1, PIK3R5* and *PIK3AP1* were mutated in 2.7% of tumors (4/151) (Figure 5B). Other components of the PI3K pathway were mutated in <2% cases (Figure 5). Major downstream effectors of the PI3K pathway, including *PDK1, AKT1* were not mutated, while *AKT2* and *MTOR* were only mutated in 1.3% (2 mutations) of HNSCC tumors (Figure 5).

Copy number variation (CNV) was analyzed in the 45 newly added tumors from the University of Pittsburgh using the Affymetrix Genome-Wide Human SNP Array 6.0 platform.(*40, 85*) In addition to commonly being mutated in our cohort, *PIK3CA* was amplified in 24.4% (11/45) of the newly added HNSCC tumors from the University of Pittsburgh. Loss of *PTEN* (≥1 allele) was identified in 8.16% of cases (4/45) in our cohort. Compared to other cancers such as glioblastoma, where *PTEN* loss can be found in up to 60% of tumors, this suggests that *PTEN* loss is not the primary mediator of PI3K pathway alteration in HNSCC.(*96, 97*)

2.3.2 Unique Features of PI3K Pathway-Mutated HNSCC Tumors

In the combined cohort of 151 HNSCC tumors we assessed, those with PI3K pathway mutations had a significantly higher mutational burden than tumors without mutations in the PI3K pathway (165.5 ± 24.1 vs 72.1 ± 6.6 mutations per tumor, $p < 0.0001$, Figure 6A). HNSCC tumors in our cohort harboring PI3K pathway mutations also harbored twice as many mutations in known cancer genes (as defined by the Cancer Gene Census, COSMIC Database) compared to those without PI3K pathway mutations (7.2 ± 0.8 vs 3.6 ± 0.3, $p < 0.0001$, Figure 6B).(*98*) Further, DNA damage/repair pathway genes, as defined by Cerami *et al.* 2012 (*ATM*, *ATR*, *CHEK1/2*, *BRCA1/2*, *FANCF*, *MLH1*, *MSH2*, *MDC1*, *PARP1* and *RAD51*), were found to be mutated at a significantly higher frequency in tumors with PI3K pathway mutations, than in those without PI3K pathway mutations (37.0%; 17 mutations in 46 tumors vs. 15.2%; 16 mutations in 105 tumors, $p = 0.0049$, Fischer's Exact Test).(*99*) Taken together, these data suggest that PI3K pathway mutations facilitate the expansion or selection of tumor cells with high levels of genomic instability that harbor more genomic aberrations, including aberrations in known cancer genes.

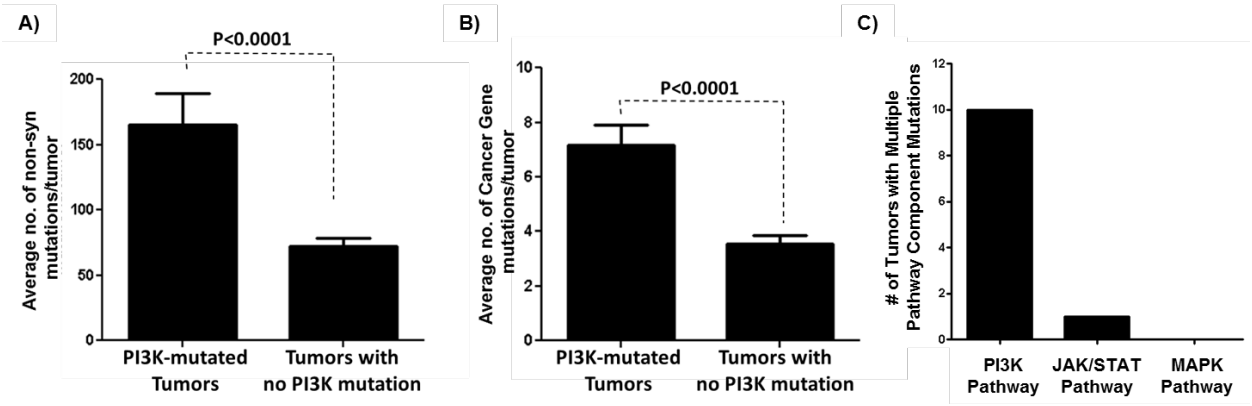

Figure 6. Co-mutational Analyses in HNSCC

(A) PI3K pathway-mutated HNSCC tumors have higher rate of non-synonymous mutations compared to HNSCC tumors without any PI3K pathway mutations. **(B)** PI3K pathway-mutated HNSCC tumors also have higher rates of non-synonymous mutations in known cancer genes when compared to HNSCC tumors without any PI3K pathway mutations. Significance calculated by Fisher's Exact Test, N=151. **(C)** Graphical representation of the number of HNSCC tumors with mutation of multiple components of the PI3K, JAK/STAT, and MAPK pathways. This figure is adapted from Lui, Hedberg, Li *et al* 2013. Sequencing data was obtained and analyzed as outlined in the methods. I performed the data analysis and interpretation for this portion of the paper, and generated this figure.

Among HNSCC tumors with PI3K pathway mutations, 21.7% (10/46), harbored mutations in more than one PI3K pathway gene, and all 10 of these tumors were advanced (Stage IV) malignancies (Figure 6C and Table 4). In contrast, HNSCC tumors rarely, if ever, harbored multiple mutations in the MAPK pathway (0 tumors), or the JAK/STAT pathway (1 tumor, *JAK3* and *STAT1* mutations; HN_63080) (Figure 6C and Table 4). This demonstrates that genetic alterations at multiple levels in the PI3K pathway are comparatively common in HNSCC, and suggests that concerted PI3K pathway aberrations may contribute to HNSCC progression. Although the association between advanced disease stage and PI3K pathway mutations was not

found to be statistically significant in this HNSCC cohort, published WES datasets in other cancers including breast, colon and lung SCC, demonstrate that only 1/25 breast tumors, 1/27 colon carcinomas, and 0/31 lung SCCs harboring multiple PI3K pathway mutations, were stage IV cancers.(*99*) This suggests that concurrent mutation of multiple PI3K pathway components may be more contributory to disease progression in HNSCC than other cancers. In the absence of models assessing the specific impact of mutation in multiple pathway components to cellular phenotypes however, it is not possible to determine the precise effect of individual or combined mutations within the PI3K pathway in HNSCC tumors.

Table 4. Characteristics of HNSCC Tumors with Multiple Pathway-Gene Mutations

Pathway	Tumor	Annotated Genes	Amino Acid Change	TNM Stage/Overall Staging
PI3K Pathway	HN_00190	***PIK3C2G***	p.V656L	T1N2bM0/ **Stage 4**
		PTEN	p.D92E	
	HN_62421	***PIK3R1***	p.D560H	T4N0M0/ **Stage 4**
		MTOR	p.L2260H	
	HN_62469	***PIK3CA***	p.H1047R	T2N2bM0/ **Stage 4**
		MTOR	p.R1161Q	
	HN_63039	***PIK3CA***	p.H1047L	T4N2bM0/ **Stage 4**
		PTEN	p.R335*	
	HN_22PT	***PIK3CG***	p.G491E	T4aN2bM0/ **Stage 4**
		PIK3AP1	p.G313R	
	HNPTS_1	***PTEN***	p.R14S	T4N0M0/ **Stage 4**
		PIK3IP1	p.A144S	
		PIK3CA	p.E545K	
	HNPTS_29	***PIK3C2G***	p.S1272L	T4N2bM0/ **Stage 4**
		PIK3R5	p.E322K	
		PIK3CA	p.E542K	
	HNPTS_38	***PIK3R5***	p.E60*	T4N2M0/ **Stage 4**
		PIK3CA	p.H1047R	
	HNPTS_42	***TSC2***	p.S1514*	T4N2BM0/ **Stage 4**
		PIK3CA	p.E545K	
		PIK3CG	p.A156V	
	HNPTS_45	***AKT2***	p.Y351C	T4N1M0/ **Stage 4**
		PIK3CA	p.H1047R	
JAK/STAT Pathway	HN_63080	***JAK3***	p.R948C	T4aN2bM0/ **Stage 4**
		STAT1	p.Q330K	
MAPK Pathway	NONE			

Fifteen of the 151 HNSCC tumors in this cohort were HPV(+), 5/15 HPV(+) tumors harbored PI3K pathway mutations (33.3%). Additionally, in 3 of the 151 tumors in our cohort, the only mutations identified by WES in known cancer genes were in the genes coding for the regulatory (*PIK3R1*) or catalytic (*PIK3CA*) subunit of PI3Kα (HN_00361, HN_63027 and HN41PT with *PIK3R1*(453_454insN), *PIK3CA*(E542K) and *PIK3CA*(H1047L) mutations, respectively). All 3 of these tumors were HPV(+), suggesting that a subset of HPV(+)HNSCC tumors (20%; 3/15 cases) may be driven by PI3K-pathway alterations alone.

2.3.3 Hotspot and Novel *PIK3CA* Mutations Identified in 151 HNSCC Tumors

PIK3CA codes for the catalytic subunit of the primary isoform of the class 1A phosphoinositol-3-kinases, p110α, and is a critical gene in the PI3K signaling pathway. Three "hotspot" amino acid residues, accounting for ≈80% of all mutations in *PIK3CA* at 542, 545, and 1047, are the most common sites of oncogenic, gain of function *PIK3CA* mutations across all cancers, including HNSCC (Table S5 in Lui, Hedberg, Li, *et al*. 2013). Four novel, previously unreported, *PIK3CA* mutations (R115L, G363A, C971R, and R975S) were identified in our cohort of 151 HNSCC tumors. Under the guidance of Dr. Ben Van Houten, I used the PyMol Molecular Graphics System to visualize the crystal structure of p110α (crystallized in complex with niSH2 of p85α, resolved to 2.9Å by Miller *et al.*), and examined the orientation of the non-hotspot residues in three dimensional space relative to the three hotspot residues.(*91, 100*) The C971 residue was found to be within 10 Angstroms of the H1047 hotspot residue in the kinase domain (Figure 7).

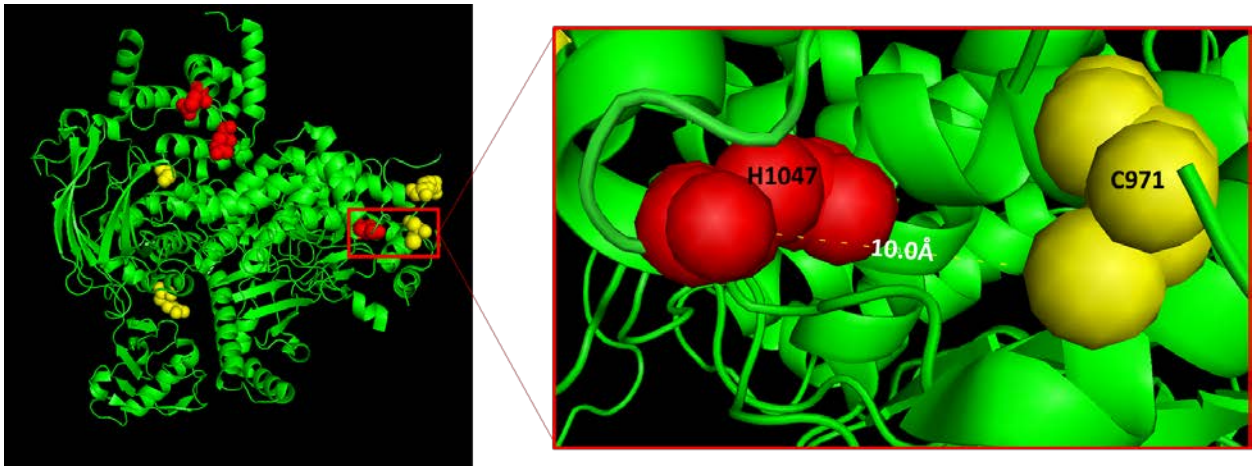

Figure 7. *PIK3CA* Hotspot and Novel Amino Acid Residues Mutated in HNSCC

A three dimensional representation of the p110α subunit (*left*) with hotspot mutation residues (E542, E545, and H1047) highlighted in red, and novel, non-hotspot mutation residues (R115, G363, C971, and R975) highlighted in yellow. A magnification of the indicated portion of the kinase domain (*right*) illustrates the proximity of the C971 residue to the H1047 hotspot residue. These images were generated under the direction of Dr. Ben Van Houten.

2.3.4 Hotspot and Novel *PIK3CA* Mutations Promote PI3K Signaling and Growth in HNSCC

To assess the impact of these novel *PIK3CA* mutations identified in our cohort of 151 HNSCC tumors we selected the HNSCC cell line PE/CA-PJ34 (known by WES to be WT for all PI3K pathway components), for initial functional experiments.(*101*) We used retroviruses to infect these cells with *EGFP* (control), WT *PIK3CA*, each of the 4 novel, non-hotspot *PIK3CA* mutations (R115L, G363A, C971R, R975S), and the kinase domain hotspot mutation (H1047R). Immunoblotting of cell lysates revealed that retroviral-infection with WT *PIK3CA* (mimicking *PIK3CA* gene amplification), and mutant *PIK3CA* constructs was associated with increased PI3K pathway activation as evidenced by increased phosphorylation of AKT (Figure 8A). Forced expression of WT *PIK3CA*, all 4 novel, non-hotspot *PIK3CA* mutants, individually, and the hotspot *PIK3CA*(H1047R) mutant, resulted in significantly enhanced growth vs *EGFP* control when proliferation over 72 hours was assessed by MTT assay (Figure 8B, $p < 0.0001$). Only the *PIK3CA*(H1047R) hotspot mutation showed significantly enhanced growth compared to simulated WT *PIK3CA* amplification (Figure 8B, $p = 0.001$). The average growth rates in cells expressing the novel, non-hotspot *PIK3CA* mutations were higher when compared to simulated WT amplification in this cell line, but not to a statistically significant degree (Figure 8B, R115L; $p = 0.1174$, G363A; $p = 0.9637$, C971R; $p = 0.6503$, R975S; $p = 0.0958$). These results demonstrate that the novel, non-hotspot *PIK3CA* mutations are not loss of function mutations, as they can drive PI3K signaling and proliferation in HNSCC at least as well as ectopic WT *PIK3CA*. But it is not clear if a significant gain of function is associated with these mutants in

this experiment as their effects over ectopic WT *PIK3CA* did not achieve statistical significance, as was seen with the hotspot (H1047R) mutation. Non-hotspot *PIK3CA* mutations identified in other cancers, different from those we identified, have similarly been shown to drive PI3K signaling and induce oncogenic transformation to a significant, but lesser, degree than hotspot mutations in avian model systems, where the oncogenic capabilities of *PIK3CA* were first discovered.(*102*)

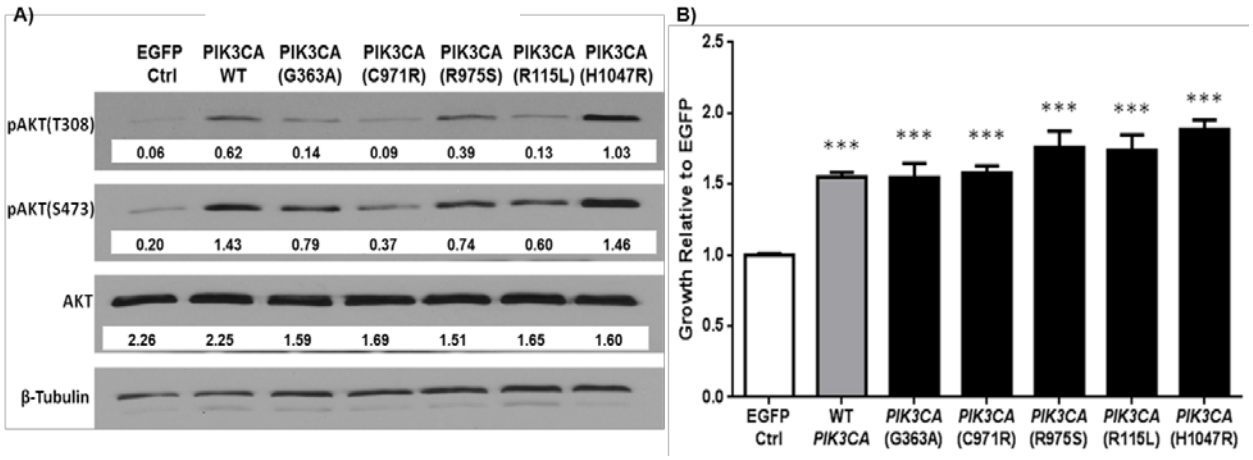

Figure 8. Effects of Mutant *PIK3CA* Expression in PE/CA-PJ34 Cells

(A) A representative Western blot with densitometry values normalized to beta-tubulin for cells expressing *EGFP*, WT *PIK3CA*, hotspot *PIK3CA* mutant H1047R, and novel mutants: R115L, G363A, C971R, and R975S, by retroviral infection. Increased phosphorylation of AKT at the T308 and/or S473 residue was observed in HNSCC cells stably expressing WT or mutant *PIK3CA* constructs relative to the EGFP expressing HNSCC cells, indicating enhanced activation of the PI3K signaling pathway. Experiment repeated three times with similar results. **(B)** Effects of *PIK3CA* mutations on PE/CA-PJ34 cell growth. HNSCC cells stably expressing WT or mutant *PIK3CA* constructs demonstrated enhanced growth at 72 hours in media with 2% FBS by MTT assay compared to cells expressing EGFP vector control ($p < 0.0001$***). *PIK3CA*(H1047R) expressing cells further demonstrated enhanced growth when compared to simulated WT *PIK3CA* amplification ($p = 0.001$). Pooled data (Mean +/- SEM) shown from three independent experiments in replicate cell lines (separate infections, n=18 for each group). This figure is adapted from Lui, Hedberg, Li *et al* 2013. I generated the vectors and engineered cell

lines as described in methods. I designed, optimized, and performed the experiments whose results are shown here. I performed data analysis and interpretation for this portion of the paper, and generated this figure.

2.3.5 Hotspot and Common *PIK3CA* Mutations in HNSCC and Other Cancers

In addition to our 151 HNSCC tumor cohort, other large scale WES studies are now contributing to our understanding of the spectrum of *PIK3CA* mutations that exist in HNSCC, and an appreciable number of *PIK3CA* mutations identified in HNSCC (≈20-30%) are non-hotspot mutations whose functional consequences are unknown (Figure 9).(*39-41, 85, 103, 104*)

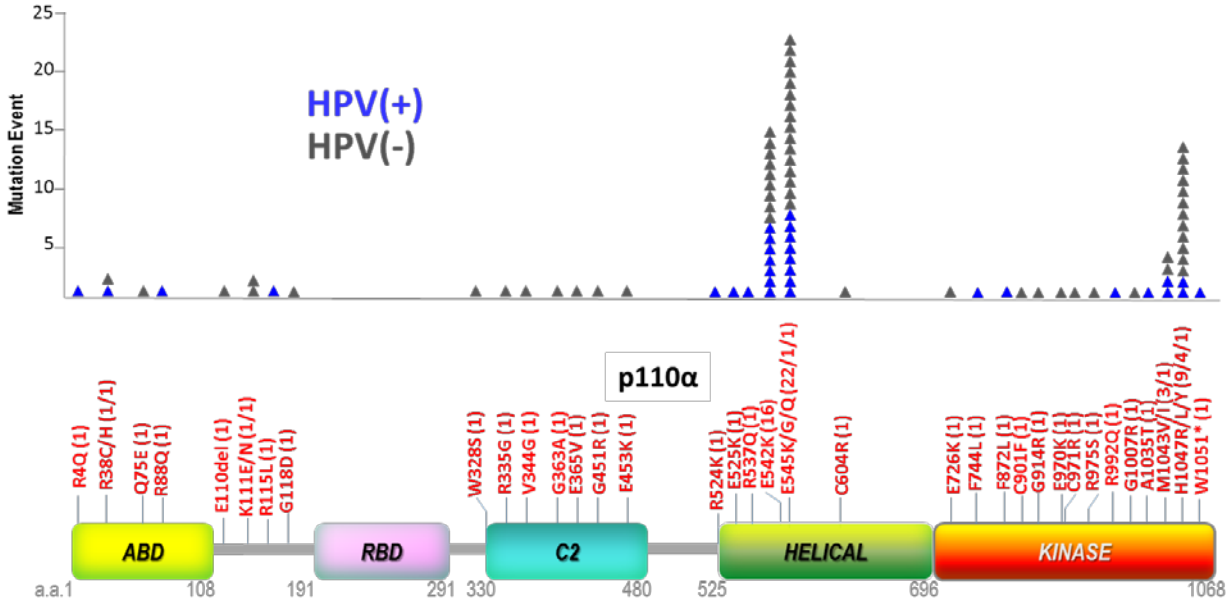

Figure 9. Schematic Diagram of *PIK3CA*/p110α Mutations Found in HNSCC Tumors.

The amino acid (a.a.) positions of each domain are shown in grey numbers below each domain. The number of mutational events at each site is indicated as filled triangle (▲) in the graph above. Blue triangles indicate mutations

that were identified in HPV(+)HNSCC tumors, grey indicates HPV(-) tumors. ABD: adaptor (p85) binding domain; RBD: Ras binding domain; C2 Superfamily; Helical: PIK domain; Kinase: kinase domain of p110α.

Individual, non-hotspot *PIK3CA* mutations are only identified in a small number of cases, often in only 1 HNSCC patient. In an attempt to predict which of these rare non-hotspot mutations might be of functional consequence, I cross-referenced the *PIK3CA* mutations identified in HNSCC with those identified in other cancers from the TCGA project. From this composite database of 1,424 shared *PIK3CA* mutations I assessed the frequency of each mutation and respective amino acid residue, and found 11 amino acid residues with a mutational frequency of at least 1% (Figure 10A). Through a collaboration facilitated by Dr. Adrian Lee, these 11 common *PIK3CA* mutations were assessed and compared to all reported *PIK3CA* mutations in HNSCC using an algorithm developed by Dr. Oliver Lichtarge. Briefly, this algorithm calculates the importance of the WT amino acid residue by evolutionary conservation, and the magnitude of change with respect to size and charge between the mutant amino acid and the WT amino acid to determine an "Evolutionary Action Score" for mutations. This score, ranging from 0-100, predicts whether a mutation is likely to be deleterious (100) with respect to the function of the protein, neutral (0) with respect to the function of the protein, or represent a potential gain of function mutation (50).(*92*) The tighter normal distribution around gain of function Evolutionary Action Scores in the subset of 11 common *PIK3CA* mutations (Figure 10C), compared to all HNSCC *PIK3CA* mutations (Figure 10B) suggests that we are selecting for mutations that are more likely to be gain of function mutations using these selection criteria.

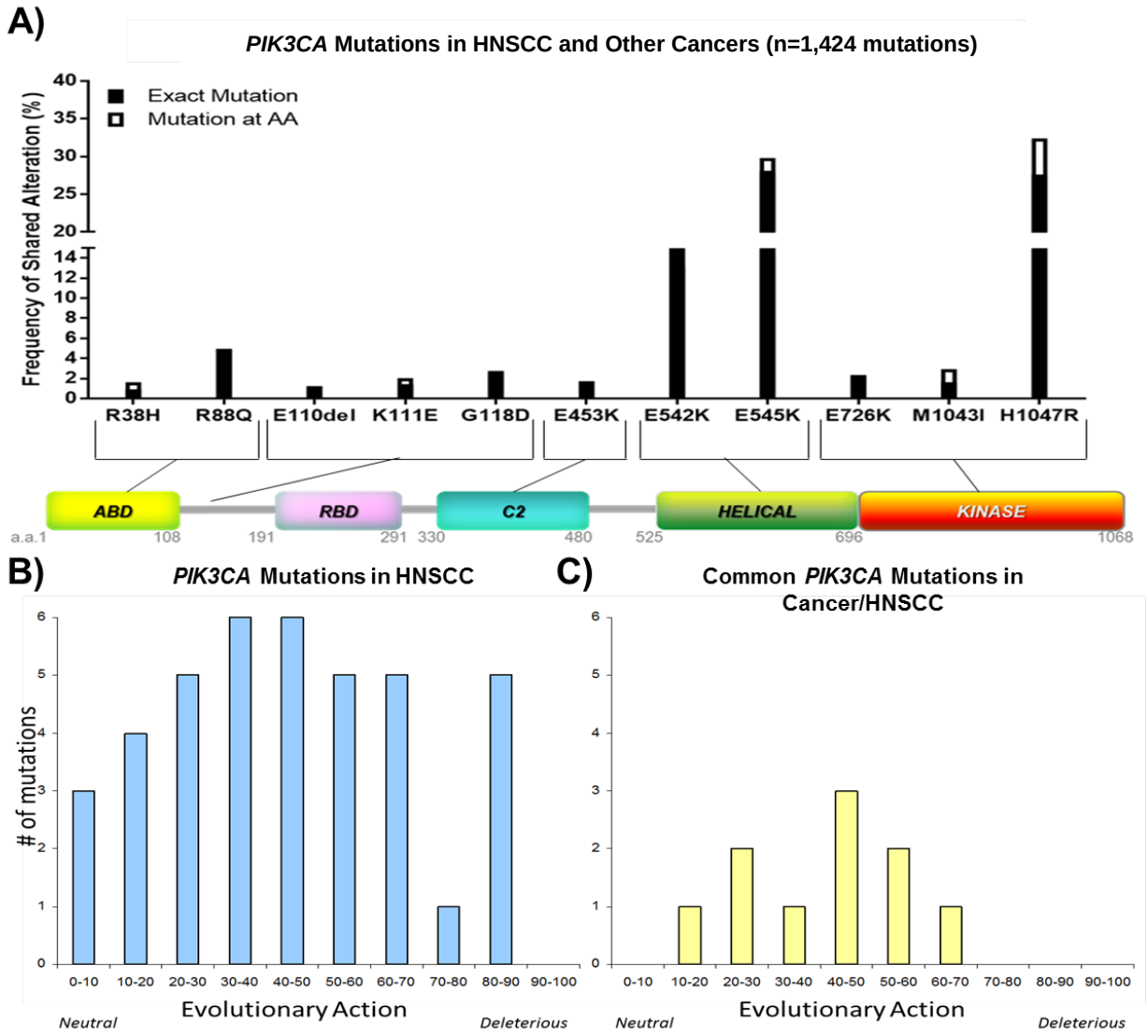

Figure 10. Common *PIK3CA* Mutations across Cancers and Comparative Functional Predictions

(A) *PIK3CA* mutations (n=1,424) identified in HNSCC and other cancers with mutational frequencies of ≥ 1% White bars represent the frequency of mutation at the specified amino acid and black bars represent the mutational frequency of the specific mutation listed. Comparative representations of the Evolutionary Action Scores for all *PIK3CA* mutations identified in HNSCC **(B)** and the common *PIK3CA* mutations **(C)**, as defined in part A, suggest that a greater proportion of the common *PIK3CA* mutations are likely to be gain of function. I supplied Dr. Panos Kastonis of Dr. Lichtarge's group with the mutational data that I utilized for part A of this figure (obtained through the cBIO portal), from which he generated parts B and C of this figure and provided interpretation.

2.3.6 Hotspot and Common *PIK3CA* Mutations Enhance Survival/Proliferation and Invasion in UPCI-52 (SD-1) Cells, but do not Confer Enhanced Sensitivity to BYL-719

To evaluate the impact of hotspot and common *PIK3CA* mutations on cancerous phenotypes in HNSCC, we conducted additional functional experiments. In these experiments, I utilized a specialized HNSCC cell line developed in our lab, UPCI-52 (SD-1). This cell line is a serum-dependent, *PIK3CA* WT, subclone isolated from the HNSCC cell line UPCI-52, that demonstrates markedly reduced survival/rates of proliferation when cultured in reduced, or serum-free media (Patent Application # PCT/US2013/051866). By engineering mutations into this cell line and assessing their effect on survival/proliferation of these cells in reduced-serum media, we have used this cell line as an HNSCC-specific screening platform to identify driver mutations.(*105*)

I used retroviruses to infect these UPCI-52 (SD-1) cells with *EGFP* control, WT *PIK3CA* (mimicking gene amplification), 4 of the common non-hotspot *PIK3CA* mutants identified in Figure 10 that are far removed from the more well-studied helical and kinase domains (R38H, R88Q, E110del and G118D), individually, and three hotspot *PIK3CA* mutants (E542K, E545K and H1047R), individually. Because they have been shown to alter the action of the p110α protein in published reports, no tag was utilized in the *PIK3CA* constructs used in these experiments.(*106*) As such, ectopic p110α cannot be readily distinguished from endogenous p110α by immunoblotting alone, and I therefore also performed RT-PCR and Sanger sequencing of the resultant cDNA, in order to confirm the expression of the appropriate mutant *PIK3CA* constructs in the respective engineered UPCI-52 (SD-1) cell lines (Figure 11).

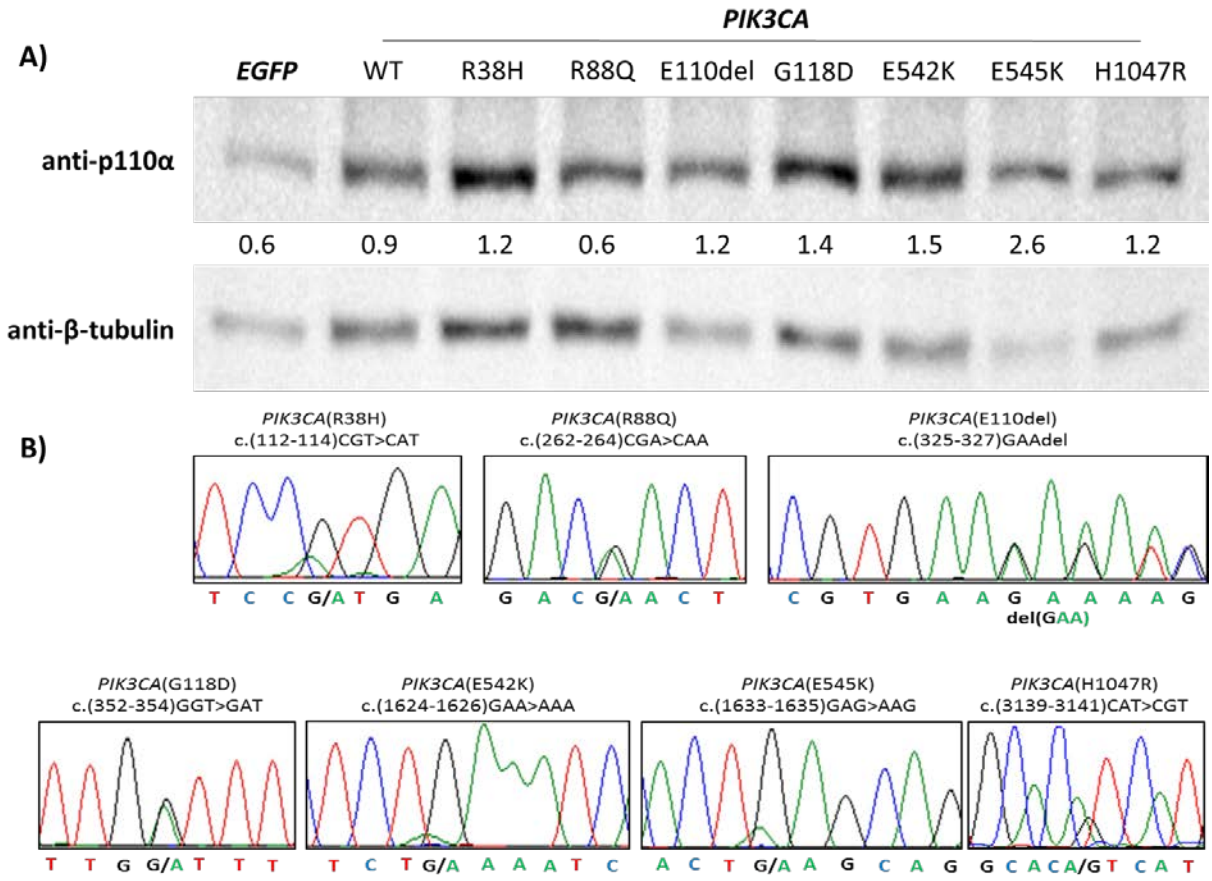

Figure 11. Expression of Hotspot and Common *PIK3CA* Mutations in UPCI-52 (SD-1) Cells

(A) A representative immunoblot with densitometry values normalized to beta-tubulin for UPCI-52 (SD-1) cells expressing *EGFP* or *PIK3CA* constructs, as indicated, by retroviral infection. 8.0 x 10^5 cells were plated overnight, serum starved for 30 hours, harvested, and assessed by SDS-PAGE and immunoblotting for p110α and β-tubulin. The experiment was repeated twice with similar results. **(B)** Sanger sequencing of cDNA generated by RT-PCR as described in methods from each engineered UPCI-52 (SD-1) cell line confirming expression of the appropriate mutant *PIK3CA* construct as indicated, at the level of transcription. The experiment was repeated twice with similar results. I generated the vectors and engineered the cell lines as described in methods. I designed, optimized, and performed the experiments whose results are shown here, and did all of the data collection and analysis. Yan Zeng performed alongside me for some of the experiments/replicates assisting in the plating of cells, harvesting of lysates, and preparation of gels and reactions.

UPCI-52 (SD-1) cells expressing WT *PIK3CA* (mimicking *PIK3CA* gene amplification), 3/4 common, non-hotspot *PIK3CA* mutants (R38H, R88Q and G118D), and all 3 hotspot *PIK3CA* mutants (E542K, E545K and H1047R) demonstrated significantly enhanced survival/proliferation in reduced serum media over 9 days compared to *EGFP* control by MTS assay (Figure 12). Further, cells expressing 3/4 common, non-hotspot mutants (R38H, R88Q and G118D), and 2/3 hotspot mutants (E542K and E545K), demonstrated significantly enhanced survival/proliferation in reduced serum media over 9 days compared to simulated WT *PIK3CA* amplification in the same experiments (Figure 12).

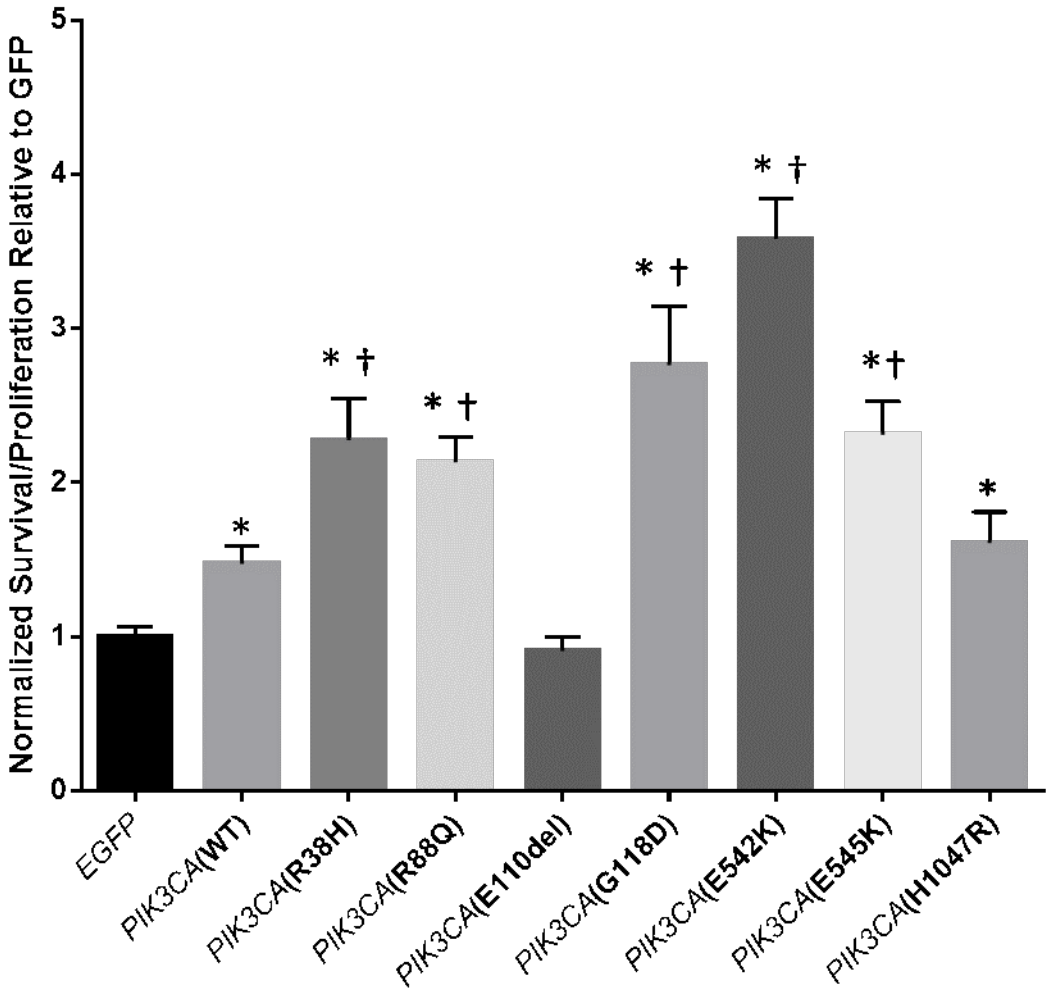

Figure 12. Effect of PIK3CA Mutants on Survival/Proliferation of UPCI-52 (SD-1) Cells

5.0 x 10^3 UPCI-52 (SD-1) cells per well, stably expressing *EGFP*, WT or mutant *PIK3CA* constructs were plated in 48-well plates, grown for 9 days in media with 2% and 10% FBS, and assessed by MTS assay. Shown is proliferation in 2% FBS media normalized by proliferation in 10% FBS media, relative to *EGFP* controls. *: significantly enhanced survival/proliferation ($p < 0.05$) vs *EGFP*, †: significantly enhanced survival/proliferation ($p < 0.05$) vs simulated *PIK3CA* amplification (ectopic WT *PIK3CA*). Pooled data (Mean +/- SEM) from 3 independent sets of experiments plated n=8 is presented. Significance was determined by unpaired T-test with Welch's correction.

I then assessed these engineered UPCI-52 (SD-1) cells in transwell assays to observe the impact of *PIK3CA* mutation on invasion/migration. In trends that roughly matched those seen in the proliferation experiments, UPCI-52 (SD-1) cells expressing WT *PIK3CA* (mimicking *PIK3CA* gene amplification), 3/4 common, non-hotspot *PIK3CA* mutants (R38H, R88Q and G118D), and all 3 hotspot *PIK3CA* mutants (E542K, E545K and H1047R) demonstrated significantly enhanced invasion compared to *EGFP* control in transwell assays over 24 hours (Figure 13). Further, cells expressing 2/4 common, non-hotspot mutants (R88Q and G118D), and all 3 hotspot mutants (E542K, E545K and H1047R), demonstrated significantly enhanced invasion compared to simulated WT *PIK3CA* amplification in the same experiments (Figure 13).

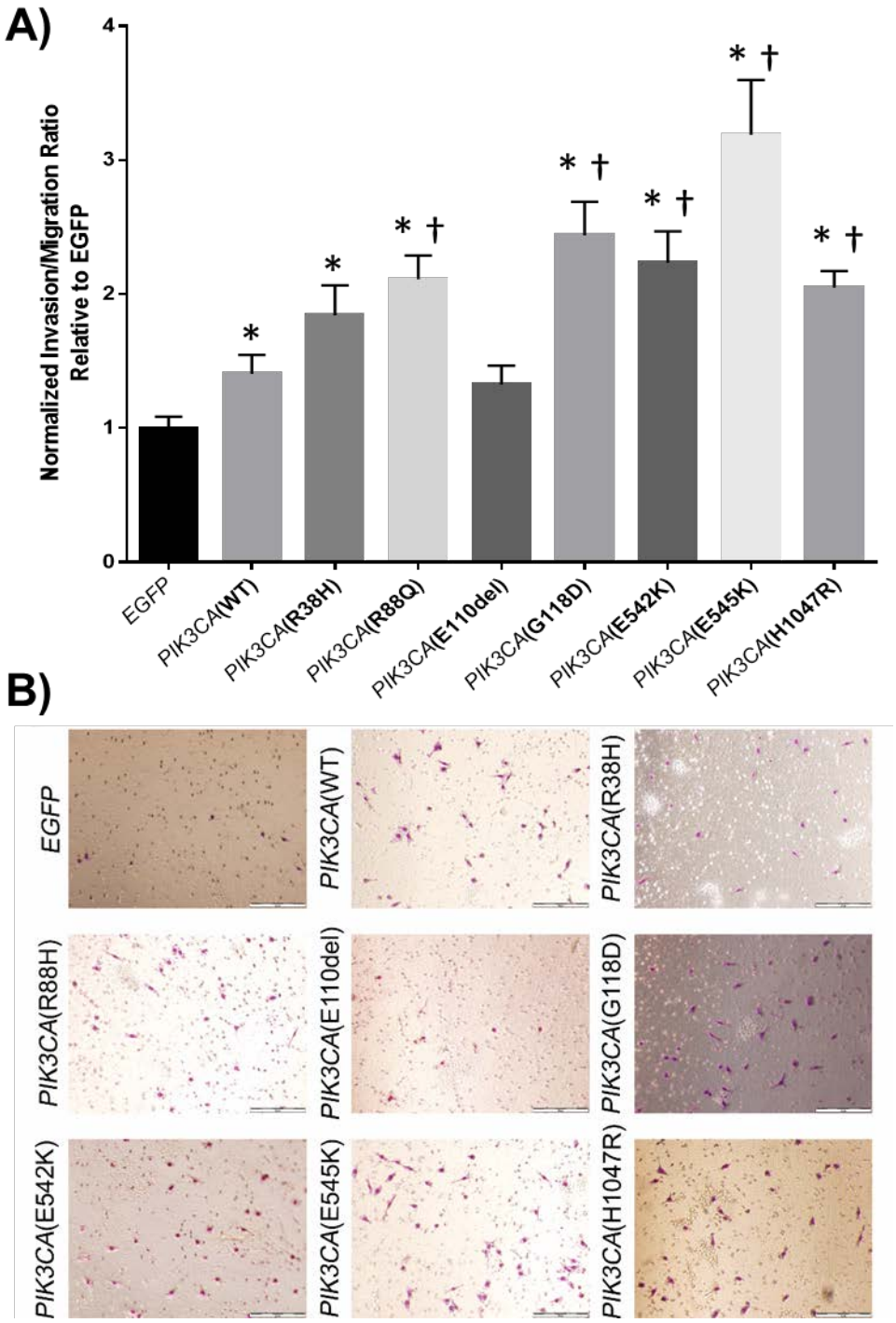

Figure 13. Effect of PIK3CA Mutants on Invasion of UPCI-52 (SD-1) Cells

3.0 x 10^4 UPCI-52 (SD-1) cells suspended in DMEM stably expressing *EGFP*, WT or mutant *PIK3CA* constructs were plated inside migration (uncoated) chambers or invasion (matrigel coated) chambers submerged in 10% FBS media for 24 hrs. Cells were counted and averaged from 4 photomicrographs (20x objective) of each membrane, and

the invasion/migration ratios were calculated. **(A)** The average Invasion:Migration ratios for each engineered line relative to *EGFP* controls. **(B)** Representative images of invasion membranes. *: significantly enhanced invasion ($p < 0.05$) vs *EGFP*, †: significantly enhanced invasion ($p < 0.05$) vs simulated *PIK3CA* amplification (WT *PIK3CA*). Pooled data (Mean +/- SEM) from 5 independent sets of experiments plated in duplicate is presented. Significance was determined by unpaired T-test with Welch's correction.

Reports in other cancers suggest that tumors with *PIK3CA* alteration may be more sensitive to PI3K pathway inhibitors.(*107*) Having demonstrated that hotspot and several common, non-hotspot *PIK3CA* mutations can contribute to cancerous phenotypes such as proliferation and invasion in UPCI-52 (SD-1) cells, we hypothesized that cells expressing these *PIK3CA* mutations would be more sensitive to treatment with a targeted PI3K inhibitor. When I treated UPCI-52 (SD-1) cells expressing *EGFP* control, WT *PIK3CA*, the four common non-hotspot *PIK3CA* mutants (R38H, R88Q, E110del and G118D), and the three hotspot *PIK3CA* mutants (E542K, E545K and H1047R), with the alpha-isoform specific p110α inhibitor BYL-719, inhibition of PI3K signaling was observed as expected (Figure 14).(*108*)

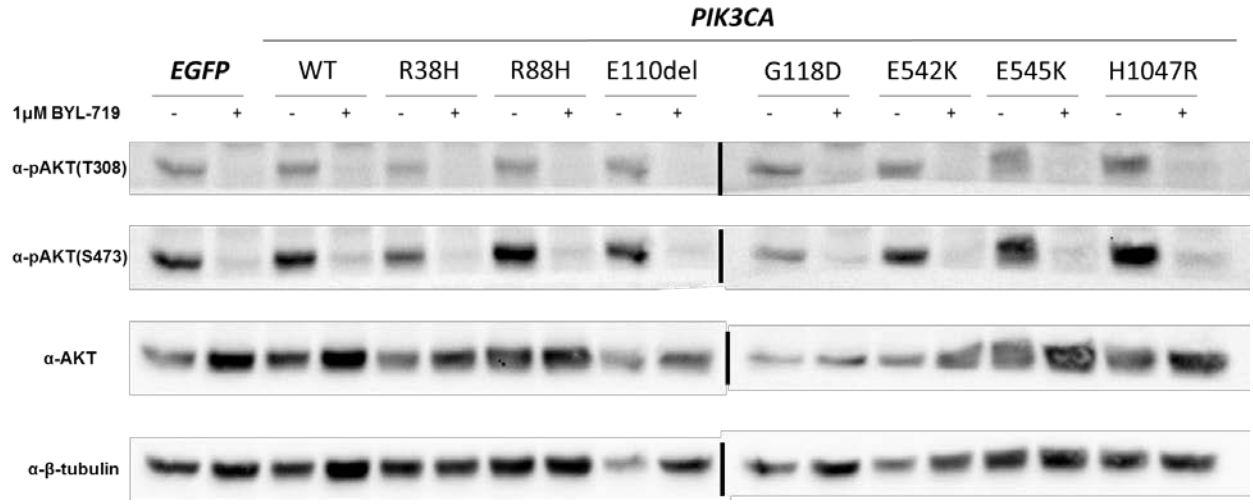

Figure 14. Inhibition of AKT Phosphorylation by BYL-719 Treatment in Engineered UPCI-52(SD-1) Cells

8.0 x 10^5 UPCI-52 (SD-1) cells expressing the indicated constructs were plated overnight, followed by 24 hours serum-starvation, after which they were re-exposed to full media for 6 hours in the presence of 1μM BYL-719 or vehicle control, harvested, and assessed by SDS-PAGE and immunoblotting. BYL-719 treatment inhibited PI3K signaling as evidenced by the reduced phosphorylation of AKT shown above. The experiment was repeated 3 times with similar results. I generated the vectors and engineered the cell lines as described in methods. I designed, optimized, and performed the experiments whose results are shown here, and did all of the data collection and analysis. Yan Zeng performed alongside me for some of these experiments/replicates assisting in the plating and treatment of cells, harvesting of lysates, and preparation of gels.

Treatment of UPCI-52 (SD-1) cells expressing the various *PIK3CA* mutant constructs with BYL-719 for 72 hours did not consistently demonstrate enhanced sensitivity compared with *EGFP* controls. Only cells expressing the *PIK3CA*(E110del) mutant were found to be more sensitive to BYL-719 than controls (Figure 15). All of the other UPCI-52 (SD-1) cells expressing *PIK3CA* mutations were less sensitive to BYL-719 treatment compared to *EGFP* controls, some to a statistically significant degree [*PIK3CA* WT, (R38H), (G118) and (E542K)], though the difference in the IC50 values is modest (Figure 15). These observations are consistent with a

prior study where forced expression of hotspot *PIK3CA* mutants in the HNSCC cell line SCC25, resulted in resistance as opposed to sensitization to treatment with the PI3K inhibitor GDC-0941.(*109*)

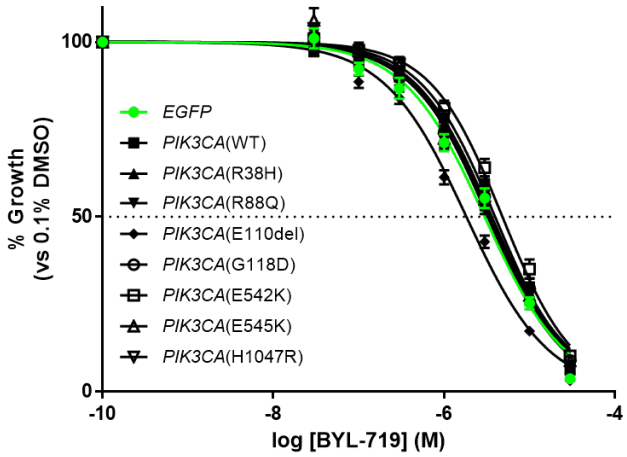

	72 Hour Treatment with BYL-719		
	Construct	**IC50 (M)**	**p-value vs *EGFP***
UPCI-52 (SD-1) Cells	*EGFP*	2.995E-06	-
	PIK3CA (WT)	3.963E-06	**0.0002**
	PIK3CA (R38H)	3.629E-06	**0.0129**
	PIK3CA (R88Q)	3.438E-06	0.0915
	PIK3CA (E110del)	1.830E-06	**< 0.0001**
	PIK3CA (G118D)	3.584E-06	**0.0435**
	PIK3CA (E542K)	4.834E-06	**< 0.0001**
	PIK3CA (E545K)	3.418E-06	0.1386
	PIK3CA (H1047R)	3.256E-06	0.2613

Figure 15. Sensitivity of Engineered UPCI-52 (SD-1) Cells to BYL-719

5.0 x 10^3 UPCI-52 (SD-1) cells per well, stably expressing *EGFP*, WT or mutant *PIK3CA* constructs were plated overnight in 48-well plates and treated with half-log doses of BYL-719 from 0μM - 30μM for 72 hours and assessed by MTS. Mean values +/- SEM were plotted in GraphPad Prism 6, and growth curves (*left*) and IC50 values (*right*) were calculated using the least squares fit log(inhibitor) vs. normalized response-variable slope equation, and compared using an extra sum of the squares F-test. Pooled data from 5 independent experiments plated at n=6 is shown.

The hypothesis that cells with *PIK3CA* alterations will be more sensitive to PI3K inhibition is predicated on the theory of oncogene addiction. This theory posits that an oncogene-addicted cancer is so highly dependent upon acquired aberrations in a cell signaling pathway for survival, that inhibition of said pathway results in massive amounts of cell death. UPCI-52 (SD-1) cells are a HNSCC cell line with a set of endogenous molecular alterations that evolved over time allowing the cells to originally become transformed and continue to proliferate limitlessly in

culture. Taken together, our data suggest that while the *PIK3CA* constructs are able to contribute to cancerous phenotypes in UPCI-52 (SD-1) cells, conferring enhanced survival/proliferation in reduced serum media and enhanced invasion in transwell assays, the engineered cells are not addicted to the added oncogene under these experimental conditions.

2.3.7 PI3K Inhibitors are Effective in Endogenous Preclinical Models of HNSCC

In light of the potential limitations of the engineered UPCI-52 (SD-1) platform, and published reports suggesting that *PIK3CA* alteration can be predictive of response to targeted therapy, we proceeded to assess the predictive value of *PIK3CA* status in endogenous preclinical models of HNSCC.(*107*) We treated a panel of 8 HNSCC cell lines of varying *PIK3CA* and HPV status (Summarized in Table 5) with 2 targeted PI3K inhibitors currently in clinical development; BKM-120, and BYL-719.(*101, 110, 111*) Both drugs are small molecules that function as competitive, reversible inhibitors of PI3Ks. BKM-120 is a pan inhibitor of the α, β, γ, and δ isoforms of the catalytic subunits of Class 1 PI3Ks.(*112*) BYL-719 is an α-isoform specific inhibitor targeted directly against p110α, the gene product of *PIK3CA*.(*108*) HNSCC cell lines were varyingly sensitive to these agents and both drugs were equipotent in HNSCC cell lines with endogenous *PIK3CA*(H1047R) mutations, which were generally found to be more sensitive to BYL-719 treatment than cell lines without *PIK3CA* mutation (Table 5 and Figure 16).

Table 5. Characteristics and BKM/BYL Sensitivity of HNSCC Cell Lines

Select characteristics of the 8 HNSCC cell lines used in the BKM/BYL treatment experiments are shown along with average IC50 values from Figure 16 (*below*). P-values are derived from extra sum-of-squares F tests comparing the logIC50 values of BKM-120 and BYL-719 for each respective cell line.

72 Hr. Treatment	Cell Line	BKM-120 IC50 (M)	BYL-719 IC50 (M)	p-value	*PIK3CA*	HPV
	PE/CA-PJ34	1.72E-06	4.75E-06	**< 0.0001**	WT	-
	Fadu	2.21E-06	4.37E-06	**< 0.0001**	WT, amp	-
	JHU 022	1.50E-06	2.56E-06	**< 0.0001**	WT, amp	-
	HSC2	1.18E-06	1.29E-06	0.4995	Mutant	-
	Det 562	1.62E-06	1.52E-06	0.6705	Mutant	-
	Cal 33	9.46E-07	9.60E-07	0.8895	Mutant	-
	UPCI 090	4.21E-06	1.04E-05	**< 0.0001**	WT	+
	UMSCC47	3.70E-07	1.98E-06	**< 0.0001**	WT	+

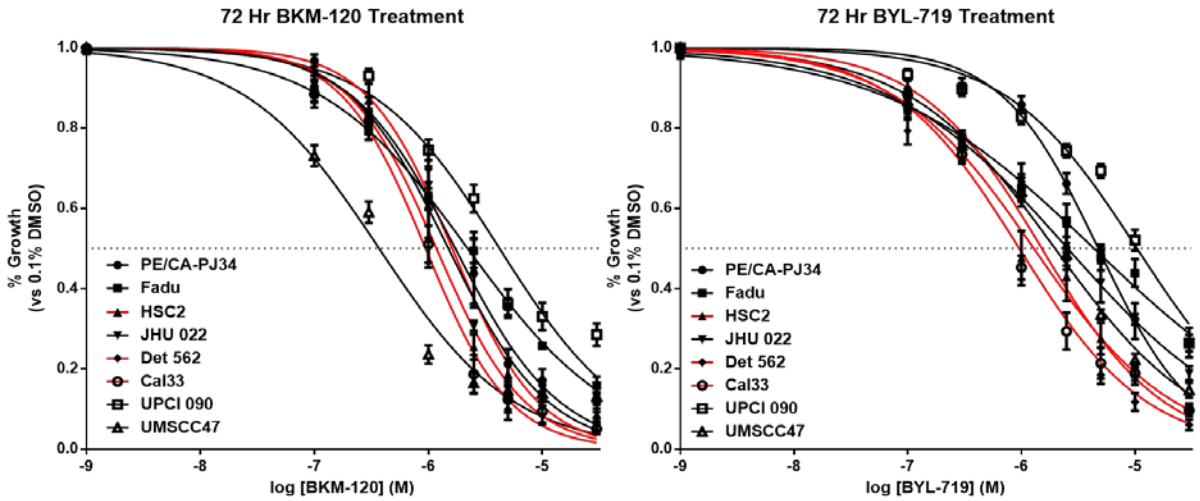

Figure 16. Sensitivity of HNSCC Cell Lines to Targeted PI3K Inhibition

6.5 x 10^3 cells per well were plated overnight in 48-well plates and treated with half-log doses of BKM-120 (*left)* or BYL-719 (*right*) from 0μM - 30μM for 72 hours and assessed by MTT. Mean values +/- SEM were plotted in GraphPad Prism 6, and growth curves and IC50 values were calculated using the least squares fit log(inhibitor) vs. normalized response-variable slope equation, and compared using an extra sum of the squares F-test. Pooled data

from three independent experiments plated in quadruplicate are displayed and IC50 results are summarized numerically in Table 2 (*above*). I designed, optimized, and performed at least one replicate of each experiment whose results are shown here, and did all of the data analysis. Yan Zeng performed some the experiments/replicates and provided raw data for my analysis.

We then proceeded to assess the efficacy of BYL-719 in 4 unique, patient-derived HNSCC xenografts (PDXs) of varying *PIK3CA* and HPV status. We chose to 4 tumorgrafts to test BYL-719 in the setting or absence of HPV and in the setting or absence of *PIK3CA* mutation. Initially, BYL-719 treatment resulted in tumor growth inhibition in the 2 PDXs with WT *PIK3CA*, and tumor regression in the 2 PDXs harboring endogenous *PIK3CA* mutations (Figure 17). After approximately two weeks of treatment, 3/4 PDXs started to demonstrate tumor growth in the BYL-719 treatment arm, suggesting the potential emergence of resistance to BYL-719. When the experiment was terminated, the average tumor volume, and fractional tumor volume change, between the BYL-719 and vehicle treated tumors of the HPV(-)/*PIK3CA*(M1043V) PDX, was no longer statistically significant (Figure 17 and Table 6).

Table 6. End Point Tumor Volumes of HNSCC PDXs Treated with BYL-719 or Vehicle

Average tumor volumes of vehicle-treated and BYL-719-treated animals in each PDX at the end of experiment were calculated and compared by T-test. Statistical significance was determined using the Sidak-Bonferroni method, α=0.05, without assuming a consistent SD.

	Mean Tumor Volume +/- SD at End of Experiment (mm^3)		Difference Significant by Bonferroni	p-value
PDX	**Treated with BYL-719**	**Treated with Vehicle Control**		
HPV(-)/*PIK3CA* (WT)	347.6 ± 156.2 (n=10)	781.0 ± 402.7 (n=12)	Yes	0.0045
HPV(+)/*PIK3CA* (WT)	833.9 ± 273.0 (n=11)	1354.9 ± 341.4 (n=8)	Yes	0.0018
HPV(-)/*PIK3CA* (M1043V)	743.4 ± 642.6 (n=10)	1279.4 ± 472.4 (n=10)	No	-
HPV(+)/*PIK3CA* (E542K, F744L)	283.6 ± 78.3 (n=10)	658.3 ± 228.5 (n=10)	Yes	0.00011

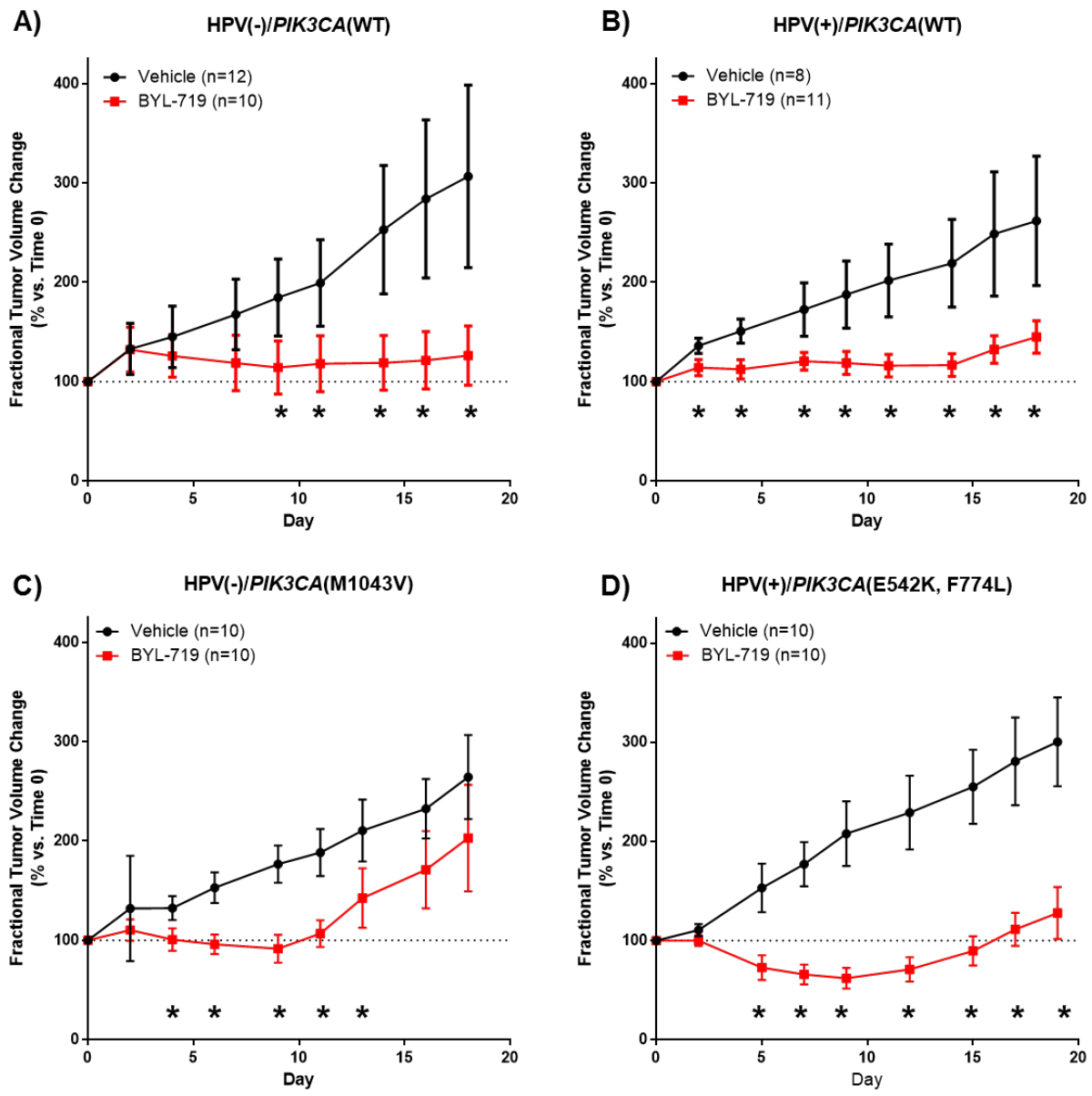

Figure 17. BYL-719 Treatment of HNSCC PDXs

HNSCC PDXs, one per mouse, were implanted bilaterally into the flanks of 12 NOD SCIDγ mice. Treatment was initiated when tumors became palpable with 5-6 mice (8-12 tumors) per PDX receiving vehicle control and 6 mice (10-11 tumors) per PDX receiving BYL-719 (1mg) daily, by oral gavage. Tumors were measured 3 times per week by digital calipers. Fractional tumor volume change +/- 95%CI was plotted in GraphPad Prism 6 and compared between the BYL-719 and vehicle treated tumors at each data/time point by T-test. *: $p<0.05$, Statistical significance was determined using the Sidak-Bonferroni method, $\alpha=0.05$, without assuming a consistent SD. I generated the vectors and engineered the cell lines as described in methods. I designed, optimized, and took part in each of the

experiments whose results are shown here, and did all of the data analysis. Yan Zeng worked alongside me for some of the initial surgeries when we expanded the PDXs up to the treatment sized cohorts, and assisted with the daily drug treatments when I was unavailable to administer them. Hua Li was blinded to the treatment groups I devised and performed the caliper tumor measurements. Providing data for my analysis.

When the experiment was terminated, samples of vehicle and BYL-719 treated PDXs were collected, lysed, and assessed by reverse phase protein array (RPPA) in collaboration with Dr. Gordon B. Mill's group at the core laboratories of the MD Anderson Cancer Center. The RPPA analysis of the HPV(-)/*PIK3CA*(WT) PDX showed statistically significant reduction in the phosphorylation of downstream effectors of the PI3K signaling cascade from the level of AKT through mTORC1 and the S6 ribosomal protein (Figure 18). This was not observed in the RPPA analysis of the other 3 HNSCC PDXs; and in the HPV(-)/*PIK3CA*(M1043V) PDX, which showed the strongest evidence of acquired resistance to BYL-719, there were significantly elevated levels of phosphorylated S6 ribosomal protein in BYL-719 treated tumors vs. vehicle treated tumors, by RPPA (Figure 18). These data may implicate mTORC1 signaling downstream of PI3K as an important mediator of response to BYL-719 treatment in these models, which would be consistent with previously published results in preclinical models of breast cancer.(*113*)

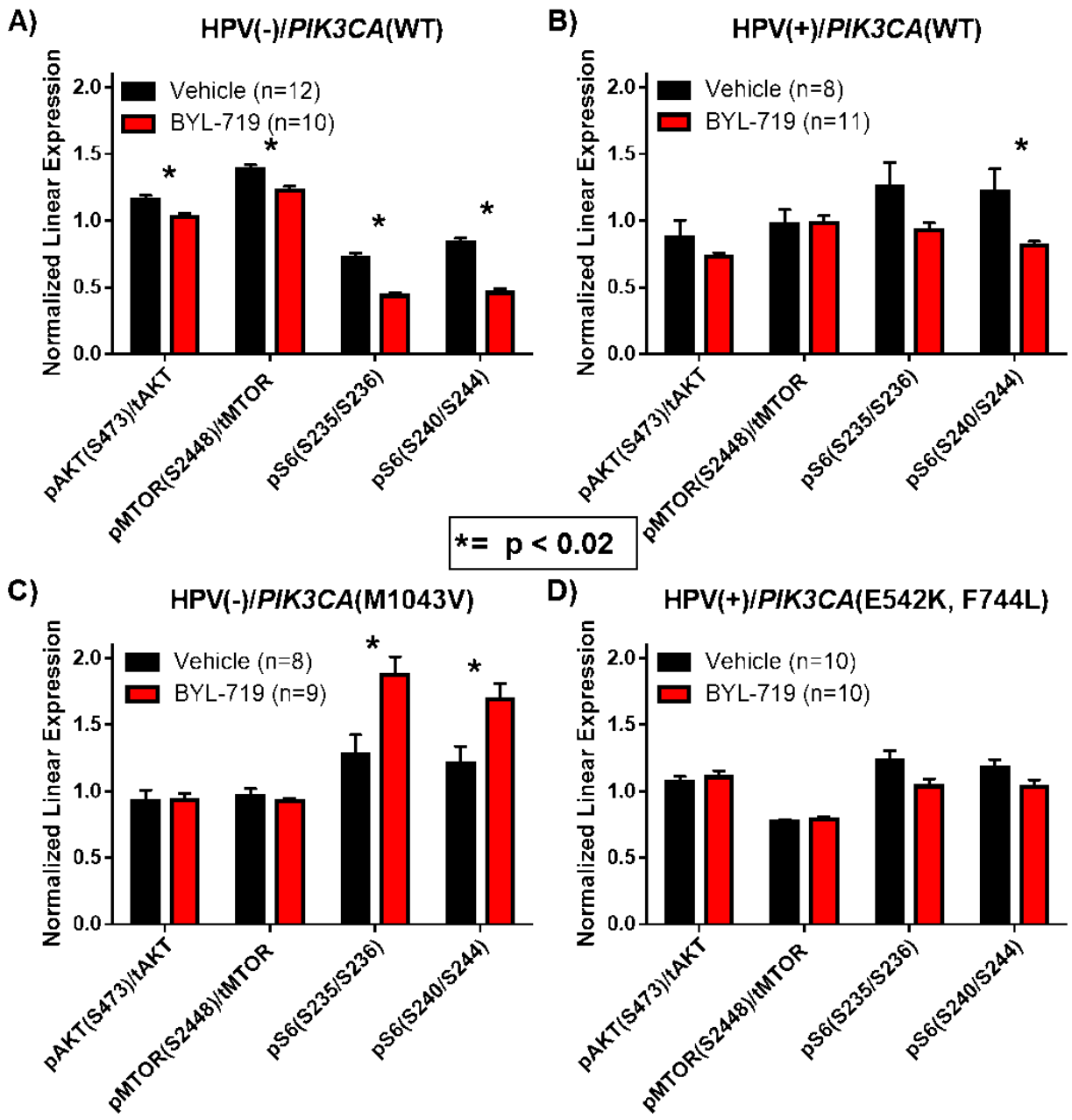

Figure 18. PI3K Signaling in BYL-719 Treated PDXs by RPPA

Normalized linear RPPA expression values (Mean +/- SEM) for phospho-specific antibodies (or ratios of phospho-specifc antibodies over total-specific antibodies) against downstream components of the PI3K signaling pathway demonstrate the level of inhibition achieved by BYL-719 treatment in each of the 4 HNSCC PDXs. Significance by unpaired T-tests. The data for this analysis was provided by the RPPA Proteomics Core at MD Anderson. I collected

all the tumor samples for this dataset at the end of the BYL-719 treatment experiments. Yan Zeng and Hua Li facilitated the preparation and export of lysates to Texas for analysis.

Elkabets *et al.* recently reported a mechanism of resistance in HNSCC to BYL-719.(*114*) In this mechanism, the AXL receptor is upregulated in response to BYL-719 treatment, it dimerizes with EGFR, and activates mTORC1 signaling in an AKT-independent manner through the activation of Phospholipase C, Gamma (PLCγ) and Protein Kinase C, Zeta (PKCζ).(*114*) Increased expression of AXL was observed across several preclinical models and patient tumor samples that were treated with BYL-719 in their study, and models with higher basal levels of AXL were more likely to be resistant to BYL-719..(*114*) Similarly, we observed elevated levels of AXL by RPPA in our BYL-719 treated PDXs vs. control, suggesting that this, or a similar mechanism may be implicated in our results (Figure 19). We also observed however, that the PDX model with the highest levels of AXL by RPPA, both basally and in the setting of BYL-719 treatment, was responsive to BYL-719 treatment. Future studies featuring sample harvesting at various time intervals will be required to address the dynamics of treatment resistance as it evolves in the face of therapy, and at this time the interpretation of RPPA data should be viewed as hypothesis generating.

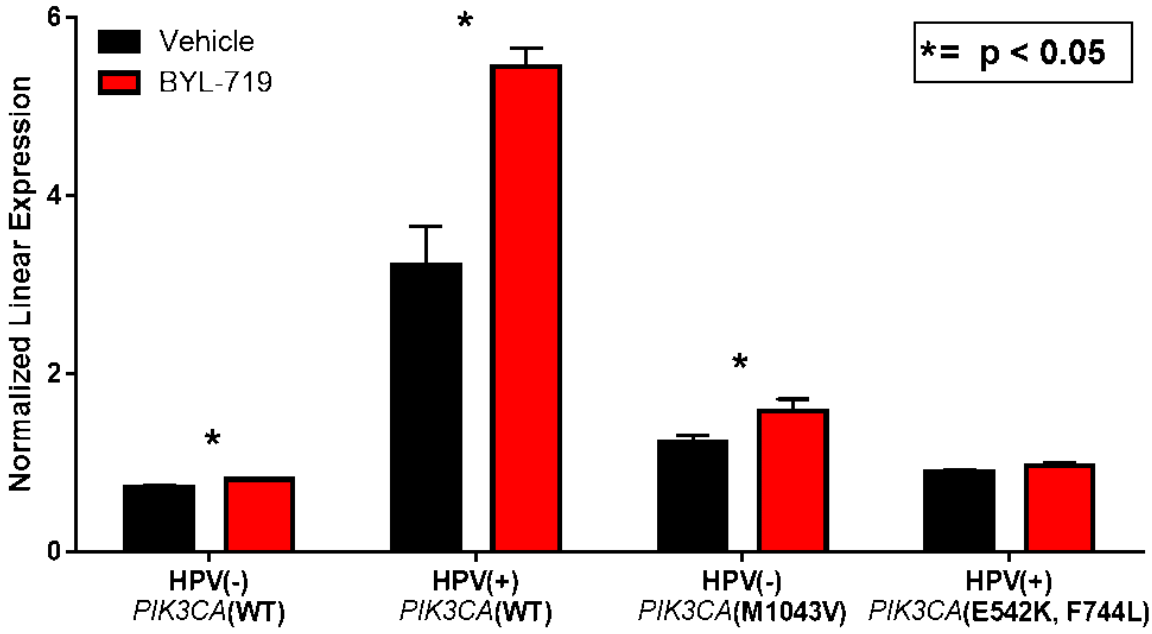

Figure 19. Effect of BYL-719 Treatment on AXL Expression in PDXs

Normalized linear RPPA expression values (Mean +/- SEM) for antibodies against AXL demonstrate the induction induced by BYL-719 treatment in each of the 4 HNSCC PDXs. Significance was determined by unpaired T-tests. The data for this analysis was provided by the RPPA Proteomics Core at MD Anderson. I collected all the tumor samples for this dataset at the end of the BYL-719 treatment experiments. Yan Zeng and Hua Li facilitated the preparation and export of lysates to Texas for analysis.

2.4 DISCUSSION

The increasing number of targeted anti-cancer agents under development presents tremendous opportunity for personalized cancer medicine. Selection of therapies based on the mutational status of molecular targets has transformed clinical management and survival of several human malignancies.(*115*) The elucidation of the mutational landscape underlying HNSCC offers an

opportunity to identify genetically-defined subgroups of HNSCC tumors with alterations in therapeutic target genes/pathways to guide treatment decisions.

Using a pathway-level approach, we analyzed WES data from 151 HNSCC tumors to identify mutationally-altered, targetable mitogenic pathways in HNSCC. We found the PI3K pathway to be the most frequently mutated oncogenic pathway in HNSCC, with the relative number of PI3K-mutated tumors compared to RAS/MAPK and JAK/STAT-mutated tumors being approximately 3-fold greater (Figure 5). Based on TCGA data downloaded from the cBio Portal, similar ratios of PI3K pathway mutations (relative to RAS/MAPK or JAK/STAT) are seen in squamous cell carcinoma of the lung, and in cervical cancer; both of which share common risk factors with HNSCC, including tobacco and HPV infection, respectively.(*90*) In contrast, the RAS/MAPK pathway is more frequently mutated than the PI3K pathway in colon and thyroid cancers, and both the PI3K and RAS/MAPK pathways are mutated at comparable rates in lung adenocarcinomas.(*99*) The percentage of HNSCC tumors harboring multiple mutations in the PI3K pathway is similar to that observed in breast cancers (4.9%, 25/507 tumors) and glioblastomas (9.1%, 25/276 tumors) , higher than in thyroid cancer (0.3%, 1/323 tumors) and lower than in most other cancers, including uterine carcinoma (65.7%, 163/248 tumors), melanoma (24.9%, 63/253 tumors), and surprisingly lung squamous cell carcinoma (17.4%, 31/178 tumors); which otherwise shares common risk factors and similar relative rates of mitogenic pathway mutations with HNSCC.(*85, 99*)

PI3K pathway-mutated HNSCC tumors were found to have a higher rate of non-synonymous mutations, including an increased number of cancer gene mutations, compared to tumors without PI3K pathway mutations (Figure 6). It is not known if or how PI3K pathway alterations could contribute to genomic instability in HNSCC tumors. Conceivably, they may

confer a “mutator” phenotype to HNSCC tumors. Either rendering them more prone to mutation directly, by somehow inhibiting DNA repair; or indirectly by, for example, enhancing the rate at which the cells divide resulting in more opportunities for the accumulation of mutations. PI3K pathway alterations may simply occur at later disease stages promoting the clonal expansion of cancer cells already harboring high numbers of mutations. Genomic gain of *PIK3CA* and increased expression of p110α have been associated with progression from dysplasia to carcinoma in pathologic studies of HNSCC.(*116*) In this latter scenario, the PI3K alterations would seem to confer an “oncogenic” advantage, even in the setting of increasing genomic instability. The “oncogenic” advantage of PI3K pathway-mutated tumors is evidenced by the behavior of “driver” *PIK3CA* mutations observed in our experiments, where they were found to promote enhanced growth in engineered PE/CA-PJ34 cells (Figure 8) and enhanced survival/proliferation in engineered UPCI-52 (SD-1) cells, cultured in reduced serum media (Figure 12). While the potential “mutator” phenotype of these tumors is supported by our finding that PI3K pathway-mutated tumors are associated with mutations in select tumor suppressors, chromatin remodelers, and DNA repair genes.(*99, 117-119*) To the extent that they each exist, both the “oncogenic” and “mutator” phenotypes associated with PI3K pathway alterations are likely to contribute to HNSCC progression; especially when they occur in the absence of other genetic mutations known to contribute to carcinogenesis in HNSCC, as was seen in 3 HPV(+) tumors in our cohort.

Our finding that all 10 HNSCC tumors with concurrent mutations of multiple PI3K-pathway genes were advanced, Stage IV cancers suggests that concurrent alterations of multiple nodes of the PI3K pathway may be involved in HNSCC progression. This aligns with reports that find, in addition to *PIK3CA* mutation, other PI3K pathway components such as *PIK3R1* and

PIK3R2, when mutated, can drive cell growth/survival.(*120*) Although the effects of multiple PI3K pathway mutations on cancer cell growth or progression have not been investigated, genetic alterations at multiple nodes in this oncogenic pathway, a common feature of many solid tumors, may identify a subgroup of cancer patients whose tumor biology is heavily dependent on the PI3K pathway, and might therefore respond to treatment with PI3K pathway inhibitors. This warrants future investigation in appropriate preclinical models.

We found *PIK3CA* to be the most commonly mutated oncogene in our cohort. Although our current data does not allow for detailed mechanistic explanations of the impact of different *PIK3CA* alterations in HNSCC at this time, it does offer the opportunity to generate hypotheses towards such explanations. Further, we implicate this classic oncogene in the molecular pathophysiology of HNSCC by demonstrating that *PIK3CA* amplification and mutation, including some non-hotspot mutations, can contribute to such cancerous phenotypes as growth, survival, and invasion in engineered models of HNSCC (Figure 8, Figure 12, Figure 13), as has been widely reported in other cancers.(*121*)

The frequency with which the PI3K pathway is altered in HNSCC, and the data we have presented showing its ability to contribute to the disease process, make it a worthwhile therapeutic target. Using endogenous and engineered HNSCC cell lines as well as PDXs, we demonstrated that the PI3K inhibitors BKM-120 and BYL-719 have cytotoxic activity in preclinical models of HNSCC. The evidence in these preclinical models that *PIK3CA* mutation may serve as a predictive biomarker for response to targeted PI3K inhibition, is mixed. Engineered UPCI-52 (SD-1) cells were not sensitized to BYL-719 treatment when expressing mutant *PIK3CA* constructs (Figure 15). However, HNSCC cell lines harboring endogenous *PIK3CA*(H1047R) mutations were generally more sensitive than *PIK3CA*(WT) cells to treatment

with BYL-719 (Figure 16). Both BYL-719 and BKM-120 demonstrated broad efficacy *in vitro* across our panel of cell lines, with IC50 values in the low μM range in almost every case (Figure 16 and Table 5). *In vivo,* 4 unique HNSCC PDXs were responsive to BYL-719 treatment. That tumor regression vs growth inhibition alone was initially seen in the *PIK3CA*-mutant PDXs vs the *PIK3CA*-WT PDXs respectively, suggests that *PIK3CA*-mutant tumors may be more sensitive to targeted PI3K inhibitors, at least initially (Figure 17). But the potential for acquired resistance to targeted treatment that was observed, most prominently in the HPV(-)/*PIK3CA*(M1043V) PDX, calls the long term efficacy of these agents in HNSCC, with or without *PIK3CA* mutations, into question (Figure 17).

The eventual development of resistance to targeted agents, including PI3K inhibitors, given as monotherapy is a well-established phenomenon in cancer, especially in solid tumors with high levels of intra-tumor mutational heterogeneity.(*122*) To date, in the advanced stage patients who have received and initially responded to BYL-719, development of resistance has been seen in virtually every case.(*113, 114, 123, 124*) Appropriate combination therapy can delay and/or overcome this resistance.(*113, 114*) When the HPV(+)/*PIK3CA*(E542K,F744L) PDX (Figure 17) was treated with a dual PI3K/MTOR inhibitor, BEZ-235, no sign of potential acquired resistance was observed with prolonged treatment (Figure 3 in Lui, Hedberg, Li, *et al*. 2013).(*85*) Early-phase clinical trial results in patients with solid tumors, and a variety of reports, including our own, in preclinical models of cancer, have demonstrated an association between response to PI3K pathway inhibitors and *PIK3CA* mutation, primarily hotspot mutations.(*85, 113, 114, 123, 125, 126*) Here, we show that treatment with BYL-719, one of the most promising PI3K inhibitors currently in clinical development, is broadly effective across HNSCC cell lines

and PDXs. Ultimately, the validity of *PIK3CA* status as a predictive biomarker for response to targeted PI3K inhibitors must established in clinical trials, and such studies are underway.

These cumulative findings identify the PI3K pathway as the most frequently mutated mitogenic pathway, and *PIK3CA* as the most commonly mutated oncogene, in HNSCC tumors. The frequency with which these alterations occur coupled with the ability of *PIK3CA* mutant and WT constructs to contribute to cancerous phenotypes such as growth, survival/proliferation, and invasion in engineered HNSCC cell lines suggests that this pathway is important to the biology of this disease. Results from experiments involving treatment with targeted PI3K inhibitors, taken together, suggest that PI3K-pathway inhibition may be an effective approach to treating HNSCC tumors, especially those with PI3K mutations. These agents are likely to be even more efficacious in the setting of combination therapies, though additional research and clinical validation of optimized combination therapies, and of *PIK3CA*/PI3K-pathway alterations as predictive biomarkers in HNSCC is required.

3.0 GENETIC ALTERATIONS IN METASTATIC/RECURRENT HNSCC

3.1 INTRODUCTION

HNSCC is the 7th most common incident cancer worldwide with more than 600,000 new cases each year.(*8*) The major risk factors for HNSCC are tobacco use, alcohol consumption, and/or infection with oncogenic strains of HPV.(*11*) Despite advances in treatment, survival has improved only modestly over three decades, and this persistent mortality is largely due to high rates of regional metastasis and locoregional recurrence.(*10*)

HNSCC metastases almost always arise first in the cervical lymph nodes.(*127*) Most patients are diagnosed with locally advanced disease and more than half have cervical lymph node metastases present at initial diagnosis.(*128*) Clinically, this is classified as *synchronous* nodal metastasis, and it is a poor prognostic indicator. Five year adjusted survival rates range from ≈30-60% for patients with synchronous nodal metastasis, compared with ≈85% for patients whose cancer has not metastasized.(*129*) Patients with synchronous nodal metastasis are also more likely to develop locoregional or distant metastatic recurrence of HNSCC after completing curative-intent therapy.(*130*)

Rates of recurrence following treatment of an index HNSCC tumor range from ≈25-50%, depending on the anatomical location of the primary tumor, stage at diagnosis, and HPV status.(*21*) Relapse after initial curative-intent treatment is known as *metachronous* recurrence.

In patients who do recur, ≈25-50% will recur more than once.(*21*) Recurrent tumors are more likely to be locoregional than distant.(*131*) Median survival following metachronous recurrence is <22 months in patients who are eligible for salvage surgery or re-irradiation, and <12 months for those receiving palliative chemotherapy alone.(*21*) Recurrence in HNSCC is often resistant to standard therapy, and is generally considered incurable.(*21, 22*)

The genetic alterations underlying nodal metastasis and recurrence are incompletely understood, and present a fundamental challenge to the development of more effective therapies. Next generation sequencing of several cancers has greatly expanded our appreciation of the genetic heterogeneity that exists in a variety of malignancies. Cumulative evidence implicates a complex, nonlinear, branched evolution model of subclonal populations within tumors that defines dynamic processes which likely mediate the expansion of minor subclones under the selective pressure of therapy, culminating in metachronous recurrences that are often treatment resistant.(*132, 133*) In hematological malignancies, distinct patterns of clonal evolution in the development of therapeutic resistance and relapse have been reported.(*134, 135*) In melanoma treated with MEK inhibitors, sequencing of recurrent tumors has identified novel, activating mutations in *MEK2* that confer resistance to targeted therapy.(*136*) WES studies have revealed mutational signatures induced by temozolomide, which alkylates guanine residues, in recurrent glioma, demonstrated inherent functional variability in recurrent clones that impact response to chemotherapy in colorectal cancer, and have shown that treatment can be guided by the sequencing of metastases or circulating tumor cells in breast cancer.(*137-140*)

To date, large scale WES studies have not characterized the genetic alterations associated with synchronous nodal metastasis or metachronous recurrence in HNSCC. Microarray-based expression profiling of unmatched normal mucosa, primary tumors, lymph node metastases, and

recurrent HNSCC lesions identified mRNA expression signatures predictive of metastasis and recurrence, but the clinical impact of these observations remains unrealized.(*141-144*) Only one study included analysis of patient-matched index primary tumors and synchronous nodal metastases, and found that the expression profiles of primary tumors were largely preserved in their respective metastatic lymph nodes.(*144*) WES studies to date in HNSCC have been conducted almost entirely in newly diagnosed primary tumors.(*39-41, 85, 86, 103-105*) In an effort to define and target the genetic alterations underlying metastasis and recurrence in HNSCC, we performed WES of patient-matched tumor pairs in the setting of synchronous nodal metastasis or metachronous recurrence.

3.2 MATERIALS AND METHODS

3.2.1 Patient Selection and DNA Extraction

The patient cohort consisted of HNSCC patients treated at the University of Pittsburgh Medical Center otolaryngology clinics who were enrolled in an observational research study supported by the University of Pittsburgh's Specialized Program of Research Excellence (SPORE) in head and neck cancer. All participants provided written informed consent and the study was approved by the University of Pittsburgh Institutional Review Board. Fresh frozen tissue was banked in the University of Pittsburgh head and neck tissue bank, and made available for sequencing in this project as previously described.(*41*) Genomic DNA for whole exome sequencing was extracted from whole blood and fresh frozen tumor tissue using the DNeasy Blood & Tissue Kit (Qiagen) according to the manufacturer's instructions.

3.2.2 Whole Exome Sequencing and Analysis

WES in this study was performed in collaboration with Dr. Richard Lifton's group at Yale University. The sequencing and bioinformatics processing described briefly below was conducted by Dr. Lifton's group and the genomics CORE laboratories at Yale. Following sequencing, alignment, and calling of mutations and copy number changes by their automated pipeline, the results were conveyed to us. From that point, Dr. Gerald Goh (a graduate student in Dr. Lifton's lab at the time) and I, performed independent analyses of the data and worked together to reach a consensus interpretation of the results which we reported together and which guided the functional experiments that I designed and performed. Targeted capture was performed using the NimbleGen 2.1 Exome reagent followed by sequencing on the Illumina platform, and downstream processing performed as previously described.(*145, 146*) Briefly, sequences were aligned to NCBI Build 37 of the human genome using the ELAND program (Illumina). Somatic mutations were called based on the significance of differences in reference and non-reference read distributions between tumor and matched normal samples. Under the assumption that few if any clonal somatic changes should occur in blood DNA, as a control the same test was applied to germline DNA using tumor DNA as reference, which as previously shown yields high validation rates of putative somatic mutations.(*147*) If a mutation was observed in a metastatic or recurrent tumor, it was considered present in the index primary tumor if there were at least 5 independent reads supporting the variant call, and vice-versa. Calls were further evaluated by manual inspection of read alignments. Additional tissue samples from 6 tumors (the primary tumors of patients PY-1, 7, 13, 19, 24, and the recurrent tumor from patient PY-3) underwent whole exome sequencing under the auspices of other studies.(*40, 41*) The alternative informatics pipeline and sequencing methods are described in the published reports.

In these 6 tumors, 78% of the mutations detected by the sequencing and bioinformatics pipeline in this study were also identified in the other studies. A lack of hotspot mutations in *PIK3CA* (AAs 542, 545 and 1047) was confirmed by Sanger sequencing of the tumor samples used in this study (data not shown).

MutSigCV (v1.3.01) was used to determine if genes were mutated more often than expected by chance.(*148*) CNVs were identified by comparing coverage depth ratios of tumor and matched normal samples after normalizing for mean coverage depth of each exome, and changes in minor allele frequency at informative SNPs. GISTIC2.0 was used to assess the significance of recurrent CNVs, and the PyClone algorithm was used to assess clonality, as described previously.(*149, 150*)

3.2.3 Cell Cultures

The HNSCC cell lines BICR 18 and PE/CA-PJ34(clone C12) were obtained from Sigma-Aldrich; UPCI 15B was a kind gift from Dr. Theresa Whiteside (University of Pittsburgh Cancer Institute). The HNSCC cell lines were grown in the following culture mediums, each containing 10% fetal calf serum and 1× penicillin/streptomycin solution (Invitrogen): UPCI 15B in Dulbecco's Modifed Eagle Medium (DMEM), BICR 18 in DMEM with 2mM glutamine (Mediatech, Inc.) and 0.4 μg/mL hydrocortisone, and the PE/CA-PJ34(clone C12) cells in Iscove's Modifed Dulbecco Minimum Essential Medium with 2mM glutamine (Mediatech, Inc.). All cell lines were maintained in a humidified cell incubator at 37°C, 5% CO_2.

3.2.4 Drug Treatment and Survival Assays

HNSCC cells were plated at the indicated concentrations in 48 well culture plates overnight and treated with the indicated concentrations of dasatinib (Bristol-Meyers Squibb) for 48 hours, at which point, MTT (Sigma-Aldrich) was performed according to manufacturer's instructions as previously described and detailed in figure legends.(*85*) Growth curves were generated using GraphPad Prism 6 software as outlined in the statistics section.

3.2.5 Invasion Assays

Invasion of BICR 18 cells in the presence or absence of dasatinib was tested using Biocoat migration and Matrigel® coated invasion Chambers (BD Biosciences), according to the manufacturer's instructions. Briefly, 2.0×10^4 BICR 18 cells suspended in DMEM were placed in migration (uncoated) chambers or invasion (matrigel-coated) chambers submerged in full media. They were treated with DMSO (n=2) or the indicated doses of Dasatinib (n=3) for 24 hrs. The experiment was repeated 3 times and cells were counted and averaged from 4 photomicrographs from each membrane. Bar graphs and statistical analysis generated in GraphPad Prism 6 as outlined in the statistics section.

3.2.6 *DDR2* Knockdown

BICR 18 cells were plated at 10% confluence in 96 well plates overnight, treated with 8μL polybrene, and infected with 15μL of MISSION® pLKO.1-puro lentiviral particles containing control or α-*DDR2* shRNA constructs (α-*EGFP* control, 121117 5′-CCGGCCCATG-

CCTATGCCACTCCATCTCGAGATGGAGTGGCATAGGCATGGGTTTTTG-3′, or 195105 5′-CCGGCGAAACTGTTTAGTGGGTAAGCTCGAGCTTACCCACTAAACAGTTTCGTTT-TTTG-3′) (Sigma-Aldrich). 72 hours later, cells were split into 96 well plates and cultured for 2 weeks in media containing puromycin to derive subclones expressing the shRNA constructs. Cells were then cultured in full medium without puromycin until sufficient volumes were obtained for phenotypic analyses (3-6 weeks).

3.2.7 Cloning and Mutagenesis

WT *EGFP* was cloned into the retroviral vector, pMXs-puro (Cell Biolabs, Inc.). WT *DDR2* cloned into a pWZL-Blast vector was a kind gift from Dr. Peter Hammerman and was used as a template for site directed mutagenesis using the QuikChange XL Site-Directed Mutagenesis Kit (Stratagene).(*151*) Mutagenesis of the *DDR2* WT gene was performed according to the manufacturer's instructions and confirmed by Sanger sequencing using the primers below.

Table 7. *DDR2* Site Directed Mutagenesis Primers

DDR2(I474M)_sense	5'-gacttacgatcgcatgtttccccttcgccct-3'
DDR2(I474M)_antisense	5'-agggcgaaggggaaacatgcgatcgtaagtc-3'
DDR2(R709*)_sense	5'-ctctcttaattttgttcactgagatctggccacacga-3'
DDR2(R709*)_antisense	5'-tcgtgtggccagatctcagtgaacaaaattaagagag-3'
DDR2(I724M)_sense	5'-gtgggtaagaactacacaatgaagatagctgactttggaa-3'
DDR2(I724M)_antisense	5'-ttccaaagtcagctatcttcattgtgtagttcttacccac-3'

Table 8. *DDR2* Sequencing Primers

Primer Name	Sequence
DDR2 Seq 1	5'-CTTTATCCAGCCCTCAC-3'
DDR2 Seq 2	5'-TCAATTACAGTCGGGATGGC-3'
DDR2 Seq 3	5'-CGGCTATGACTATGTGGGCT-3'
DDR2 Seq 4	5'-CCCACAACCTATGATCCAATG-3'
DDR2 Seq 5	5'-CCACTATGCAGAGGCTGACA-3'
DDR2 Seq 6	5'-TCACTGAATACATGGAGAATGGA-3'
DDR2 Seq 7	5'-CAAGAACAGCCCTATTCCCA-3'
DDR2 Seq 8	5'-CCCTCAACCAGCCATTTGTC-3'

3.2.8 Mutant *DDR2* Expression

Retroviruses were generated using the Platinum Retrovirus Expression Systems (Cell Biolabs), Fugene® HD (Promega), and retroviral vectors carrying the gene of interest (pMXs-puro-*EGFP* as control, pWZL-Blast-*DDR2*(WT), pWZL-Blast-*DDR2*(mutants)), according to manufacturer's instructions. Briefly, $2x10^6$ PLAT-A cells were plated overnight in 10cm tissue culture dishes without antibiotics and transfected the next day with 3 µg of retroviral vector carrying the gene of interest (pMXs-puro-*EGFP* as control, pWZL-Blast-*DDR2*(WT), pWZL-Blast-*DDR2*(mutants)) using the Fugene HD kit (Promega) according to manufacturer's instructions. Two days after transfection, fresh retroviruses (in the supernatant of the PLAT-A cells) were collected by filtering through a 0.45 µm syringe filter. Fresh retroviruses were used for infection of UPCI-15B cells. UPCI-15B cells were plated to 20% confluence in a T75 flasks without antibiotics one day before infection. Infection of UPCI-15B cells was performed by adding 4.5ml of retrovirus to the cells mixed with 5.5ml of complete culture media without antibiotics. Then, 18-20 µl of polybrene (4 µg/µl, Sigma-Aldrich, St. Louis, MO) was added to the cells with

gentle mixing. Cells were then incubated at 37°C and 5% CO_2 for additional 72 hrs, and the infection medium was replaced with fresh complete medium after infection.

3.2.9 Western/Immuno Blotting

Lysates were collected as described and resolved on sodium dodecyl sulfate polyacrylamide gel electrophoresis (SDS-PAGE) gels and transferred to nitrocellulose membranes prior to antibody staining. Primary antibodies: α-DDR2 (#12133, Cell Signaling Technology, Inc.), α-β-tubulin (ab6046, Abcam), goat anti-rabbit IgG (H+L)-HRP conjugated secondary antibodies (#170-6515, BioRad), and Luminol reagent (sc-2048, Santa Cruz Biotech) were utilized.

3.2.10 Statistics

Mean values with SEM, from replicate experiments plated as indicated in figure legends, were plotted as mean values +/- SEM in Graphpad Prism 6. A sigmoidal dose response curve with automatic outlier elimination was applied to generate optimized datasets. The finalized datasets, with outliers removed, were used to generate growth curves using the least squares fit log(inhibitor) vs. normalized response-variable slope equation. The logIC50 values were compared using an extra sum of the squares F-test (null hypothesis = the logIC50 values are identical, the null hypothesis was rejected in cases where $p < 0.05$). For bar graphs, mean values with SEM were calculated and plotted as above, and compared using an unpaired, two-tailed T test with Welch's correction.

3.2.11 Study Approval

This study was approved by the University of Pittsburgh Institutional Review Board. All tissue samples were obtained from patients who provided written informed consent and were enrolled in an observational research study supported by the University of Pittsburgh's Specialized Program of Research Excellence (SPORE) in head and neck cancer.

3.3 RESULTS

3.3.1 Patient Characteristics and WES

The cohorts analyzed in this study were two groups of patients with HNSCC from the University of Pittsburgh; the "synchronous nodal metastasis" group and the "metachronous recurrence" group (Figure 20). The synchronous nodal metastasis group consisted of 13 patients contributing blood, primary tumor, and synchronous nodal metastases. The metachronous recurrence group consisted of 10 patients contributing blood, primary tumor, and recurrent tumor. All patients were treated with curative intent for the index tumor, and all metachronous recurrences underwent salvage therapy.

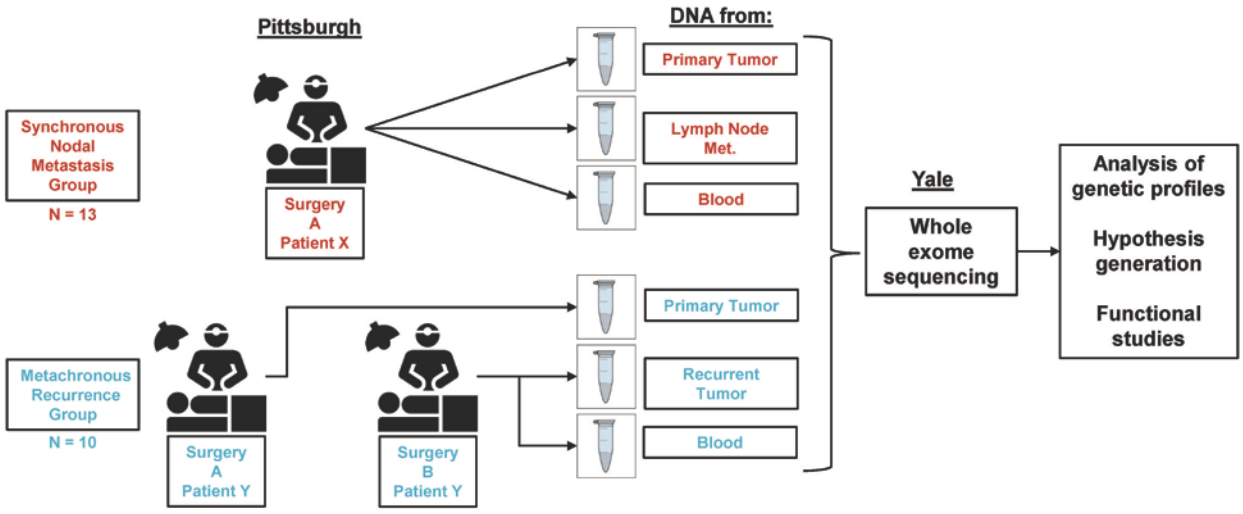

Figure 20. Patient Cohorts and Study Design.

To define and interrogate the genetic alterations underlying metastasis and recurrence in HNSCC, we analyzed two groups of patients. The synchronous nodal metastasis group consisted of 13 HNSCC patients that contributed normal tissue (blood), primary tumor tissue, and metastatic lymph node tumor tissue from a single time point. The metachronous recurrence group consisted of 10 HNSCC patients that contributed normal tissue (blood), primary tumor tissue, and recurrent tumor tissue from a later time point following relapse. Genomic DNA was isolated from this fresh frozen tissue and assessed by whole exome sequencing.

Clinical and pathologic characteristics were typical of a surgically treated HNSCC population, and are summarized in Table 9. Briefly, all patients were Caucasian, 83% of the patients were male (19/23), mean age at diagnosis was 61.9 ± 11.2 years (range: 44-79), 87% (20/23) had a history of significant tobacco exposure (generally >20 pack years), 74% (17/23) had documented alcohol use, and only 1 patient had HPV(+) disease. Of the 5 patients in the metachronous recurrence group with nodal disease at the time of initial diagnosis, all had evidence of extracapsular spread; as did 10 of the 13 patients in the synchronous nodal metastasis group.

The majority of the index primary tumors were located in the oral cavity (61%; n=14), with the remainder distributed between the larynx (22%; n=5) and pharynx (17%; n=4). As is commonly seen in HNSCC, most patients presented with advanced disease. Of the newly diagnosed index primary tumors, 25% and 70% were AJCC Stage III or IVA, respectively; metachronous recurrent tumors are not staged (Table 9).(*17*) All metachronous recurrences sequenced in this study were locoregional and, compared to their paired index primary tumors, 7/10 were located in different anatomic subsites of the head and neck (Table 9). Median time to recurrence in the metachronous recurrence group was 5.5 months (range 2.2-33.9) (Table 9). Two of 10 patients in the metachronous recurrence group received adjuvant radiation therapy, and 3 received adjuvant chemotherapy in combination with radiation, after resection of the index primary tumor (Table 9).

Table 9. Clinical Characteristics of HNSCC Patient Cohort.

All index primary tumors, synchronous nodal metastases, and metachronous recurrences were surgically resected. Site = anatomic location of primary tumor; OC = Oral Cavity, P = Pharynx, L = Larynx, LN = Lymph Node (cervical). RT = Radiation Therapy. Index primary tumors for patients PY-6, PY-8, and PY-10 were recurrences, which are not staged.

Metchronous Recurrence Group								
General Characteristics			Index Primary Tumor				Metachronous Recurrent Tumor	
Patient ID #	Gender	Age @ Dx (Yrs)	Site	Path. Stage	AJCC Stage	Adjuvant Treatment	Time to Recurrence (Months)	Site
PY-1	M	78	OC	T3 N1 M0	III	None	2.3	P
PY-3	F	67	OC	T2 N2B M0	IVA	RT	6.3	OC
PY-4	M	44	OC	T4A N2B M0	IVA	RT& Cisplatin & Vectibix	6.8	P
PY-5	M	52	OC	T3 N0 M0	III	None	4.3	L
PY-6	M	52	P	TX NX MX	n.a.	IMRT & Cetuximab & Pemetrexed	10.5	LN
PY-7	M	49	L	T4A N1 M0	IVA	None	2.9	LN
PY-8	M	76	OC	TX NX MX	n.a.	RT	33.9	P
PY-9	M	60	OC	T2 N0 MX	II	None	4.7	LN
PY-10	M	58	OC	TX NX MX	n.a.	None	2.2	OC
PY-11	M	74	OC	T3 N2C M0	IVA	RT & Cisplatin	9.7	OC

Synchronous Nodal Metastasis Group					
General Characteristics			Index Primary Tumor		
Patient ID #	Gender	Age @ Dx (Yrs)	Site	Path. Stage	AJCC Stage
PY-12	F	46	OC	T3 N2C M0	IVA
PY-13	M	53	OC	T3 N2B M0	IVA
PY-14	M	71	L	T3 N1 MX	III
PY-15	M	63	L	T3 N2C M0	IVA
PY-16	M	70	P	T1 N2B MX	IVA
PY-17	F	68	L	T4A N2A MX	IVA
PY-19	M	73	P	T2 N1 MX	III
PY-20	F	79	OC	T1 N1 MX	III
PY-21	M	49	L	T4A N2C MO	IVA
PY-22	M	49	OC	T4A N2C M0	IVA
PY-23	M	56	P	T4A N2B M0	IVA
PY-24	M	73	OC	T4A N2C M0	IVA
PY-25	M	64	OC	T1 N2 M0	IVA

Genomic DNA from patient matched tumor-pairs and peripheral blood mononuclear cells (PBMCs), was subjected to exome sequencing as described in methods. By design, tumors were sequenced to higher depth of coverage than normal samples (PBMCs). Normal samples were sequenced to a mean depth of 123 independent reads per targeted base, and tumors to a mean of 202 independent reads (Table S1 Hedberg, Goh, Chiosea, *et al.*, 2015 in press *JCI*). Somatic single nucleotide variants (SSNVs) and somatic copy number variants (SCNVs) were called (see methods), and tumor purity was estimated from deviation in minor allele frequency of heterozygous SSNVs in segments showing loss of heterozygosity (LOH) (Table S2 Hedberg,

Goh, Chiosea, *et al.*, 2015 in press *JCI*). In one primary tumor, two synchronous metastases, and one metachronous recurrence, estimated tumor purity was too low to yield high quality sequencing data (Table S2 Hedberg, Goh, Chiosea, *et al.*, 2015 in press *JCI*). These patients were not included in the analysis of genetic concordance between matched tumor pairs, but the tumors obtained from them that did yield high quality sequencing data were included when reporting overall mutation rates in each tumor type (11 total synchronous metastases and 9 total metachronous recurrences).

3.3.2 Genetic Profiles of Index Primary Tumors

Among 22 primary tumors, 1,961 SSNVs were identified in 1,666 genes. Tumors averaged 89.1 SSNVs (range 3 – 413), and the ratio of non-synonymous:synonymous variants in coding regions was 3.14:1. Analysis of mutation burden with MutSigCV revealed a single gene, *TP53,* with a significant excess of SSNVs (mutated in 13 tumors, $q=2.66x10^{-6}$).(*148*) We utilized the findings of Vogelstein *et al* (n=124), the TCGA Pan Cancer Effort (n=127), and the TCGA HNSCC cohort (n=11), to generate a composite list of 191 genes, which have either been established as cancer driving genes, and/or as genes which are significantly mutated in HNSCC (Cancer driver genes) (Table S3 Hedberg, Goh, Chiosea, *et al.*, 2015 in press *JCI*).(*40*, *152*, *153*) Forty-seven nonsynonymous SSNVs were identified in 28/191 cancer driver genes, which is significantly greater than expected by chance ($p=5.2 \times 10^{-5}$, Monte Carlo) (Table S4 Hedberg, Goh, Chiosea, *et al.*, 2015 in press *JCI*).

GISTIC2 analysis of SCNVs in the primary tumors of our cohort identified 8 significantly amplified regions, including portions of 3q and 8q which were amplified in a majority of tumors in the TCGA HNSCC cohort, as well as 3q26.32 ($q=4.95x10^{-6}$), 7p11.2

($q=2.62x10^{-3}$), 11q13.3 ($q=1.14x10^{-3}$), which were also significantly amplified in the TCGA HNSCC cohort, and overlap well-known cancer driver genes *PIK3CA*, *EGFR*, and *CCND1*, respectively (Figure S2 Hedberg, Goh, Chiosea, *et al.*, 2015 in press *JCI*).(*40, 149*) We observed 8 segments with significant recurrent somatic deletions, including portions of 3p and 8p which were lost in a majority of tumors in the TCGA HNSCC cohort, as well as 9p21.3 ($q=0.15$), which was also significantly deleted in the TCGA HNSCC cohort, and overlaps *CDKN2A* and *CDKN2B* (Figure S2 Hedberg, Goh, Chiosea, *et al.*, 2015 in press *JCI*).(*40, 149*) Overall, the genetic profiles of the index primary tumors in this cohort are similar to those reported in other WES studies of primary HNSCC.(*39-41, 85, 86, 103-105*)

Index primary tumors from patients in the synchronous nodal metastasis group had a significantly greater mutational burden than those from patients in the metachronous recurrence group (125.9 ± 103.2 versus 36.0 ± 31.6 SSNVs, $p=9.94 \times 10^{-3}$, two-tailed T-test). Even after excluding PY-15 (413 SSNVs) as an outlier, there is a significant difference in number of SSNVs between the two groups (102.0 ± 59.2 versus 36.0 ± 31.6, $p=4.21 \times 10^{-3}$, two-tailed T-test). Similarly, SCNV burden in the index primary tumors differed significantly, with a higher fraction of the genome in index primary tumors from the synchronous nodal metastasis group harboring SCNVs than those in the metachronous recurrence group (0.36 ± 0.13 versus 0.19 ± 0.13, n=13 and n=9, p=0.017, Mann-Whitney) (Table S5 Hedberg, Goh, Chiosea, *et al.*, 2015 in press *JCI*).

3.3.3 Genetic Profiles of Synchronous Nodal Metastases

In the synchronous nodal metastasis group, we obtained high quality sequencing data from the matched PBMCs, primary tumor, and synchronous nodal metastases of 11 patients, allowing for the analysis of genetic concordance within matched tumor pairs in these patients (Figure 21A). The nodal metastases in these patients harbored 1,499 SSNVs in 1,310 genes (Figure 21A). Thirty-three nonsynonymous SSNVs in the metastases were found in 23/191 cancer driver genes, which is significantly greater than expected by chance (p=0.0013, Monte Carlo) (Table S6 Hedberg, Goh, Chiosea, *et al.*, 2015 in press *JCI*).(*40, 152, 153*) In the primary tumors of these 11 patients, 84.8% (979/1154) of nonsynonymous SSNVs, and 94.1% (32/34) of nonsynonymous SSNVs in cancer driver genes, were transmitted to the nodal metastases (not a significantly different rate of transmission, p=0.15, Fisher test) (Figure 21A). In the nodal metastases of these 11 patients, 13.9% (208/1499) of the SSNVs were identified as newly arisen, i.e. absent in the primary tumor (see methods), including one new mutation in a cancer driver gene, *MLL4*, in PY-15 (Figure 21A, and Table S6 Hedberg, Goh, Chiosea, *et al.*, 2015 in press *JCI*).

The PyClone algorithm was used to identify and quantify clonal populations in the primary and metastatic tumors.(*150*) In 10 of 11 patients, ≥80% of the SSNVs identified in the nodal metastases were transmitted from the primary tumor. In those 10 patients, PyClone analysis revealed that the majority of SSNVs were transmitted in a stable fashion, with the primary clone (containing >50% of SSNVs) being present at similar cellular prevalence in both the primary and metastatic tumors (Table S7 Hedberg, Goh, Chiosea, *et al.*, 2015 in press *JCI*). In the 11th patient, PY-16, 44% of SSNVs were unique to the metastatic tumor (clusters 4 and 5

in Figure 21B), which had lost 25.2% of the SSNVs found in the primary tumor (cluster 1 in Figure 21B).

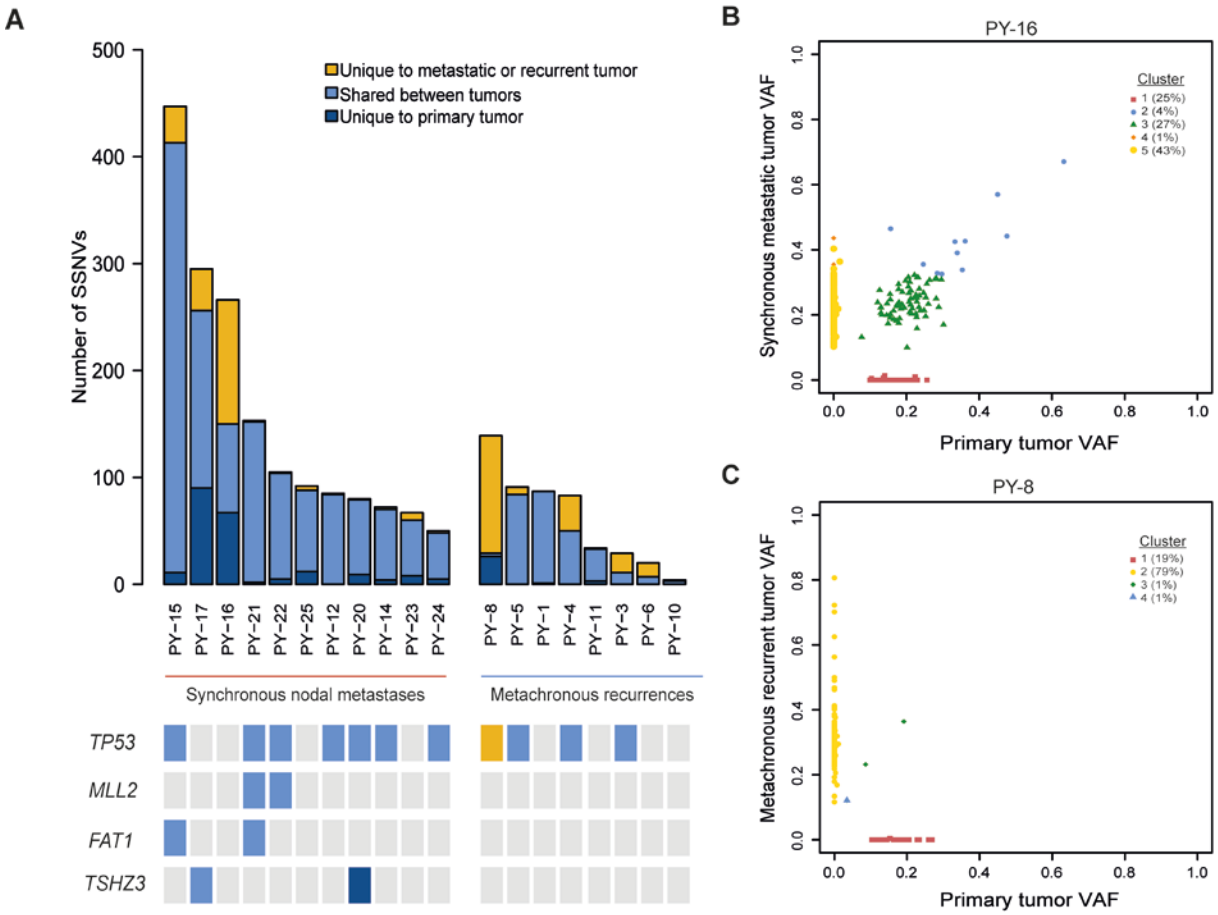

Figure 21. Somatic SSNVs in HNSCC Tumors.

(A) Top panel: Distribution of somatic SNVs (SSNVs) in each tumor pair; synchronous nodal metastases on the left, metachronous recurrences on the right. Lower panel: panels describing presence of SSNVs in select cancer driver genes in each tumor pair. SSNVs were identified as unique to primary tumor (dark blue), shared between paired tumors (cornflower blue), or unique to metastasis or recurrent tumor (gold). **(B)** Differences in subclonal architecture in the primary and synchronous nodal metastatic tumors from patient PY-16. 44% of SSNVs were private to the metastatic tumor (clusters 4 and 5) and 25% private to the primary tumor (cluster 1). **(C)** SSNVs in the samples from patient PY-8 are unique to the primary tumor (cluster 1) or the recurrent tumor (cluster 2), shared SSNVs (clusters 3 and 4) are germline. VAF: Variant Allele Frequency. Sequencing data for this figure was

generated in collaboration with Yale University as described in methods. The consensus interpretation and figure preparation represents a collaborative effort between myself and Dr. Goh, based upon our independent analyses of the sequencing results Dr. Goh applied the PyClone algorithm to our data.

GISTIC2 analysis of SCNVs in the synchronous nodal metastases revealed 4 regions of significant focal amplification and 4 regions of significant focal deletion with copy number gains encompassing *EGFR*, and *CCND1*, and copy number losses encompassing *CDKN2A* and *CDKN2B* (Figure S3 Hedberg, Goh, Chiosea, *et al.*, 2015 in press *JCI*).(*149*) The copy number profiles between matched primary tumors and synchronous nodal metastases were not significantly different (fraction of genome harboring SCNVs 0.38 ± 0.14 versus 0.32 ± 0.14, n=11, p=0.48, Mann-Whitney, Table S5 and Figure 2A Hedberg, Goh, Chiosea, *et al.*, 2015 in press *JCI*). Many of the significant SCNV peaks identified in the nodal metastases of these patients arose in the primary tumor; 3/4 regions of significant focal amplification identified in the nodal metastases were also significantly amplified in the primary tumors (3q26.32, 7p11.2, and 11q13.3) (Figure 2B Hedberg, Goh, Chiosea, *et al.*, 2015 in press *JCI*).

Among these 11 patients, 60 genes harbored nonsynonymous mutations in 2 or more patients (Figure 21A). Three of those 60 genes: *TP53*, *FAT1*, and *MLL2*, are cancer driver genes. Two genes were newly mutated in the synchronous metastases of 2 patients: *C17orf104*, and *ITPR3* (p=0.37, Monte Carlo) (Table 10). The precise function(s) of *C17orf104* has not been described. Whereas *ITPR3* encodes a calcium channel receptor that binds inositol 1,4,5-trisphosphate, mediates intracellular calcium levels, and is important to exocrine functions that influence metabolism and growth.(*154, 155*) *ITPR3* has been implicated in breast cancer proliferation, and elevated expression levels correlate with increased invasion, metastasis and decreased survival in colorectal cancer, and with dissemination of gastric cancers.(*156-158*)

Table 10. Genes that are Exclusively Mutated in Two Synchronous Nodal Metastases.

AA: amino acid, Ref: # of reference sequence reads, Nonref: # of nonreference sequence reads, MAF: minor allele frequency (adjusted for estimated tumor purity).

Gene	Patient	AA Change	Primary			Metastasis		
			Ref	Nonref	MAF	Ref	Nonref	MAF
C17orf104	PY-16	H846Y	217	0	0	176	56	0.241
	PY-21	Q145*	234	0	0	215	34	0.137
ITPR3	PY-15	R149L	44	0	0	55	32	0.368
	PY-16	R64H	164	0	0	137	31	0.185

3.3.4 Genetic Profiles of Metachronous Recurrent Tumors

In the metachronous recurrence group, we obtained high quality sequencing data from the matched PBMCs, primary tumor, and metachronous recurrent tumors of 8 patients, allowing for the analysis of genetic concordance in matched tumor pairs from these patients (Figure 21A, and Table S2 Hedberg, Goh, Chiosea, *et al.*, 2015 in press *JCI*). The metachronous recurrent tumors in these 8 patients harbored 457 SSNVs in 441 genes. Nine nonsynonymous SSNVs were found in 6/191 cancer driver genes, this number being significantly greater than expected by chance (p = 0.019, Monte Carlo) (Table S9 Hedberg, Goh, Chiosea, *et al.*, 2015 in press *JCI*).(*40, 152, 153*) In the primary tumors from these 8 patients, 90.1% (274/304) of SSNVs overall, and 100% (5/5) of SSNVs in cancer driver genes, were transmitted to the metachronous recurrent tumors (Figure 21A). In the metachronous recurrences of these 8 patients, 40.0% (183/457) of SSNVs were identified as newly arisen (Figure 21A). The copy number profiles between matched primary tumors and metachronous recurrent tumors were not significantly different (fraction of

genome harboring SCNVs 0.21 ± 0.13 versus 0.34 ± 0.12, p=0.05, n=8, Mann-Whitney, Table S5 and Figure 2C Hedberg, Goh, Chiosea, *et al.*, 2015 in press *JCI*). GISTIC2 analysis of these 8 primary tumor-metachronous recurrence pairs identified no regions of significant focal amplification or deletion in the primary tumors, whereas 4 and 6 regions of significant focal amplification and deletion were observed in the recurrent tumors, respectively, with copy number gains overlapping *PIK3CA, NFIB,* and *CCND1*, and copy number losses overlapping *TATDN2*, and *FAT1* (Figure 2D and Figure S5 Hedberg, Goh, Chiosea, *et al.*, 2015 in press *JCI*).(*149*)

The PyClone algorithm was used to determine if the metachronous recurrent tumors were largely clonal, as was observed in the synchronous nodal metastases.(*150*) The total mutation load in the tumor pairs from patients PY-3, PY-6, PY-7 and PY-10 was too low (<30 SSNVs per pair) for analysis with this technique. In the metachronous recurrent tumors from patients PY-1, PY-5, and PY-11, ≥90% of the SSNVs identified were transmitted from the primary index tumor and present at similar cellular prevalence (Table S7 Hedberg, Goh, Chiosea, *et al.*, 2015 in press *JCI*). In the metachronous recurrent tumor from patient PY-4, 60.2% of the SSNVs identified were transmitted from the primary index tumor, and the recurrence is composed of a set of SSNVs seeded from the primary tumor, present at high cellular prevalence (0.9-1.0), and set of SSNVs unique to the metachronous recurrent tumor (40%) present at a moderate cellular frequency (a subclonal population) (Figure S4 Hedberg, Goh, Chiosea, *et al.*, 2015 in press *JCI*). In patient PY-8, the metachronous recurrent tumor is genetically distinct from the index primary tumor, with 110 and 26 SSNVs unique to the metachronous recurrent and index primary tumors respectively (clusters 1 and 2); only 3 SNVs, all of which were also detected at trace levels in the matched normal tissue, were shared between the two tumors (clusters 3 and 4), demonstrating

that this is a true second primary tumor (SPT) (Figure 21C). Also, newly arisen mutations were identified in 4 cancer driver genes of this SPT: *KDM5C, POLQ*, *SF3B1*, and *TP53* (Table S8 Hedberg, Goh, Chiosea, *et al.*, 2015 in press *JCI*).

Among the 8 patients with high quality sequencing data from all three tissue samples, 4 genes: *DDR2*, *OR7A5*, *SYNE1*, and *TP53* harbored nonsynonymous mutations in 2 or more patients. *DDR2* was the only gene with newly acquired mutations in the metachronous tumors of 2 patients, PY-3 and PY-8 (Table 11, Figure 22 and Figure 23). *DDR2* encodes the discoidin domain receptor 2, which is a collagen-stimulated receptor tyrosine kinase implicated in a wide range of processes including regulation of epithelial to mesenchymal transition (EMT), and osteogenic/chondrogenic differentiation.(*159, 160*) Although the functional mechanisms of *DDR2* expression and/or mutation in disease are incompletely understood, it has been implicated in cellular adhesion, migration, invasion, and metastasis; in prostate cancer, breast cancer, and recently, HNSCC.(*161-164*) In total, *DDR2* mutations were observed in 3 of the 19 patients whose tumor pairs had reliable WES data (Table 11). A *DDR2*(I724M) mutation was identified in both the index primary tumor and synchronous nodal metastasis of patient PY-22 (Table 11).

Table 11. *DDR2* is Exclusively Mutated in Two Metachronous HNSCC Recurrences.

AA: amino acid, Ref: # of reference sequence reads, Nonref: # of nonreference sequence reads, MAF: minor allele frequency (adjusted for estimated tumor purity).

Gene	Patient	AA Change	Primary			Metachronous Recurrence		
			Ref	Nonref	MAF	Ref	Nonref	MAF
DDR2	PY-3	p.R709*	77	0	0	91	16	0.15
	PY-8	p.I474M	190	0	0	141	50	0.262
Gene	**Patient**	**AA Change**	**Primary**			**Synchronous Nodal Metastasis**		
			Ref	**Nonref**	**MAF**	**Ref**	**Nonref**	**MAF**
DDR2	PY-22	p.I724M	104	74	0.42	111	50	0.31

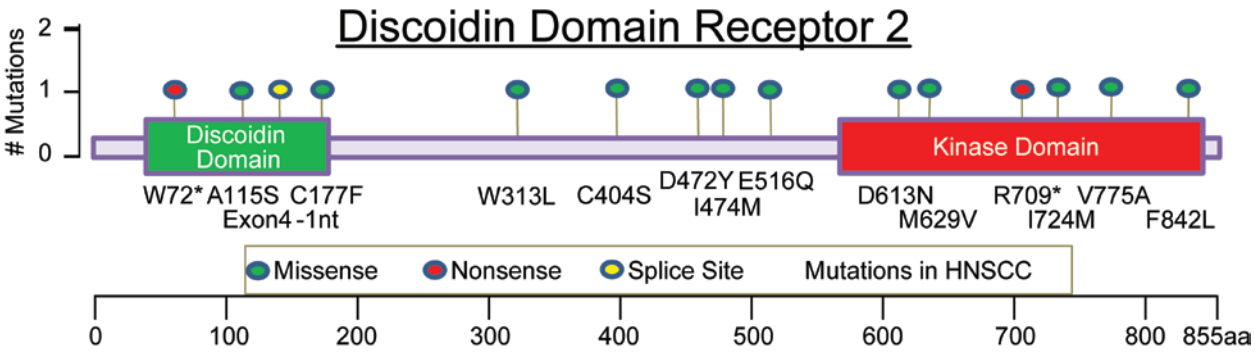

Figure 22. *DDR2* Mutations in HNSCC.

The genetic alterations in *DDR2* identified in our cohort, and the previously reported, transcript-altering, *DDR2* mutations identified in other sequencing studies of primary HNSCC tumors are displayed. 2/9 (22.2%) metachronous recurrent tumors sequenced in this study had newly arisen *DDR2* mutations vs. 12/658 (1.8%) newly diagnosed primary HNSCC tumors in other studies. aa: amino acid

Patients PY-3 and PY-8 both developed metachronous recurrences within the field of radiation therapy following resection of their index primary tumors. *DDR2*(R709*) and *DDR2*(I474M) mutations were identified in their metachronous recurrent tumors, respectively, and appear to be newly arisen; as they were not identified in the paired index primary tumors from these patients. However, the depth of sequencing achieved in this study was not sufficient to rule out the possibility that these mutations were present in rare subclones in the primary tumors. The spectrum of *DDR2* mutations in human HNSCC, including the new mutations reported here, is shown in figure 3.(*39-41, 85, 86, 103-105*) Figure 23 summarizes the clinical history of the two patients (PY-3 and PY-8) whose recurrent tumors were found to harbor new *DDR2* mutations. Several *DDR2* mutations, identified in squamous cell carcinoma of the lung, have been shown to be oncogenic, and/or confer high sensitivity to Src-family kinase (SFK)

inhibitors both in vitro and in vivo.(*151*, *165*) *DDR2* mutations in recurrent/metastatic HNSCC could have important clinical implications, as significant clinical response to the SFK inhibitor, dasatinib, has been reported in two patients with squamous cell carcinoma of the lung harboring *DDR2*(S768R) mutations.(*151*, *166*)

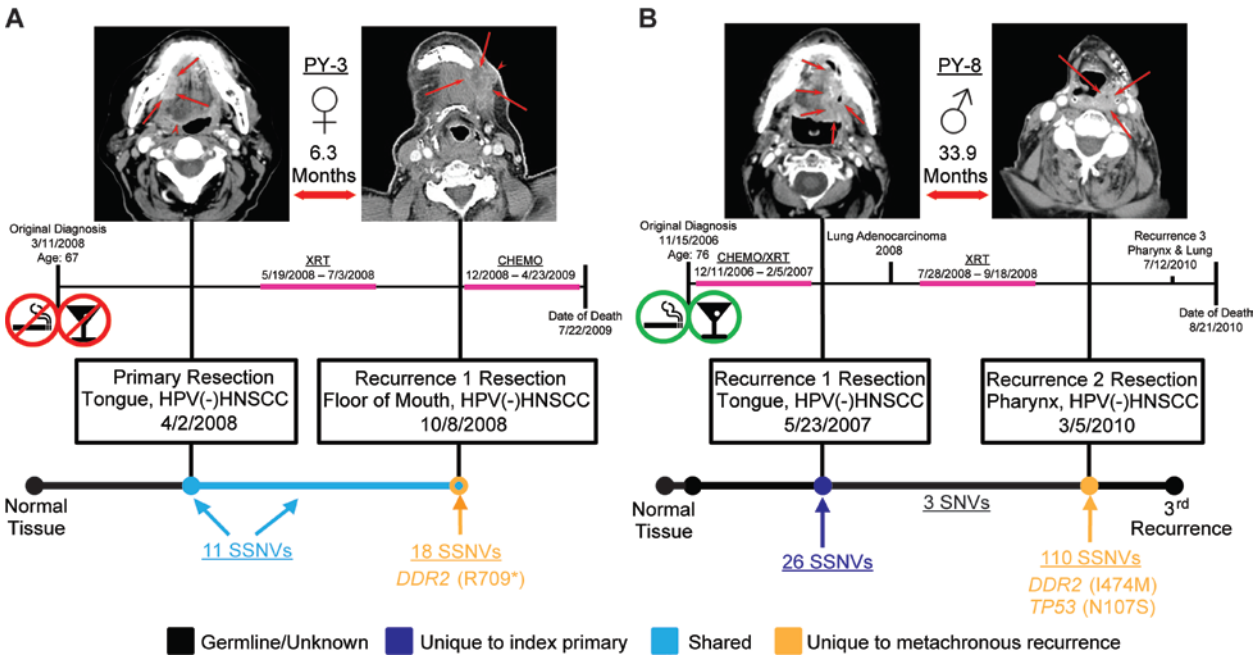

Figure 23. Disease Evolution in Patients with Newly Arisen DDR2 Mutations

The clinical histories of patient PY-3 **(A)** and patient PY-8 **(B)** are shown. Index primary and metachronous recurrent tumors assessed via WES are outlined and presented with CT imaging of the respective tumors. Treatments between cancer events are illustrated on the timeline, and the time to recurrence between sequenced tumors is indicated in months. Below each timeline is the mutational burden of each sequenced tumor for PY-3 and PY-8, respectively. SSNVs are defined as germline/unknown (black), unique to index primary tumor (dark blue), shared between paired tumors (cornflower blue), or unique to metachronous recurrent tumor (gold). XRT: radiation therapy, CHEMO: chemotherapy

3.3.5 HNSCC Cell Lines with *DDR2* Mutations are Sensitive to Dasatinib

To investigate whether *DDR2* mutations might serve as predictive biomarkers of dasatinib (a multi-kinase inhibitor with off-target activity against *DDR2)* sensitivity in HNSCC, we treated a panel of HNSCC cell lines with dasatinib. BICR 18 harbors an endogenous *DDR2*(D590G) mutation, whereas PE/CA-PJ34 (clone C12) is known to have WT *DDR2*, and UPCI 15B also has WT *DDR2*, by Sanger sequencing (data not shown).(*101*) By MTT assay, following 48 hours of dasatinib treatment, these three cell lines were found to have IC50 values of 5.608×10^{-8} (M), 5.426×10^{-7} (M), and 2.211×10^{-6} (M), respectively (Figure 24A). In addition to its potent cytotoxic effect on BICR 18 cells at 48 hours, administration of dasatinib in the setting of 24 hour matrigel invasion assays significantly inhibited the invasion of BICR 18 cells in a dose-dependent fashion (Figure 24B&C). The sensitivity of BICR 18 cells to dasatinib was attenuated to a statistically significant degree in the setting of *DDR2* knockdown, implicating *DDR2* in the marked sensitivity of this mutant HNSCC cell line to dasatinib (Figure 25). Similarly, when the most dasatinib-resistant HNSCC cell line from our panel, UPCI 15B, was engineered to express the *DDR2*(R709*) mutation, identified in the metachronous recurrent tumor of patient PY-3, statistically significant sensitization to dasatinib treatment compared to *EGFP* control and WT *DDR2* was observed (Figure 26). Taken together, these data suggest that *DDR2* status may serve as a biomarker for response to SFK inhibitors in HNSCC.

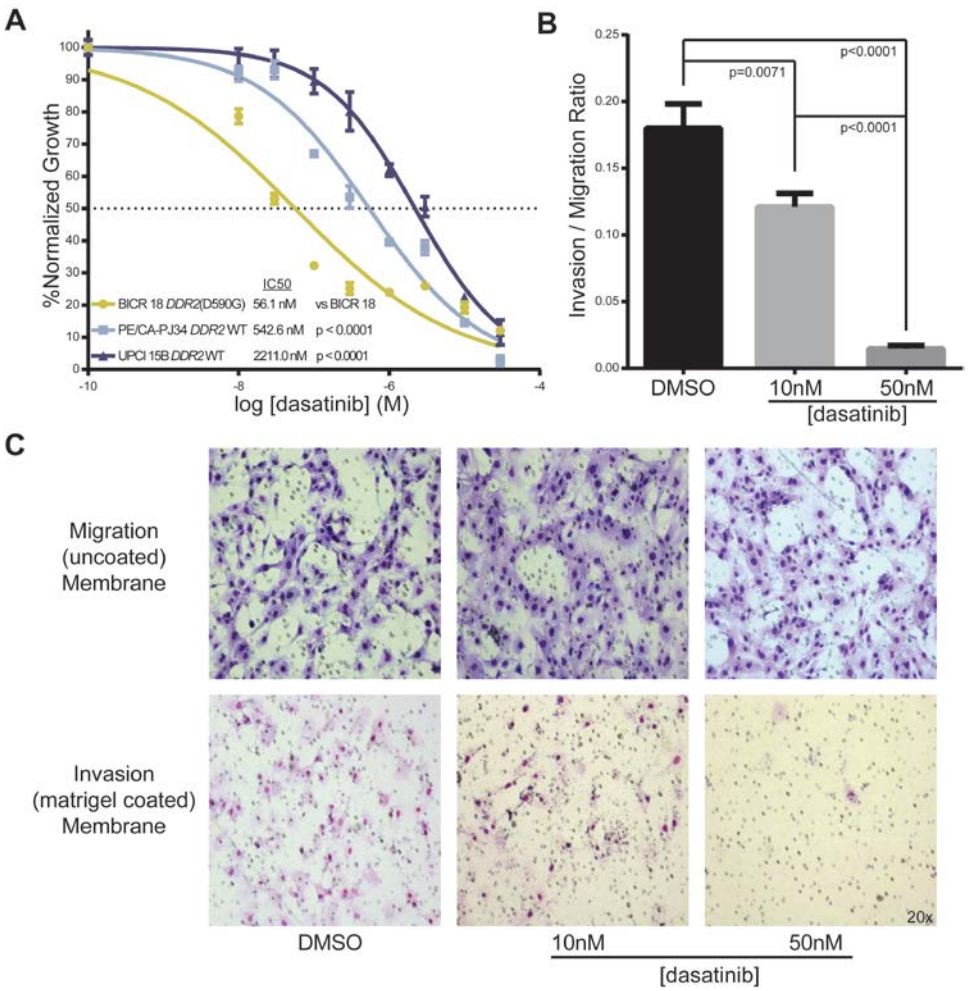

Figure 24. HNSCC Cells with an Endogenous *DDR2* Mutation are Sensitive to Dasatinib.

(A) 6.5 x 10^3 BICR 18 (*DDR2* mutant), PE/CA-PJ34, and UPCI 15B (both *DDR2* WT) cells were plated in triplicate in a 48-well plate, treated with half-log doses of dasatinib from 10nM to 30μM for 48 hours, and assessed by MTT. Pooled data (Mean +/- SEM) from 3 replicate experiments is shown and demonstrates exquisite sensitivity to dasatinib in the case of BICR 18. PE/CA-PJ34 and UPCI 15B cells are one and two orders of magnitude less sensitive, respectively, to treatment with dasatinib. **(B)** 2.0 x 10^4 BICR 18 cells suspended in DMEM were placed in migration (uncoated) chambers or invasion (matrigel coated) chambers submerged in full media, and treated in duplicate with DMSO or in triplicate with the indicated doses of dasatinib for 24 hrs. Cells were counted and averaged from 4 photomicrographs (20x objective) of each membrane, and the invasion/migration ratios were calculated. Pooled data (Mean +/- SEM) from 3 replicate experiments is shown along with representative images of the membranes **(C)**. The invasion of BICR 18 cells in matrigel invasion assays is inhibited by dasatinib in a dose-

dependent manner. Growth curves and statistics (extra sum of the squares F-test and unpaired, two-tailed T test with Welch's correction) are described in methods.

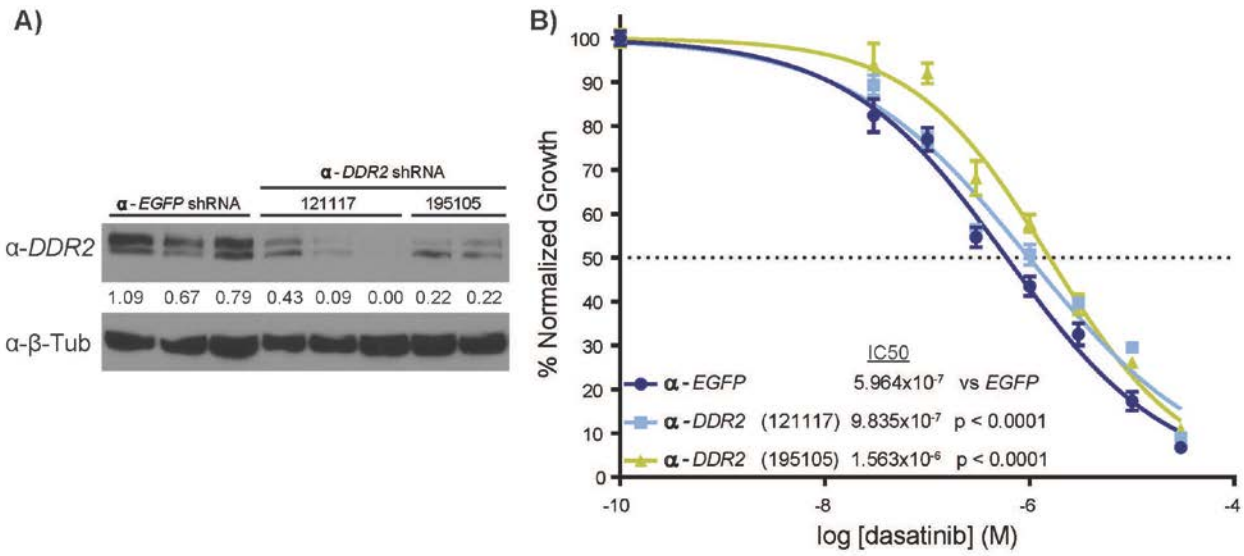

Figure 25. *DDR2* Knockdown in BICR 18 Modulates Sensitivity to Dasatinib.

BICR 18 cells (HNSCC cells with an endogenous *DDR2*(D590G) mutation), were engineered with lenti-viruses to express one of two different anti-*DDR2* shRNAs, or an anti-*EGFP* shRNA. **(A)** A representative immunoblot with densitometry normalized to β-tubulin from 8 unique subclones demonstrates the level of *DDR2* knock-down that was achieved. Experiment repeated at least twice with similar results observed. **(B)** BICR 18 cells expressing anti-*DDR2* shRNA (121117) and anti-*DDR2* shRNA (195105) were 1.6x and 2.6x less sensitive, respectively, to dasatinib treatment than BICR 18 cells expressing anti-*EGFP* shRNA. Pooled data from each of the 8 subclones pictured in part A (Mean +/- SEM) is presented in part B from at least 8 replicate experiments per group (2-4/subclone). Cells of each subclone were plated in triplicate overnight in a 48-well plate (10 x 10^3 cells/well) and treated with half-log doses of dasatinib ranging from 30nM to 3μM for 48 hours, and assessed by MTT. Growth curves and statistics described in methods.

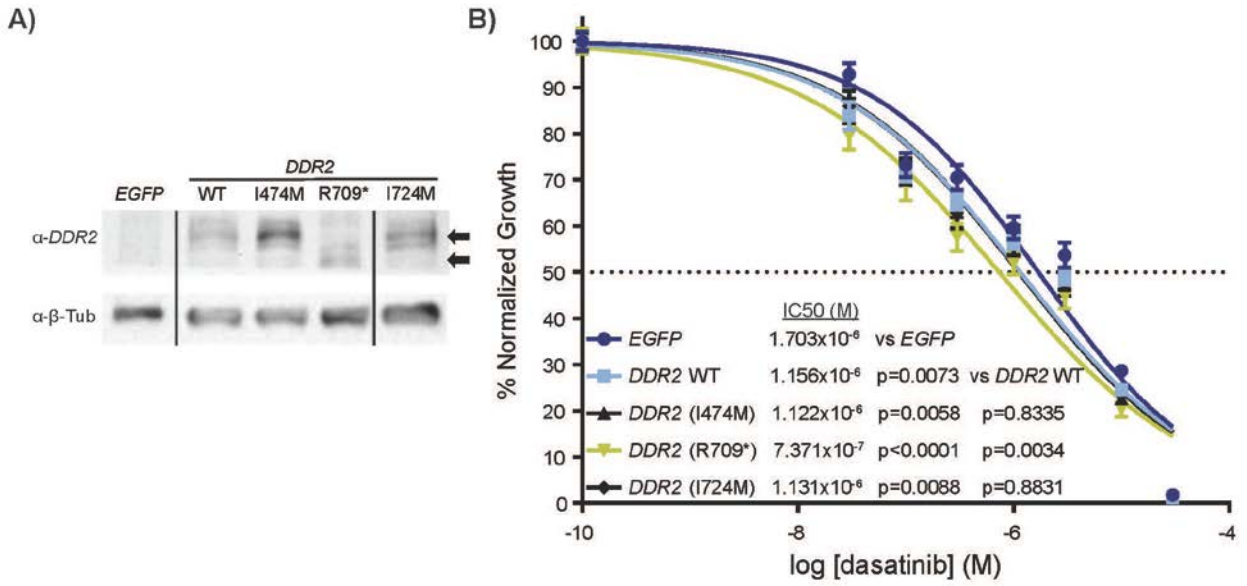

Figure 26. *DDR2* Enhances Dasatinib Sensitivity in the HNSCC Cell Line, UPCI 15B.

UPCI 15B cells (HNSCC cells with WT *DDR2* that was the most dasatinib resistant cell line in Figure 24A were engineered with retroviruses to express *EGFP*, WT *DDR2*, or one of the three mutant forms of *DDR2* that were identified in our cohort. **(A)** A representative immunoblot demonstrates the expression of the *DDR2* constructs, including a downshifted band corresponding to the truncation mutation R709*, in these engineered cells. Experiment repeated at least twice including independent subclones showing similar results. Lanes separated by black dividing lines were run on the same gel but were noncontiguous. **(B)** UPCI 15B cells expressing WT *DDR2*, *DDR2*(I474M), or *DDR2*(I724M) were ~1.5x more sensitive to dasatinib treatment than *EGFP* control cells; whereas cells expressing the *DDR2*(R709*) mutant construct were ~2.3x more sensitive to dasatinib than *EGFP* control cells, and ~1.6x more sensitive to dasatinib treatment than UPCI 15B cells engineered with WT *DDR2* constructs. Pooled data (Mean +/- SEM) is presented from 5 experiments composed of both technical and biologic replicates (2 and 3, respectively). Cells were plated in triplicate overnight in a 48-well plate (10×10^3 cells/well) and treated with half-log doses of dasatinib ranging from 30nM to 3μM for 48 hours, and assessed by MTT. Growth curves and statistics described in methods.

3.4 DISCUSSION

Whole exome sequencing of patient-matched tumor pairs from 23 individuals with HNSCC demonstrates the inter-tumor genetic heterogeneity of this cancer. To our knowledge, this is the first study in HNSCC to examine inter-tumor genetic heterogeneity in synchronous nodal metastases and metachronous recurrence across multiple patients, and provides a model to determine patterns of mutation and clonal evolution that may be targetable for the treatment of recurrent/metastatic disease.

Primary tumors in our study averaged 67.6 nonsynonymous SSNVs per tumor, including mutations in tumor suppressor genes, oncogenes, and genes that have previously been found to be significantly mutated in HNSCC; such as *AJUBA*, *CASP8*, *FAT1*, *FBXW7*, *NFE2L2*, and *TP53* (Table S4 Hedberg, Goh, Chiosea, *et al.*, 2015 in press *JCI*). Interestingly, primary tumors were not found to harbor mutations in several tumor suppressor genes and oncogenes previously implicated in HNSCC including *CCND1*, *PIK3CA*, *NOTCH1*, *PTEN*, *CDKN2A*, *HRAS*, and *EGFR*. However, copy number alterations, consistent with previously published reports, were seen in several of these genes, and the overall genetic profiles of primary tumors in our study appear similar to those reported in other WES studies of primary HNSCC tumors (Figure S2 Hedberg, Goh, Chiosea, *et al.*, 2015 in press *JCI*).(*39-41, 85, 86, 103-105*)

Approximately 86% (1290/1499) of the SSNVs identified in synchronous nodal metastases from 11 patient-matched tumor pairs were transmitted from their respective index primary tumors. This high degree of mutational similarity between primary tumors and synchronous nodal metastases in individual patients was also seen in the only other published sequencing report of patient-matched HNSCC tumors to date, in which whole genome

sequencing was performed on three regions of a primary HPV(+)HNSCC tumor, and two regions of a single synchronous cervical lymph node metastasis, from one patient.(*167*) In that study, Zhang *et al* used multiple samples of the same tumor to study intra-tumor genetic heterogeneity, and approximated the phylogenetic evolution and timeline of cancer development in that patient. They estimated that the clones making up the nodal metastasis evolved at a significantly later point in time than the clones of the index primary tumor.(*167*) We are unable to estimate the timeline of clonal evolution as our study design does not allow for the analysis of intra-tumor genetic heterogeneity. However, if metastatic potential is acquired in later stages of HNSCC progression, as posited by Zhang *et al*, then mutated genes identified in multiple nodal metastases, but not in the primary tumors, may confer metastatic ability. Newly arisen mutations in *C17orf104*, and *ITPR3* were seen in the nodal metastases of two patients in the synchronous nodal metastases group, and represent plausible targets for investigation in future studies (Table 10). Alternatively, if metastatic ability is developed early in HNSCC development, as is the commonly held clinical belief, then commonly transmitted mutations may confer metastatic ability. In 8/11 patient-matched tumor pairs in the synchronous metastasis group, fewer SSNVs were identified in the metastases than in their paired primary tumors, suggesting that clones developed the ability to metastasize and did so early on, while the primary tumor continued to evolve. These observations may be limited by differences in sample purity however, and future studies with multiple samples from each tumor and deeper sequencing must be performed to validate this finding.

Approximately 60% (274/457) of the SSNVs identified in metachronous recurrences from 8 patient-matched tumor pairs were transmitted from their respective index primary tumors. This finding suggests a greater degree of inter-tumor genetic heterogeneity in the setting of

metachronous recurrence, versus synchronous nodal metastasis, in HNSCC. This was largely expected given that, compared to their matched index primary tumors, metachronous recurrent tumors sequenced in this study were malignancies that arose in different anatomical microenvironments, at later points in time, often following genotoxic therapy, including radiation and/or chemotherapy.

The field cancerization theory suggests that there are numerous malignant and premalignant fields present in the mucosa of HNSCC patients.(*168*) This can lead to a high degree of inter-tumor genetic heterogeneity in the setting of recurrent disease, as metachronous tumors can be recurrences, which evolved from cells in the initial primary tumor that survived treatment, or they may arise from malignant clones that developed in a field unrelated to the initial cancer event, known as a "second primary," or "second field" tumor (SPT).(*10*) To date, the differentiation of recurrence and SPT has been based on histologic appearance, anatomic location, and kinetics of tumor formation, with earlier events (<24 months) generally considered to represent recurrences. Molecular diagnostic studies using mutated *TP53* and patterns of genetic changes as markers suggest that as many as 50% of recurrent HNSCC tumors that arise within 3 years of initial treatment and occur within 2 cm of the original index tumor location, may in fact be "second primary" tumors.(*131*) In patient PY-8, we conclusively demonstrate an instance in which the metachronous tumor represents a true SPT. The metachronous tumor was found to harbor newly arisen mutations in multiple cancer driving genes, and shared no SSNVs with the index primary tumor studied from that patient, apart from 3 SNVs of uncertain, potentially germline, origin. Identification of the unique mutational profiles in recurrences and SPTs will be vital to the rational design of personalized therapy that appropriately targets the

newly aberrant cellular processes contributing to the formation of metachronous head and neck tumors.

Although this cohort is small, it is striking that 2/9 metachronous recurrent tumors, including one true SPT, harbored *DDR2* mutations that were not identified in their matched primary tumors. Sequencing data, utilizing platforms sufficient for detection of *DDR2* mutations, is available for at least 658 newly diagnosed primary HNSCC tumors to date, and only 12 have been found to harbor transcript-altering *DDR2* mutations (Figure 22).(*39-41, 85, 86, 103-105, 167, 169*) The HNSCC cell line BICR 18, which harbors an endogenous *DDR2* mutation, HNSCC cells engineered to express the *DDR2* mutations identified in metachronous recurrent HNSCC tumors, and *DDR2* mutant tumors in two lung cancer case reports demonstrated increased sensitivity to dasatinib (Figure 24 and Figure 26).(*151, 165*) While the precise mechanism(s) underlying dasatinib sensitivity are beyond the scope of this report, the general mechanisms and consequences of discoidin domain receptor signaling in cancer are areas of ongoing research.(*151, 163-165, 170*) The *DDR2*(R709*) mutation identified in the metachronous recurrent tumor of patient PY-3, which conferred the greatest degree of sensitization to dasatinib in the present study, has also been reported in gastric and endometrial cancers. It is among the most common recurrent mutations, and is the only recurrent truncation mutation, identified in *DDR2* across all cancers in the TCGA and COSMIC database.(*90, 171-173*) Patient PY-3 is HPV-negative, had no history of smoking or significant alcohol use, and had a low mutational burden, further implicating *DDR2* as a potential driver in the metachronous recurrence.

If validated in larger cohorts, our observation that *DDR2* mutations may be enriched in metachronous recurrences, and may confer enhanced sensitivity to SFK inhibitors, has important

implications for the treatment of recurrent disease. Especially in light of the exceptional clinical response to dasatinib reported in two patients with lung squamous cell carcinoma harboring *DDR2*(S768R) mutations. As such, further mechanistic investigations to define the role of *DDR2* mutations as predictive biomarkers in HNSCC are warranted. While SFK inhibitors are FDA approved in several hematological malignancies, their role has not been defined in solid tumors, and is the subject of ongoing preclinical and clinical investigations.(*174*) A 12-patient, single-arm, phase II study of dasatinib in unselected patients with recurrent/metastatic HNSCC failed to demonstrate significant activity, however the *DDR2* status of patients' tumors was unknown.(*175*) A biomarker-guided trial in which patients with *DDR2* mutated tumors are selected to receive a SFK inhibitor has not been performed. A variety of sequencing platforms in common clinical use are capable of rapidly assessing the mutational status of *DDR2* and other genes in HNSCC tumor samples.(*176*) The implementation of such techniques will be required to determine to what degree, if any, *DDR2* mutations are enriched in metastatic/recurrent disease overall, and to correlate mutational status with treatment response and outcomes.

Limitations of the present study include the relatively small sample size, the use of a cohort of convenience where adequate biologic material was available for sequencing, a lack of distant metastases, variations in tumor sample purity, and the assessment of a single sample per tumor; thereby precluding assessment of intra-tumor heterogeneity. While these findings will require validation in future, larger sequencing studies, this is the first mutational analysis of patient matched tumor pairs in the setting of synchronous nodal metastasis, and metachronous recurrence in HNSCC. The findings provide an opportunity to guide future investigations.

4.0 GENERAL SUMMARY DISCUSSION AND FUTURE DIRECTIONS

HNSCC is characterized by phenotypic, etiological, biological and clinical heterogeneity resulting in a difficult to treat malignancy. The first two WES studies of HNSCC were published in 2011 and demonstrated a mutational landscape in which HNSCCs were found to harbor anywhere from 2, to as many as 527 nonsynonymous mutations per tumor (mean = 73 +/- 99). These mutations were largely found in a range of tumor suppressor genes and rarely, oncogenes.(*39, 41*) Both studies reported that HPV(+) tumors harbored fewer mutations than HPV(-) tumors, and identified novel, inactivating mutational patterns in *NOTCH1*, suggesting that it functions as a tumor suppressor in HNSCC.

The studies differed with respect to whether or not the mutational spectrum in smoking-associated cancers was enriched for G:C>T:A transversions, as has been reported in lung cancer. They reported markedly different rates of mutation in genes found to be commonly mutated in HNSCC (e.g. 47% vs 62% of tumors harboring *TP53* mutations in each study, respectively). Neither report identified an oncogene that was mutated in more than 8% of patients, and Agrawal *et al.* remarked: “Our finding that HNSCCs have few directly targetable mutations … suggests that prevention, careful surveillance of patients at risk, and early detection are the optimal approaches for reducing morbidity and mortality from this disease.” The goal of identifying genetic alterations that can guide treatment in subsets of HNSCC patients was not realized by

these initial studies, and its fulfillment would represent a much-needed advance in HNSCC therapy.

4.1 THE PI3K PATHWAY IN HNSCC

By analyzing WES data from an expanded cohort of 151 tumors, including the previously studied samples (*39*, *41*), we interrogated several mitogenic pathways, and found the PI3K pathway, and *PIK3CA*, to be the most frequently mutated oncogenic pathway and oncogene in HNSCC (mutated in 30.5% and 12.6% of tumors in our cohort, respectively Figure 5). The frequency with which the PI3K pathway and *PIK3CA* are altered suggest that they are likely to be important contributors to the aberrant molecular biology underlying HNSCC. We found that 3 HPV(+) tumors harbored no mutations in known cancer genes, except for mutations in PI3K genes, suggesting that PI3K pathway alterations may play an especially important role in HPV(+)HNSCC. We demonstrated that *PIK3CA* alterations including simulated amplification and/or hotspot and non-hotspot mutations can contribute to cancerous phenotypes including growth, survival, and invasion in HNSCC cell lines (Figure 8, Figure 12, and Figure 13). We showed that PI3K inhibitors were effective in preclinical models of HNSCC that we tested including endogenous cell lines and PDXs (Figure 16 and Figure 17). These data suggest that targeting the PI3K pathway may be a clinically feasible approach, and we conclude that the PI3K pathway represents a promising target for therapy in a substantial subset of HNSCC patients. Overall, we believe further investigation of targeted PI3K inhibition in HNSCC, and further investigation regarding the validity of PI3K alterations as predictive biomarkers of response to

targeted PI3K inhibition and/or combination therapy, is warranted in future preclinical and clinical studies.

Many of our findings with regard to the PI3K pathway have since been validated by subsequent, larger, and more comprehensive studies; including most prominently the TCGA HNSCC project, which is the largest, multi-platform cohort-study of HNSCC to date.(*40*) These studies confirm that *PIK3CA* is the most commonly mutated and/or amplified oncogene in HNSCC (~37% overall), that mutation and amplification of *PIK3CA* is significantly enriched in HPV(+)HNSCC vs HPV(-)HNSCC (~56% vs ~34%, respectively), and that in total, approximately half of all patients have a somatic alteration somewhere in the pathway that may be activating.(*18, 40*) These cumulative findings, exemplified by a concluding statement in the abstract of the TCGA HNSCC report: "Therapeutic candidate alterations were identified in most HNSCCs." represent a sharp departure from the observations of Agrawal *et al.*

The impact of this work can be greatly expanded through future studies that are able to elucidate the signaling mechanisms of these various *PIK3CA* driver mutations in HNSCC preclinical models. To do this, we intend to engineer driver *PIK3CA* mutations into HNSCC cell lines using the newly developed CRISPR/Cas9 genetic engineering techniques, and assess them with the RPPA platform. The RPPA platform measures the expression and phosphorylation of more than 200 proteins composing most of the major mitogenic pathways that have been implicated in cancer. By assessing the parental and engineered cell lines, treated with BYL-719 or vehicle control, we can determine the effect of each *PIK3CA* driver mutation and PI3K inhibition by BYL-719 on these pathways. Should any of the *PIK3CA* driver mutations be found to upregulate non-canonical signaling pathways that are not successfully targeted by PI3K

inhibitors, these experiments can guide us towards rationally designed combination therapies with other targeted inhibitors.

Increasing amounts of preclinical data confirming and defining both the efficacy and limitations of PI3K inhibitors in HNSCC, has spurred great interest in what ultimately represents the future direction of this work; targeting this pathway in patients.(*109*, *114*, *177-179*) This future is being realized as at least 16 clinical trials evaluating PI3K inhibitors in HNSCC are now active across the country, including NCT02277197 and NCT02277184 at the University of Pittsburgh. Our studies, and their clinical extensions, represent an important step forward in the search for new HNSCC treatment options, and will continue to influence future research efforts.

4.2 GENETICS OF METASTASIS AND RECURRENCE IN HNSCC

WES studies in primary HNSCC are rapidly expanding our knowledge of the underlying disease biology and impacting the course of translational research. Recurrence and metastasis are the primary cause of the persistent cancer-associated mortality seen in HNSCC. Challenges inherent to the collection of multiple paired normal and tumor tissue samples of sufficient quantity and quality for whole exome sequencing from separate clinical time points throughout a patient's course of treatment, represents a significant barrier to evaluating the mutations that arise in paired primary tumors, metastatic tumors, and/or recurrent tumors that develop in individual head and neck cancer patients. Only a small number of academic centers are equipped to assemble such cohorts. Leaving this critical area of HNSCC largely unstudied by these powerful methodologies, and the genetic alterations underlying these processes largely unknown.

In what is the first WES study of a cohort of patient-matched HNSCC tumor pairs in 13 patients with synchronous lymph node metastases, and 10 patients who recurred, we have outlined the first compendium of somatic mutations in primary, metastatic and/or recurrent HNSCC. With ~86% vs ~60% of the mutations identified in synchronous nodal metastases or metachronous recurrent tumors respectively, found to be transmitted from their matched index primary tumors, we observed a higher degree of genetic concordance between paired index primary tumors and synchronous lymph node metastases than between paired index primary tumors and metachronous recurrent tumors.

Additionally, the range of genetic concordance varies widely in the recurrent tumor pairs we assessed. In 3 pairs >90% of the mutations identified in each patient-matched tumor were shared, whereas 1 patient had a recurrent tumor that shared virtually no mutations with its paired index primary tumor (Figure 21). The evolution of such genetic differences is likely to underlie important changes in tumor biology and response to therapy throughout the course of treatment. Our cohorts are not large enough to identify genetic alterations with a prevalence high enough to suggest that they are likely contributors to metastasis or recurrence in large subsets of patients. But even in these small cohorts, we were able to identify some genes that appear to be newly mutated in the metastases or recurrences of multiple patients.

One such example that may have implications for targeted therapy are the *DDR2* mutations that arose in the metachronous recurrences of two otherwise very dissimilar patients (Figure 23). *DDR2* mutations have been shown to confer sensitivity to SFK inhibitors in other cancers. We similarly found evidence in endogenous and engineered HNSCC cell lines that *DDR2* mutations may be predictive of enhanced sensitivity to treatment with dasatinib (Figure 24, Figure 25, and Figure 26). The true translational potential of sequencing studies in the setting

of metastasis and recurrence can only be realized once a critical mass of data is obtained, as has begun to be achieved in primary disease. Should the prevalence of *DDR2* mutations and/or activation truly be enriched in recurrent disease, further mechanistic study of the role it plays in this disease setting would be warranted. In UPCI15B cells engineered to express the various *DDR2* mutations we identified in our sequencing study, we did not appreciate any reduction in the phosphorylation of downstream targets, primarily SHP2 (data not shown). However we have not yet performed the appropriate studies to determine whether or not the mutations we observed in *DDR2* are truly activating, nor have we dissected their effect on, or requirement for, downstream effectors known to be a part of the *DDR2* signaling cascade. It is conceivable that *DDR2* signaling could play an important role in the setting of recurrent disease as its natural ligand is collagen, which is often enriched (primarily types I and III) in the cellular microenvironment of recurrent tumors that arise in the setting of radiation induced fibrosis. Although we found BICR18 cells to be invasive in transwell assays, the collagen component of matrigel is collagen IV, which has been shown to bind *DDR1,* but not *DDR2*.(*180*) Further, the timeframe for these experiments was only 24 hours; and *DDR2* has been shown to take up to 24 hours to achieve maximal phosphorylation.(*170*) Therefore, the experiments we have conducted may not have been conducted with the appropriate ligand(s) and/or timeframe(s) to appreciate specific mechanistic contributions made by *DDR2*, beyond the enhanced sensitivity to SFK inhibitors it seems to confer. Growth studies of HNSCC cells with WT and modified *DDR2* in a variety of collagen-spiked matrices, coupled with phosphoproteomic analyses and RNAi screens, could help to identify the functional and molecular effects of *DDR2* in preclinical models of HNSCC, and start to tease apart the required components of the signaling pathway. Ultimately tumorigenic studies could be conducted *in vivo* with HNSCC cells harboring WT or modified

DDR2 being seeded either in matrigel solutions +/- fibrillary collagen, or into a fibrotic field induced by pre-irradiation, to observe the effect of stimulated *DDR2* on HNSCC tumor growth, invasion, and metastasis *in vivo*. First and foremost however, future directions of these studies will necessitate more sequencing in larger cohorts of patient-matched tumor pairs to validate our findings and any potential biomarkers in collaboration with other academic centers. In the near term future, we plan to assess the *DDR2* mutational status of tumors from patients enrolled in NCT01488318, an ongoing phase II trial of dasatinib plus cetuximab in recurrent/metastatic HNSCC that is currently being conducted at the University of Pittsburgh.

4.3 CONCLUDING REMARKS

This dissertation, and my work as a graduate student, has focused on the application and analysis of WES in cohorts of HNSCC patient tumors, paired with functional analyses and treatment studies in preclinical models of HNSCC. With the goal of expanding our understanding of the important genomic changes that drive these tumors, and identifying promising targets for novel therapeutic approaches in HNSCC. I have led and contributed to studies, described in this dissertation, that have made significant progress towards this stated goal.

By identifying *PIK3CA* as the most commonly mutated oncogene in HNSCC, demonstrating that it can contribute to cancerous phenotypes in HNSCC cell lines, and demonstrating efficacy of small molecule PI3K inhibitors in preclinical models of HNSCC. We have laid significant groundwork for continued mechanistic studies into this pathway, and for rapid translation of this preliminary data into the development and implementation of clinical trials.

By reporting the first landscape of exomic alterations in a cohort of metastatic/recurrent HNSCC, we have described important, novel genetic characteristics of these understudied and high risk disease states. By demonstrating that newly acquired genetic alterations, such as *DDR2* mutations, may result in new or enhanced sensitivity to targeted therapeutics in the setting of relapse, we offer an example after which future studies may be designed to monitor the evolution of disease in individual patients and one day modify therapy over time as guided by pharmacogenomics.

The era of personalized molecular medicine in HNSCC is on the near horizon. It has been my distinct privilege to play a small role in its early development. Thank you for reading.

APPENDIX

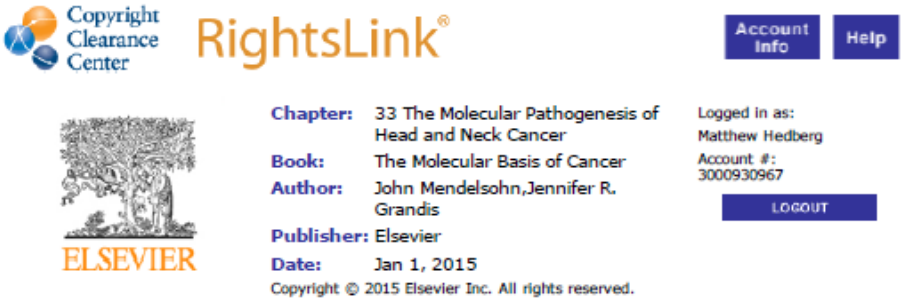

Copyright Clearance Center RightsLink®

Account Info | Help

ELSEVIER

Chapter: 33 The Molecular Pathogenesis of Head and Neck Cancer
Book: The Molecular Basis of Cancer
Author: John Mendelsohn,Jennifer R. Grandis
Publisher: Elsevier
Date: Jan 1, 2015

Logged in as:
Matthew Hedberg
Account #: 3000930967
LOGOUT

Order Completed

Thank you for your order.

This Agreement between Matthew Hedberg ("You") and Elsevier ("Elsevier") consists of your order details and the terms and conditions provided by Elsevier and Copyright Clearance Center.

License number	Reference confirmation email for license number
License date	Jun 26, 2015
Licensed content publisher	Elsevier
Licensed content publication	Elsevier Books
Licensed content title	The Molecular Basis of Cancer
Licensed content author	John Mendelsohn,Jennifer R. Grandis
Licensed content date	2015
Number of pages	10
Type of Use	reuse in a thesis/dissertation
Portion	full chapter
Format	both print and electronic
Are you the author of this Elsevier chapter?	Yes
How many pages did you author in this Elsevier book?	8
Will you be translating?	No
Title of your thesis/dissertation	Leveraging Next Generation Sequencing to Elucidate the Spectrum of Genetic Alterations Underlying Head and Neck Cancer and Identify Potential Translational Targets
Expected completion date	Jul 2015
Elsevier VAT number	GB 494 6272 12
Billing Type	Invoice
Billing address	Matthew Hedberg 229 Stratford Avenue Apartment 1 PITTSBURGH, PA 15206 United States Attn: Matthew Hedberg
Permissions price	0.00 USD
VAT/Local Sales Tax	0.00 USD / 0.00 GBP
Total	0.00 USD

BIBLIOGRAPHY

1. C. International Human Genome Sequencing, Finishing the euchromatic sequence of the human genome. *Nature* **431**, 931-945 (2004).

2. S. Brenner *et al.*, Gene expression analysis by massively parallel signature sequencing (MPSS) on microbead arrays. *Nat Biotechnol* **18**, 630-634 (2000).

3. A. A. Durmaz *et al.*, Evolution of genetic techniques: past, present, and beyond. *Biomed Res Int* **2015**, 461524 (2015).

4. B. A. Kohler *et al.*, Annual report to the nation on the status of cancer, 1975-2011, featuring incidence of breast cancer subtypes by race/ethnicity, poverty, and state. *J Natl Cancer Inst* **107**, djv048 (2015).

5. NCI. (www.cancer.gov, 2015).

6. M. L. Hedberg, J. R. Grandis, in *The Molecular Basis of Cancer,* J. Mendelsohn, P. M. Howley, M. A. Israel, J. W. Gray, C. B. Thompson, Eds. (Elsevier Inc., Philadelphia, PA, 2015), chap. 33, pp. 491-498.

7. L. C. van Imhoff *et al.*, The prognostic value of continued smoking on survival and recurrence rates in head and neck cancer patients: A systematic review. *Head Neck,* (2015).

8. S. I. Ferlay J, Ervik M, Dikshit R, Eser S, Mathers C, Rebelo M, Parkin DM, Forman D, Bray F., GLOBOCAN 2012 v1.0, Cancer Incidence and Mortality Worldwide. *IARC CancerBase No. 11 [Internet]* **1**, (2013).

9. C. Centers for Disease, Prevention, Human papillomavirus-associated cancers - United States, 2004-2008. *MMWR Morb Mortal Wkly Rep* **61**, 258-261 (2012).

10. C. Leemans, B. Braakhuis, R. Brakenhoff, The molecular biology of head and neck cancer. *Nature reviews. Cancer* **11**, 9-22 (2011).

11. S. Marur, G. D'Souza, W. Westra, A. Forastiere, HPV-associated head and neck cancer: a virus-related cancer epidemic. *The lancet oncology* **11**, 781-789 (2010).

12. J. B. Hebnes *et al.*, Prevalence of genital human papillomavirus among men in Europe: systematic review and meta-analysis. *J Sex Med* **11**, 2630-2644 (2014).

13. K. K. Ang *et al.*, Human papillomavirus and survival of patients with oropharyngeal cancer. *N Engl J Med* **363**, 24-35 (2010).

14. M. Okano, T. G. Gross, Acute or Chronic Life-Threatening Diseases Associated With Epstein-Barr Virus Infection. *Am J Med Sci*, (2011).

15. S. Dogan *et al.*, Human papillomavirus and Epstein-Barr virus in nasopharyngeal carcinoma in a low-incidence population. *Head Neck* **36**, 511-516 (2014).

16. J. W. Park *et al.*, Deficiencies in the Fanconi anemia DNA damage response pathway increase sensitivity to HPV-associated head and neck cancer. *Cancer Res* **70**, 9959-9968 (2010).

17. S. B. Edge *et al.*, *AJCC cancer staging manual*. (Springer New York, 2010), vol. 649.

18. P. S. Hammerman, D. N. Hayes, J. R. Grandis, Therapeutic insights from genomic studies of head and neck squamous cell carcinomas. *Cancer Discov* **5**, 239-244 (2015).

19. D. G. Pfister *et al.*, Head and neck cancers, Version 2.2014. Clinical practice guidelines in oncology. *J Natl Compr Canc Netw* **12**, 1454-1487 (2014).

20. D. J. Givens *et al.*, Adverse events associated with concurrent chemoradiation therapy in patients with head and neck cancer. *Arch Otolaryngol Head Neck Surg* **135**, 1209-1217 (2009).

21. A. Ho *et al.*, Decision making in the management of recurrent head and neck cancer. *Head & neck* **36**, 144-151 (2014).

22. X. León *et al.*, Second, third, and fourth head and neck tumors. A progressive decrease in survival. *Head & neck* **34**, 1716-1719 (2012).

23. S. Morgan, J. R. Grandis, ErbB receptors in the biology and pathology of the aerodigestive tract. *Exp Cell Res* **315**, 572-582 (2009).

24. J. A. Bonner *et al.*, Radiotherapy plus cetuximab for locoregionally advanced head and neck cancer: 5-year survival data from a phase 3 randomised trial, and relation between cetuximab-induced rash and survival. *Lancet Oncol* **11**, 21-28 (2010).

25. J. B. Vermorken *et al.*, Platinum-based chemotherapy plus cetuximab in head and neck cancer. *N Engl J Med* **359**, 1116-1127 (2008).

26. K. K. Ang *et al.*, Randomized phase III trial of concurrent accelerated radiation plus cisplatin with or without cetuximab for stage III to IV head and neck carcinoma: RTOG 0522. *J Clin Oncol* **32**, 2940-2950 (2014).

27. J. B. Vermorken *et al.*, Open-label, uncontrolled, multicenter phase II study to evaluate the efficacy and toxicity of cetuximab as a single agent in patients with recurrent and/or metastatic squamous cell carcinoma of the head and neck who failed to respond to platinum-based therapy. *J Clin Oncol* **25**, 2171-2177 (2007).

28. P. J. Bradley, P. T. Bradley, Searching for metachronous tumours in patients with head and neck cancer: the ideal protocol! *Curr Opin Otolaryngol Head Neck Surg* **18**, 124-133 (2010).

29. J. S. Cooper *et al.*, Precisely defining high-risk operable head and neck tumors based on RTOG #85-03 and #88-24: targets for postoperative radiochemotherapy? *Head Neck* **20**, 588-594 (1998).

30. T. P. Dang, Notch, apoptosis and cancer. *Adv Exp Med Biol* **727**, 199-209 (2012).

31. G. P. Dotto, Notch tumor suppressor function. *Oncogene* **27**, 5115-5123 (2008).

32. M. Nicolas *et al.*, Notch1 functions as a tumor suppressor in mouse skin. *Nat Genet* **33**, 416-421 (2003).

33. J. W. Rocco, C. O. Leong, N. Kuperwasser, M. P. DeYoung, L. W. Ellisen, p63 mediates survival in squamous cell carcinoma by suppression of p73-dependent apoptosis. *Cancer Cell* **9**, 45-56 (2006).

34. A. Yang *et al.*, p63 is essential for regenerative proliferation in limb, craniofacial and epithelial development. *Nature* **398**, 714-718 (1999).

35. T. Yugawa *et al.*, DeltaNp63alpha repression of the Notch1 gene supports the proliferative capacity of normal human keratinocytes and cervical cancer cells. *Cancer Res* **70**, 4034-4044 (2010).

36. M. Roesch-Ely *et al.*, Proteomic analysis reveals successive aberrations in protein expression from healthy mucosa to invasive head and neck cancer. *Oncogene* **26**, 54-64 (2007).

37. M. Olivier, M. Hollstein, P. Hainaut, TP53 mutations in human cancers: origins, consequences, and clinical use. *Cold Spring Harb Perspect Biol* **2**, a001008 (2010).

38. D. Hanahan, R. A. Weinberg, Hallmarks of cancer: the next generation. *Cell* **144**, 646-674 (2011).

39. N. Agrawal *et al.*, Exome sequencing of head and neck squamous cell carcinoma reveals inactivating mutations in NOTCH1. *Science (New York, N.Y.)* **333**, 1154-1157 (2011).

40. N. Cancer Genome Atlas, Comprehensive genomic characterization of head and neck squamous cell carcinomas. *Nature* **517**, 576-582 (2015).

41. N. Stransky *et al.*, The mutational landscape of head and neck squamous cell carcinoma. *Science (New York, N.Y.)* **333**, 1157-1160 (2011).

42. M. L. Poeta *et al.*, TP53 mutations and survival in squamous-cell carcinoma of the head and neck. *N Engl J Med* **357**, 2552-2561 (2007).

43. A. Cardesa, A. Nadal, Carcinoma of the head and neck in the HPV era. *Acta Dermatovenerol Alp Panonica Adriat* **20**, 161-173 (2011).

44. K. H. Vousden, D. P. Lane, p53 in health and disease. *Nat Rev Mol Cell Biol* **8**, 275-283 (2007).

45. R. Sailasree *et al.*, Differential roles of p16INK4A and p14ARF genes in prognosis of oral carcinoma. *Cancer Epidemiol Biomarkers Prev* **17**, 414-420 (2008).

46. G. Pannone *et al.*, Evaluation of a combined triple method to detect causative HPV in oral and oropharyngeal squamous cell carcinomas: p16 Immunohistochemistry, Consensus PCR HPV-DNA, and In Situ Hybridization. *Infect Agent Cancer* **7**, 4 (2012).

47. E. Higuchi *et al.*, Prognostic significance of cyclin D1 and p16 in patients with intermediate-risk head and neck squamous cell carcinoma treated with docetaxel and concurrent radiotherapy. *Head Neck* **29**, 940-947 (2007).

48. E. A. Musgrove, C. E. Caldon, J. Barraclough, A. Stone, R. L. Sutherland, Cyclin D as a therapeutic target in cancer. *Nat Rev Cancer* **11**, 558-572 (2011).

49. K. H. Kim *et al.*, The clinicopathological significance of epithelial mesenchymal transition associated protein expression in head and neck squamous cell carcinoma. *Korean J Pathol* **48**, 263-269 (2014).

50. S. Y. Lee *et al.*, Gain-of-function mutations and copy number increases of Notch2 in diffuse large B-cell lymphoma. *Cancer Sci* **100**, 920-926 (2009).

51. X. S. Puente *et al.*, Whole-genome sequencing identifies recurrent mutations in chronic lymphocytic leukaemia. *Nature* **475**, 101-105 (2011).

52. A. P. Weng *et al.*, Activating mutations of NOTCH1 in human T cell acute lymphoblastic leukemia. *Science* **306**, 269-271 (2004).

53. M. Nicolas *et al.*, Notch1 functions as a tumor suppressor in mouse skin. *Nat Genet* **33**, 416-421 (2003).

54. W. S. Pear *et al.*, Exclusive development of T cell neoplasms in mice transplanted with bone marrow expressing activated Notch alleles. *J Exp Med* **183**, 2283-2291 (1996).

55. E. L. Rosenthal, L. M. Matrisian, Matrix metalloproteases in head and neck cancer. *Head Neck* **28**, 639-648 (2006).

56. B. Fabre, A. Ramos, B. de Pascual-Teresa, Targeting matrix metalloproteinases: exploring the dynamics of the s1' pocket in the design of selective, small molecule inhibitors. *J Med Chem* **57**, 10205-10219 (2014).

57. H. Ikushima, K. Miyazono, TGFbeta signalling: a complex web in cancer progression. *Nat Rev Cancer* **10**, 415-424 (2010).

58. S. Bornstein *et al.*, Smad4 loss in mice causes spontaneous head and neck cancer with increased genomic instability and inflammation. *J Clin Invest* **119**, 3408-3419 (2009).

59. W. Qiu, F. Schonleben, X. Li, G. H. Su, Disruption of transforming growth factor beta-Smad signaling pathway in head and neck squamous cell carcinoma as evidenced by mutations of SMAD2 and SMAD4. *Cancer Lett* **245**, 163-170 (2007).

60. D. Wang *et al.*, Mutation and downregulation of the transforming growth factor beta type II receptor gene in primary squamous cell carcinomas of the head and neck. *Carcinogenesis* **18**, 2285-2290 (1997).

61. J. Cohen *et al.*, Attenuated transforming growth factor beta signaling promotes nuclear factor-kappaB activation in head and neck cancer. *Cancer Res* **69**, 3415-3424 (2009).

62. C. Freudlsperger *et al.*, TGF-beta and NF-kappaB signal pathway cross-talk is mediated through TAK1 and SMAD7 in a subset of head and neck cancers. *Oncogene*, (2012).

63. J. Fei *et al.*, Prognostic significance of vascular endothelial growth factor in squamous cell carcinomas of the tonsil in relation to human papillomavirus status and epidermal growth factor receptor. *Ann Surg Oncol* **16**, 2908-2917 (2009).

64. M. Kamal *et al.*, Loss of CSMD1 expression is associated with high tumour grade and poor survival in invasive ductal breast carcinoma. *Breast Cancer Res Treat* **121**, 555-563 (2010).

65. J. A. Engelman, Targeting PI3K signalling in cancer: opportunities, challenges and limitations. *Nat Rev Cancer* **9**, 550-562 (2009).

66. Y. Bian *et al.*, Loss of TGF-beta signaling and PTEN promotes head and neck squamous cell carcinoma through cellular senescence evasion and cancer-related inflammation. *Oncogene*, (2011).

67. A. H. Berger, A. G. Knudson, P. P. Pandolfi, A continuum model for tumour suppression. *Nature* **476**, 163-169 (2011).

68. A. K. Murugan, N. T. Hong, Y. Fukui, A. K. Munirajan, N. Tsuchida, Oncogenic mutations of the PIK3CA gene in head and neck squamous cell carcinomas. *Int J Oncol* **32**, 101-111 (2008).

69. F. E. Henken *et al.*, PIK3CA-mediated PI3-kinase signalling is essential for HPV-induced transformation in vitro. *Mol Cancer* **10**, 71 (2011).

70. F. E. Henken *et al.*, PIK3CA-mediated PI3-kinase signalling is essential for HPV-induced transformation in vitro. *Mol Cancer* **10**, 71 (2011).

71. S. K. Kundu, M. Nestor, Targeted therapy in head and neck cancer. *Tumour Biol* **33**, 707-721 (2012).

72. E. Castellano, J. Downward, RAS Interaction with PI3K: More Than Just Another Effector Pathway. *Genes Cancer* **2**, 261-274 (2011).

73. S. L. Lu, H. Herrington, X. J. Wang, Mouse models for human head and neck squamous cell carcinomas. *Head Neck* **28**, 945-954 (2006).

74. M. Narisawa-Saito *et al.*, A critical role of MYC for transformation of human cells by HPV16 E6E7 and oncogenic HRAS. *Carcinogenesis* **33**, 910-917 (2012).

75. A. T. Baines, D. Xu, C. J. Der, Inhibition of Ras for cancer treatment: the search continues. *Future Med Chem* **3**, 1787-1808 (2011).

76. M. E. Sharafinski, R. L. Ferris, S. Ferrone, J. R. Grandis, Epidermal growth factor receptor targeted therapy of squamous cell carcinoma of the head and neck. *Head Neck* **32**, 1412-1421 (2010).

77. T. Hama *et al.*, Prognostic significance of epidermal growth factor receptor phosphorylation and mutation in head and neck squamous cell carcinoma. *Oncologist* **14**, 900-908 (2009).

78. J. C. Sok *et al.*, Mutant epidermal growth factor receptor (EGFRvIII) contributes to head and neck cancer growth and resistance to EGFR targeting. *Clin Cancer Res* **12**, 5064-5073 (2006).

79. B. Szabo *et al.*, Clinical significance of genetic alterations and expression of epidermal growth factor receptor (EGFR) in head and neck squamous cell carcinomas. *Oral oncology* **47**, 487-496 (2011).

80. S. E. Wheeler *et al.*, Lyn Kinase Mediates Cell Motility and Tumor Growth in EGFRvIII-Expressing Head and Neck Cancer. *Clin Cancer Res* **18**, 2850-2860 (2012).

81. T. Y. Seiwert *et al.*, The MET receptor tyrosine kinase is a potential novel therapeutic target for head and neck squamous cell carcinoma. *Cancer Res* **69**, 3021-3031 (2009).

82. L. V. Sequist *et al.*, Genotypic and histological evolution of lung cancers acquiring resistance to EGFR inhibitors. *Sci Transl Med* **3**, 75ra26 (2011).

83. E. L. Kwak *et al.*, Anaplastic lymphoma kinase inhibition in non-small-cell lung cancer. *N Engl J Med* **363**, 1693-1703 (2010).

84. G. Pacchiana *et al.*, Monovalency unleashes the full therapeutic potential of the DN-30 anti-Met antibody. *J Biol Chem* **285**, 36149-36157 (2010).

85. V. Lui *et al.*, Frequent mutation of the PI3K pathway in head and neck cancer defines predictive biomarkers. *Cancer discovery* **3**, 761-769 (2013).

86. T. Y. Seiwert *et al.*, Integrative and comparative genomic analysis of HPV-positive and HPV-negative head and neck squamous cell carcinomas. *Clinical cancer research : an official journal of the American Association for Cancer Research*, (2014).

87. X. Liao *et al.*, Aspirin use, tumor PIK3CA mutation, and colorectal-cancer survival. *N Engl J Med* **367**, 1596-1606 (2012).

88. C. C. Bancroft *et al.*, Effects of pharmacologic antagonists of epidermal growth factor receptor, PI3K and MEK signal kinases on NF-kappaB and AP-1 activation and IL-8 and VEGF expression in human head and neck squamous cell carcinoma lines. *Int J Cancer* **99**, 538-548 (2002).

89. J. R. Grandis *et al.*, Requirement of Stat3 but not Stat1 activation for epidermal growth factor receptor- mediated cell growth in vitro. *J Clin Invest* **102**, 1385-1392. (1998).

90. E. Cerami *et al.*, The cBio cancer genomics portal: an open platform for exploring multidimensional cancer genomics data. *Cancer discovery* **2**, 401-404 (2012).

91. L. Grell, C. Parkin, L. Slatest, P. A. Craig, EZ-Viz, a tool for simplifying molecular viewing in PyMOL. *Biochem Mol Biol Educ* **34**, 402-407 (2006).

92. P. Katsonis, O. Lichtarge, A formal perturbation equation between genotype and phenotype determines the Evolutionary Action of protein-coding variations on fitness. *Genome Res* **24**, 2050-2058 (2014).

93. Q. Zhang *et al.*, Antitumor mechanisms of combined gastrin-releasing peptide receptor and epidermal growth factor receptor targeting in head and neck cancer. *Mol Cancer Ther* **6**, 1414-1424 (2007).

94. K. Kozaki *et al.*, PIK3CA mutation is an oncogenic aberration at advanced stages of oral squamous cell carcinoma. *Cancer Sci* **97**, 1351-1358 (2006).

95. Y. Cohen *et al.*, Mutational analysis of PTEN/PIK3CA/AKT pathway in oral squamous cell carcinoma. *Oral Oncol* **47**, 946-950 (2011).

96. J. Li *et al.*, PTEN, a putative protein tyrosine phosphatase gene mutated in human brain, breast, and prostate cancer. *Science* **275**, 1943-1947 (1997).

97. P. A. Steck *et al.*, Identification of a candidate tumour suppressor gene, MMAC1, at chromosome 10q23.3 that is mutated in multiple advanced cancers. *Nat Genet* **15**, 356-362 (1997).

98. S. Bamford *et al.*, The COSMIC (Catalogue of Somatic Mutations in Cancer) database and website. *Br J Cancer* **91**, 355-358 (2004).

99. E. Cerami *et al.*, The cBio cancer genomics portal: an open platform for exploring multidimensional cancer genomics data. *Cancer Discov* **2**, 401-404 (2012).

100. M. S. Miller *et al.*, Structural basis of nSH2 regulation and lipid binding in PI3Kalpha. *Oncotarget* **5**, 5198-5208 (2014).

101. J. Barretina *et al.*, The Cancer Cell Line Encyclopedia enables predictive modelling of anticancer drug sensitivity. *Nature* **483**, 603-607 (2012).

102. M. Gymnopoulos, M. A. Elsliger, P. K. Vogt, Rare cancer-specific mutations in PIK3CA show gain of function. *Proc Natl Acad Sci U S A* **104**, 5569-5574 (2007).

103. C. India Project Team of the International Cancer Genome, Mutational landscape of gingivo-buccal oral squamous cell carcinoma reveals new recurrently-mutated genes and molecular subgroups. *Nature communications* **4**, 2873 (2013).

104. C. Pickering *et al.*, Integrative genomic characterization of oral squamous cell carcinoma identifies frequent somatic drivers. *Cancer discovery* **3**, 770-781 (2013).

105. V. Lui *et al.*, Frequent mutation of receptor protein tyrosine phosphatases provides a mechanism for STAT3 hyperactivation in head and neck cancer. *Proceedings of the National Academy of Sciences of the United States of America* **111**, 1114-1119 (2014).

106. M. Sun, J. R. Hart, P. Hillmann, M. Gymnopoulos, P. K. Vogt, Addition of N-terminal peptide sequences activates the oncogenic and signaling potentials of the catalytic subunit p110alpha of phosphoinositide-3-kinase. *Cell Cycle* **10**, 3731-3739 (2011).

107. L. Groesser *et al.*, Postzygotic HRAS and KRAS mutations cause nevus sebaceous and Schimmelpenning syndrome. *Nat Genet* **44**, 783-787 (2012).

108. P. Furet *et al.*, Discovery of NVP-BYL719 a potent and selective phosphatidylinositol-3 kinase alpha inhibitor selected for clinical evaluation. *Bioorg Med Chem Lett* **23**, 3741-3748 (2013).

109. E. D. Wirtz, D. Hoshino, A. T. Maldonado, D. R. Tyson, A. M. Weaver, Response of Head and Neck Squamous Cell Carcinoma Cells Carrying PIK3CA Mutations to Selected Targeted Therapies. *JAMA Otolaryngol Head Neck Surg* **141**, 543-549 (2015).

110. S. S. De Buck *et al.*, Population pharmacokinetics and pharmacodynamics of BYL719, a phosphoinositide 3-kinase antagonist, in adult patients with advanced solid malignancies. *Br J Clin Pharmacol* **78**, 543-555 (2014).

111. J. F. Vansteenkiste *et al.*, Safety and Efficacy of Buparlisib (BKM120) in Patients With PI3K Pathway-Activated Non-Small Cell Lung Cancer (NSCLC): Results From the Phase II BASALT-1 Study. *J Thorac Oncol*, (2015).

112. M. T. Burger *et al.*, Identification of NVP-BKM120 as a Potent, Selective, Orally Bioavailable Class I PI3 Kinase Inhibitor for Treating Cancer. *ACS Med Chem Lett* **2**, 774-779 (2011).

113. M. Elkabets *et al.*, mTORC1 inhibition is required for sensitivity to PI3K p110alpha inhibitors in PIK3CA-mutant breast cancer. *Sci Transl Med* **5**, 196ra199 (2013).

114. M. Elkabets *et al.*, AXL mediates resistance to PI3Kalpha inhibition by activating the EGFR/PKC/mTOR axis in head and neck and esophageal squamous cell carcinomas. *Cancer Cell* **27**, 533-546 (2015).

115. C. Rodríguez-Antona, M. Taron, Pharmacogenomic biomarkers for personalized cancer treatment. *Journal of internal medicine* **277**, 201-217 (2015).

116. J. Woenckhaus *et al.*, Genomic gain of PIK3CA and increased expression of p110alpha are associated with progression of dysplasia into invasive squamous cell carcinoma. *J Pathol* **198**, 335-342 (2002).

117. S. Jones *et al.*, Frequent mutations of chromatin remodeling gene ARID1A in ovarian clear cell carcinoma. *Science* **330**, 228-231 (2010).

118. K. Wang *et al.*, Exome sequencing identifies frequent mutation of ARID1A in molecular subtypes of gastric cancer. *Nat Genet* **43**, 1219-1223 (2011).

119. Y. Watanabe *et al.*, Frequent alteration of MLL3 frameshift mutations in microsatellite deficient colorectal cancer. *PLoS One* **6**, e23320 (2011).

120. L. W. Cheung *et al.*, High frequency of PIK3R1 and PIK3R2 mutations in endometrial cancer elucidates a novel mechanism for regulation of PTEN protein stability. *Cancer discovery* **1**, 170-185 (2011).

121. B. Karakas, K. E. Bachman, B. H. Park, Mutation of the PIK3CA oncogene in human cancers. *Br J Cancer* **94**, 455-459 (2006).

122. S. J. Klempner, A. P. Myers, L. C. Cantley, What a tangled web we weave: emerging resistance mechanisms to inhibition of the phosphoinositide 3-kinase pathway. *Cancer Discov* **3**, 1345-1354 (2013).

123. A. Bosch *et al.*, PI3K inhibition results in enhanced estrogen receptor function and dependence in hormone receptor-positive breast cancer. *Sci Transl Med* **7**, 283ra251 (2015).

124. D. Juric *et al.*, Convergent loss of PTEN leads to clinical resistance to a PI(3)Kalpha inhibitor. *Nature* **518**, 240-244 (2015).

125. F. Janku *et al.*, PIK3CA mutation H1047R is associated with response to PI3K/AKT/mTOR signaling pathway inhibitors in early-phase clinical trials. *Cancer Res* **73**, 276-284 (2013).

126. K. E. Bachman *et al.*, The PIK3CA gene is mutated with high frequency in human breast cancers. *Cancer Biol Ther* **3**, 772-775 (2004).

127. P. Roepman *et al.*, Maintenance of head and neck tumor gene expression profiles upon lymph node metastasis. *Cancer research* **66**, 11110-11114 (2006).

128. Surveillance, Epidemiology, and End Results (SEER) Program (www.seer.cancer.gov) SEER*Stat Database: Incidence - SEER 9 Regs Research Data (with SEER Delay Factors), Nov 2013 Sub (1973-2011) <Katrina/Rita Population Adjustment> - Linked To County Attributes - Total U.S., 1969-2012 Counties, National Cancer Institute, DCCPS, Surveillance Research Program, Surveillance Systems Branch, released April 2014, based on the November 2013 submission.

129. J. de Juan *et al.*, Inclusion of extracapsular spread in the pTNM classification system: a proposal for patients with head and neck carcinoma. *JAMA otolaryngology-- head & neck surgery* **139**, 483-488 (2013).

130. X. Wan, A. Egloff, J. Johnson, Histological assessment of cervical lymph node identifies patients with head and neck squamous cell carcinoma (HNSCC): who would benefit from chemoradiation after surgery? *The Laryngoscope* **122**, 2712-2722 (2012).

131. A. P. Graveland *et al.*, Molecular diagnosis of minimal residual disease in head and neck cancer patients. *Cellular oncology (Dordrecht)* **35**, 367-375 (2012).

132. R. A. Burrell, N. McGranahan, J. Bartek, C. Swanton, The causes and consequences of genetic heterogeneity in cancer evolution. *Nature* **501**, 338-345 (2013).

133. M. Gerlinger *et al.*, Intratumor heterogeneity and branched evolution revealed by multiregion sequencing. *The New England journal of medicine* **366**, 883-892 (2012).

134. L. Ding *et al.*, Clonal evolution in relapsed acute myeloid leukaemia revealed by whole-genome sequencing. *Nature* **481**, 506-510 (2012).

135. C. G. Mullighan *et al.*, Genomic analysis of the clonal origins of relapsed acute lymphoblastic leukemia. *Science (New York, N.Y.)* **322**, 1377-1380 (2008).

136. N. Wagle *et al.*, MAP kinase pathway alterations in BRAF-mutant melanoma patients with acquired resistance to combined RAF/MEK inhibition. *Cancer discovery* **4**, 61-68 (2013).

137. F. André *et al.*, Comparative genomic hybridisation array and DNA sequencing to direct treatment of metastatic breast cancer: a multicentre, prospective trial (SAFIR01/UNICANCER). *The Lancet. Oncology* **15**, 267-274 (2014).

138. B. E. Johnson *et al.*, Mutational analysis reveals the origin and therapy-driven evolution of recurrent glioma. *Science (New York, N.Y.)* **343**, 189-193 (2014).

139. A. Kreso *et al.*, Variable clonal repopulation dynamics influence chemotherapy response in colorectal cancer. *Science (New York, N.Y.)* **339**, 543-548 (2013).

140. M. Yu *et al.*, Cancer therapy. Ex vivo culture of circulating breast tumor cells for individualized testing of drug susceptibility. *Science (New York, N.Y.)* **345**, 216-220 (2014).

141. A. Cromer *et al.*, Identification of genes associated with tumorigenesis and metastatic potential of hypopharyngeal cancer by microarray analysis. *Oncogene* **23**, 2484-2498 (2004).

142. M. Ginos *et al.*, Identification of a gene expression signature associated with recurrent disease in squamous cell carcinoma of the head and neck. *Cancer research* **64**, 55-63 (2004).

143. P. Reis *et al.*, A gene signature in histologically normal surgical margins is predictive of oral carcinoma recurrence. *BMC cancer* **11**, 437 (2011).

144. S. van Hooff *et al.*, Validation of a gene expression signature for assessment of lymph node metastasis in oral squamous cell carcinoma. *Journal of clinical oncology : official journal of the American Society of Clinical Oncology* **30**, 4104-4110 (2012).

145. G. Goh *et al.*, Recurrent activating mutation in PRKACA in cortisol-producing adrenal tumors. *Nature genetics* **46**, 613-617 (2014).

146. U. I. Scholl *et al.*, Somatic and germline CACNA1D calcium channel mutations in aldosterone-producing adenomas and primary aldosteronism. *Nature genetics* **45**, 1050-1054 (2013).

147. M. Choi *et al.*, K+ channel mutations in adrenal aldosterone-producing adenomas and hereditary hypertension. *Science* **331**, 768-772 (2011).

148. M. Lawrence *et al.*, Mutational heterogeneity in cancer and the search for new cancer-associated genes. *Nature* **499**, 214-218 (2013).

149. C. Mermel *et al.*, GISTIC2.0 facilitates sensitive and confident localization of the targets of focal somatic copy-number alteration in human cancers. *Genome biology* **12**, (2011).

150. A. Roth *et al.*, PyClone: statistical inference of clonal population structure in cancer. *Nature methods* **11**, 396-398 (2014).

151. P. Hammerman *et al.*, Mutations in the DDR2 kinase gene identify a novel therapeutic target in squamous cell lung cancer. *Cancer discovery* **1**, 78-89 (2011).

152. N. Cancer Genome Atlas Research *et al.*, The Cancer Genome Atlas Pan-Cancer analysis project. *Nature genetics* **45**, 1113-1120 (2013).

153. B. Vogelstein *et al.*, Cancer Genome Landscapes. *Science* **339**, 1546-1558 (2013).

154. A. Maranto, Primary structure, ligand binding, and localization of the human type 3 inositol 1,4,5-trisphosphate receptor expressed in intestinal epithelium. *The Journal of biological chemistry* **269**, 1222-1230 (1994).

155. M. Srivastava *et al.*, Anx7 is required for nutritional control of gene expression in mouse pancreatic islets of Langerhans. *Molecular medicine (Cambridge, Mass.)* **8**, 781-797 (2002).

156. C. Sakakura *et al.*, Possible involvement of inositol 1,4,5-trisphosphate receptor type 3 (IP3R3) in the peritoneal dissemination of gastric cancers. *Anticancer research* **23**, 3691-3697 (2003).

157. K. Shibao *et al.*, The type III inositol 1,4,5-trisphosphate receptor is associated with aggressiveness of colorectal carcinoma. *Cell calcium* **48**, 315-323 (2010).

158. A. Mound, L. Rodat-Despoix, S. Bougarn, H. Ouadid-Ahidouch, F. Matifat, Molecular interaction and functional coupling between type 3 inositol 1,4,5-trisphosphate receptor and BKCa channel stimulate breast cancer cell proliferation. *European journal of cancer (Oxford, England : 1990)* **49**, 3738-3751 (2013).

159. Y. Zhang *et al.*, An essential role of discoidin domain receptor 2 (DDR2) in osteoblast differentiation and chondrocyte maturation via modulation of Runx2 activation. *Journal of bone and mineral research : the official journal of the American Society for Bone and Mineral Research* **26**, 604-617 (2011).

160. L. Walsh, A. Nawshad, D. Medici, Discoidin domain receptor 2 is a critical regulator of epithelial-mesenchymal transition. *Matrix biology : journal of the International Society for Matrix Biology* **30**, 243-247 (2011).

161. B. Leitinger, Discoidin domain receptor functions in physiological and pathological conditions. *International review of cell and molecular biology* **310**, 39-87 (2014).

162. Z. Yan *et al.*, Discoidin domain receptor 2 facilitates prostate cancer bone metastasis via regulating parathyroid hormone-related protein. *Biochimica et biophysica acta*, (2014).

163. K. Zhang *et al.*, The collagen receptor discoidin domain receptor 2 stabilizes SNAIL1 to facilitate breast cancer metastasis. *Nature cell biology* **15**, 677-687 (2013).

164. J. Xu *et al.*, Overexpression of DDR2 contributes to cell invasion and migration in head and neck squamous cell carcinoma. *Cancer biology & therapy* **15**, (2014).

165. E. M. Beauchamp *et al.*, Acquired resistance to dasatinib in lung cancer cell lines conferred by DDR2 gatekeeper mutation and NF1 loss. *Molecular cancer therapeutics* **13**, 475-482 (2014).

166. V. Pitini, C. Arrigo, C. Di Mirto, P. Mondello, G. Altavilla, Response to dasatinib in a patient with SQCC of the lung harboring a discoid-receptor-2 and synchronous chronic myelogenous leukemia. *Lung cancer (Amsterdam, Netherlands)* **82**, 171-172 (2013).

167. X. C. Zhang *et al.*, Tumor evolution and intratumor heterogeneity of an oropharyngeal squamous cell carcinoma revealed by whole-genome sequencing. *Neoplasia (New York, N.Y.)* **15**, 1371-1378 (2013).

168. D. P. Slaughter, H. W. Southwick, W. Smejkal, Field cancerization in oral stratified squamous epithelium; clinical implications of multicentric origin. *Cancer* **6**, 963-968 (1953).

169. S. Tabatabaeifar, T. A. Kruse, M. Thomassen, M. J. Larsen, J. A. Sørensen, Use of next generation sequencing in head and neck squamous cell carcinomas: A review. *Oral oncology*, (2014).

170. L. Iwai *et al.*, Phosphoproteomics of collagen receptor networks reveals SHP-2 phosphorylation downstream of wild-type DDR2 and its lung cancer mutants. *The Biochemical journal* **454**, 501-513 (2013).

171. Exome sequencing identifies frequent mutation of ARID1A in molecular subtypes of gastric cancer. *Nature Genetics* **43**, 1219-1223 (2011).

172. N. Cancer Genome Atlas Research *et al.*, Integrated genomic characterization of endometrial carcinoma. *Nature* **497**, 67-73 (2013).

173. S. Forbes *et al.*, COSMIC (the Catalogue of Somatic Mutations in Cancer): a resource to investigate acquired mutations in human cancer. *Nucleic acids research* **38**, 7 (2010).

174. M. Lindauer, A. Hochhaus, Dasatinib. *Recent results in cancer research. Fortschritte der Krebsforschung. Progrès dans les recherches sur le cancer* **201**, 27-65 (2013).

175. H. D. Brooks *et al.*, Phase 2 study of dasatinib in the treatment of head and neck squamous cell carcinoma. *Cancer* **117**, 2112-2119 (2011).

176. L. E. MacConaill *et al.*, Prospective Enterprise-Level Molecular Genotyping of a Cohort of Cancer Patients. *The Journal of molecular diagnostics : JMD,* (2014).

177. R. B. Erlich *et al.*, Preclinical evaluation of dual PI3K-mTOR inhibitors and histone deacetylase inhibitors in head and neck squamous cell carcinoma. *Br J Cancer* **106**, 107-115 (2012).

178. L. Lattanzio *et al.*, Treatment effect of buparlisib, cetuximab and irradiation in wild-type or PI3KCA-mutated head and neck cancer cell lines. *Invest New Drugs* **33**, 310-320 (2015).

179. T. Mazumdar *et al.*, A comprehensive evaluation of biomarkers predictive of response to PI3K inhibitors and of resistance mechanisms in head and neck squamous cell carcinoma. *Mol Cancer Ther* **13**, 2738-2750 (2014).

180. H. Xu *et al.*, Collagen binding specificity of the discoidin domain receptors: binding sites on collagens II and III and molecular determinants for collagen IV recognition by DDR1. *Matrix Biol* **30**, 16-26 (2011).